

Data Assimilation in the Geosciences

An overview on methods, issues and perspectives

Alberto Carrassi*, Marc Bocquet[†], Laurent Bertino* and Geir Evensen^{‡*}

Article Type: Overview

Abstract

We commonly refer to state-estimation theory in geosciences as *data assimilation*. This term encompasses the entire sequence of operations that, starting from the observations of a system, and from additional statistical and dynamical information (such as a dynamical evolution model), provides an estimate of its state. Data assimilation is standard practice in numerical weather prediction, but its application is becoming widespread in many other areas of climate, atmosphere, ocean and environment modeling; in all circumstances where one intends to estimate the state of a large dynamical system based on limited information. While the complexity of data assimilation, and of the methods thereof, stands on its interdisciplinary nature across statistics, dynamical systems and numerical optimization, when applied to geosciences an additional difficulty arises by the continually increasing sophistication of the environmental models. Thus, in spite of data assimilation being nowadays ubiquitous in geosciences, it has so far remained a topic mostly reserved to experts. We aim this overview article at geoscientists with a background in mathematical and physical modeling, who are interested in the rapid development of data assimilation and its growing domains of application in environmental science, but so far have not delved into its conceptual and methodological complexities.

*Nansen Environmental and Remote Sensing Center, Bergen, Norway

[†]CEREA, joint laboratory École des Ponts ParisTech and EDF R&D, Université Paris-Est, Champs-sur-Marne, France

[‡]IRIS, Bergen, Norway

1 Introduction

The purpose of this article is to provide a comprehensive, state-of-the-art overview of the methods and challenges of data assimilation (DA) in the geosciences. We aim the article at geoscientists confronted with the problem of combining data with models and need to learn DA, but who are intimidated by the vast, and technical, literature. This work may guide them through a first journey into the topic while being at the same time as complete and precise as possible.

The finest mathematical details, at the crossing between different areas such as numerical methods, algebra, statistics or dynamical systems, are essential to grasp the sense of the DA problem, to reveal its interdisciplinary nature and, for many, its beauty. We have nevertheless avoided all technicalities that were not, in our opinion, strictly necessary and have worked to make the narrative intelligible for geoscientists, or climate scientists, who do not usually possess a strong background in mathematics.

We provide the readers with an extensive bibliography, but also recognize that it is beyond the scope of this work to make it entirely exhaustive. In the last decade or so, DA has attracted much attention. The topic has recently reached the rank of a discipline per se, as testified by the appearance of books such as *van Leeuwen et al. (2015)*, *Reich and Cotter (2015)*, *Law et al. (2015)* or *Asch et al. (2016)*. These works have mainly addressed the mathematical dimension and formulation of the DA problem and complement seminal books on DA (e.g., *Daley, 1993*; *Kalnay, 2002*; *Evensen, 2009b*), that had spread the knowledge about DA and shaped it as an independent discipline. The present article places itself somehow in between these two classes of textbooks and aims at bridging the mathematical side of the DA methods with the practicalities and the physical intuitions and know-how that have guided its dramatic development in climate science and geosciences in general.

The paper is structured to provide a first general formulation of the state estimation problem, from a Bayesian perspective, in Sect. 2. Having defined the issue, and illustrated the intrinsic difficulties to adopt the Bayesian approach in the geosciences, the two most popular families of DA algorithms, both based on a Gaussian approximation, namely the Kalman filter and the variational methods, are described in Sect. 3 and in the complementary Appendices A–D. Section 4 is entirely devoted to the ensemble methods, from their origin, through the most relevant successful variants and up to the new frontier of hybrid ensemble-variational methods. Four selected topics, characterizing the DA problems in the geosciences, are the subjects of Sect. 5, and are examples of the specific type of approximations and compromises, as well as the level of innovations DA has achieved. Finally Sect. 6 presents a prospect of the recent challenges and current directions of research and developments, with special attention to two, the particle filter and coupled DA.

2 State estimation: formulation of the problem

2.1 Premises

The problem we intend to solve is the estimation of the state of a system, say the atmosphere, the ocean or any component of the Earth system or its whole, at any arbitrary past,

present and future time. We possess two complementary, but both incomplete and inaccurate, sources of information: the *observations* and the *model*. Data assimilation provides the conceptual and methodological tools to tackle the problem by extracting synergies between model and observations and by exploiting their respective informational content. Given the nature of the modeling and observation infrastructure in the geosciences, DA is conveniently formalized as a discrete-model/discrete-observation estimation problem, as we will do in this overview. We remark however that, the *nudging method* (e.g., *Hoke and Anthes, 1976; Lakshmivarahan and Lewis, 2013*), one of the simplest and most straightforward approach to assimilate data in a dynamical model, is better formulated as continuous-model/continuous-data problem. Nudging will not be addressed in this overview, but it is worth mentioning that it has recently awoken new attention that has brought the introduction of new advanced formulations (e.g., *Auroux and Blum, 2008; Pazo et al., 2016*), and to the study of its connection with the synchronization problem (*Duane et al., 2006*). Interested readers can find a complete treatment of the continuous-continuous and discrete-continuous cases in many textbooks on estimation theory (see, e.g., *Jazwinski, 1970; Bain and Crisan, 2009*).

Throughout the text the following notation convention is used: $\mathbf{x} \in \mathbb{R}^m$ means that \mathbf{x} is a m -dimensional vector whose components are real numbers; $f : \mathbb{R}^l \rightarrow \mathbb{R}^n$ signifies that the function f transforms an l -dimensional vector into an n -dimensional one; model values at discrete times are indicated as $\mathbf{x}(t_k) = \mathbf{x}_k$. We can now formalize the two ingredients entering the estimation problem.

The dynamical model - Let us assume that a model of the natural processes of interest is available as a discrete stochastic-dynamical system,

$$\mathbf{x}_k = \mathcal{M}_{k:k-1}(\mathbf{x}_{k-1}, \boldsymbol{\lambda}) + \boldsymbol{\eta}_k. \quad (1)$$

Here $\mathbf{x}_k \in \mathbb{R}^m$ and $\boldsymbol{\lambda} \in \mathbb{R}^p$ are the model state and parameter vectors respectively, $\mathcal{M}_{k:k-1} : \mathbb{R}^m \rightarrow \mathbb{R}^m$ is usually a nonlinear, possibly chaotic, function from time t_{k-1} to t_k , and $\boldsymbol{\eta}_k \in \mathbb{R}^m$ is the model error, represented here as a stochastic additive term, although it could be included into the parenthesis without loss of generality. The model parameters may include the external forcings or the boundary conditions.

The model error, $\boldsymbol{\eta}_k$, is intended to represent the error of a model prediction of the true unknown process at time t_k , initialized from the true state (perfect initial condition) at time t_{k-1} . It accounts for the cumulative effect, over the interval $t_k - t_{k-1}$, of errors in the parameters, $\boldsymbol{\lambda}$, errors in the numerical schemes used to integrate Eq. (1) as well as the effect of the unresolved scales. The two latter arise from the spatio-temporal discretization from physical laws (e.g., the Navier Stokes equations) expressed as partial differential equations on a continuous media, into difference equations on a discrete grid or finite spectral modes. The appropriateness of the stochastic formulation of the model error is questionable in many cases (see, e.g., *Nicolis, 2003*). Nevertheless it has the advantage of fitting very well to the probabilistic Bayesian approach to the DA problem, as we will clarify later. Alternative forms of model error treatment in DA have been proposed recently, including a deterministic one (see *Carrassi and Vannitsem, 2016*, and references therein), but they will not be developed in this overview.

The dynamical model can also include an explicit dependence on time (i.e., be non-autonomous), as can be the case if the system is subject to climate change driven by a time-

dependent forcing, such as radiative forcing, anthropogenic changes in greenhouse gases and aerosol concentrations. In such case the system may not have an attractor nor an invariant measure on it (in practice it does not possess statistical equilibrium), a situation that again would hamper the development of a consistent statistical framework for DA. Recent studies on the pullback or random attractor (*Chekroun et al.*, 2011; *Dijkstra*, 2013) may open the path to suitable formulations of the estimation problem for non-autonomous systems.

The observation model - Noisy observations of \mathbf{x}_k are available at discrete times and are represented as components of the observation vector $\mathbf{y}_k \in \mathbb{R}^d$. Assuming the noise is additive, they are related to the model state vector through

$$\mathbf{y}_k = \mathcal{H}_k(\mathbf{x}_k) + \epsilon_k. \quad (2)$$

Equation (2) defines the, generally nonlinear, observation operator, $\mathcal{H} : \mathbb{R}^m \rightarrow \mathbb{R}^d$, from model to observational space, which often involve spatial interpolations, convolutions or spectral-to-physical space transformation in spectral models. Transformations based on physical laws for indirect measurements, such as radiative fluxes used to measure temperatures, can also be represented in this way (e.g., *Kalnay*, 2002). To simplify the notation, we have assumed the observation dimension is constant, so that $d_k = d$.

Similarly to model error, the observational error, ϵ_k , is also represented as a stochastic (i.e., random) additive term, and accounts for the instrumental error of the observing devices, deficiencies in the formulation of the observation operator itself, and the *error of representation (or representativeness)* (*Lorenç*, 1986; *Janjić et al.*, 2017). The latter arises from the presence of unresolved scales and represents their effect on the scales explicitly resolved by the model. The error of representativeness is difficult to estimate due to lack of information at small scales, but ubiquitous in Earth science, because the description of a continuum fluid is made by an inevitably limited (albeit always growing) number of discrete grid points (or spectral bands); see *Cohn* (1997) for a discussion on this issue and the related “change of support” techniques in geostatistics (*Chilès and Delfiner*, 2012). Note that the additivity of noise is also a simplification since more general noisy observations $\mathbf{y}_k = \mathcal{H}_k(\mathbf{x}_k, \epsilon_k)$ could be considered.

Confronting model with data is inherent to the scientific methods since Galileo’s era. Nevertheless, the DA problem in Earth science has some characteristic criticalities that makes it unique. In geosciences we usually have $d \ll m$, i.e., the amount of available data is insufficient to fully describe the system and one cannot strongly rely on a data-driven approach: the model is paramount. It is the model that fills the spatial and temporal gaps in the observational network: it propagates information from observed-to-unobserved areas and from the observing times to any other causally related. This capability has been pivotal in DA for numerical weather prediction (NWP) with notable examples being the ocean areas and the Southern Hemisphere, where the lack of routine observations platforms has been compensated by the dynamical model (see, e.g., *Daley*, 1993; *Kalnay*, 2002). The other peculiarity is the use of massive dataset ($d \approx \mathcal{O}(10^7)$) and huge models states ($m \approx \mathcal{O}(10^9)$). Thus, DA methods are designed to achieve the best possible use of a never sufficient (albeit constantly growing) amount of data, and to attain an efficient data-model fusion, in a short

period of time (typically 3 – 6 hours for NWP). This poses a formidable computational challenge, and makes DA an example of big-data problems.

2.2 Bayesian formulation of the state estimation problem

With the two complementary pieces of information in hand, model and data, we can move forward and formalize their fusion. Because of the assumed random nature of both the model and observational error, they can be described in terms of *probability density functions* (pdfs), and the Bayesian approach offers a natural framework to understand the DA problem. Our main focus here is on state estimation, i.e., the issue of estimating \mathbf{x} , based on the model and the observation. Nevertheless, in many physical applications, one is often interested in the joint estimate of the system’s state and of its parameters, $\boldsymbol{\lambda}$ (see, e.g., Evensen, 2009a, and references therein). We shall allude to parameter estimation later, but its extensive exposition is beyond the scope of this overview.

In the Bayesian formulation, the output of the estimation process is the *posterior distribution* $p(\mathbf{x}|\mathbf{y})$ of the unknown process \mathbf{x} conditioned on the data \mathbf{y} , which can be obtained using *Bayes’ rule*

$$p(\mathbf{x}|\mathbf{y}) = \frac{p(\mathbf{y}|\mathbf{x})p(\mathbf{x})}{p(\mathbf{y})}. \quad (3)$$

In Eq. (3), the three components of the Bayesian inference appear: $p(\mathbf{x})$ is the *prior pdf* that gathers all the knowledge before assimilating the new observations, $p(\mathbf{y}|\mathbf{x})$ is the *likelihood of the data* conditioned on the state \mathbf{x} (i.e., what would be the observation if the true state were known?), and $p(\mathbf{y})$ is the distribution of the observation, whichever the value of the state, $p(\mathbf{y}) = \int d\mathbf{x} p(\mathbf{y}|\mathbf{x})p(\mathbf{x})$. The latter is independent of \mathbf{x} and is treated as a normalization coefficient. The postulate of a prior is a distinctive feature of the Bayesian approach, which allows the introduction of arbitrary information about the system before data are included. Its choice is subjective and one can in principle use any distribution that suits a study’s specific purposes, either based on climatology (i.e., from historical knowledge about the system), on theoretical physical principles or even on subjective expert’s opinion. However, in many practical cases, the search for a good informative prior is not straightforward, although its choice may strongly affect the results, sometimes adversely.

So far, we have left the times of \mathbf{x} and \mathbf{y} undefined. Both the model and the observational error sequences, $\{\boldsymbol{\eta}_k : k = 1, \dots, K\}$ and $\{\boldsymbol{\epsilon}_k : k = 1, \dots, K\}$ are assumed to be uncorrelated in time, mutually independent, and distributed according to the pdfs p_η and p_ϵ , respectively. These pdfs are related to the prior and likelihood terms of Bayes’ rule as follows:

$$p(\mathbf{x}_k|\mathbf{x}_{k-1}) = p_\eta[\mathbf{x}_k - \mathcal{M}_{k:k-1}(\mathbf{x}_{k-1})], \quad (4)$$

$$p(\mathbf{y}_k|\mathbf{x}_k) = p_\epsilon[\mathbf{y}_k - \mathcal{H}_k(\mathbf{x}_k)], \quad (5)$$

where the model dependency on the parameters, $\boldsymbol{\lambda}$, has been dropped to simplify the notation. Let us define the sequences of system states and observations within the interval $[t_0, t_K]$ as $\mathbf{x}_{K:0} = \{\mathbf{x}_K, \mathbf{x}_{K-1}, \dots, \mathbf{x}_0\}$ and $\mathbf{y}_{K:1} = \{\mathbf{y}_K, \mathbf{y}_{K-1}, \dots, \mathbf{y}_1\}$ respectively. Since the observational errors are assumed to be uncorrelated in time we can split the products of the

probabilities

$$p(\mathbf{y}_{K:1}|\mathbf{x}_{K:0}) = \prod_{k=1}^K p(\mathbf{y}_k|\mathbf{x}_k) = \prod_{k=1}^K p_\epsilon[\mathbf{y}_k - \mathcal{H}_k(\mathbf{x}_k)], \quad (6)$$

meaning that the mutual likelihood of all the observations in the interval $t_K - t_0$ is the product of the individual likelihoods at each time. We will further assume that the process is Markovian, which means that the state \mathbf{x} at time t_k , conditioned on all past states, only depends on the most recent state at time t_{k-1} and split the prior pdf accordingly

$$p(\mathbf{x}_{K:0}) = p(\mathbf{x}_0) \prod_{k=1}^K p(\mathbf{x}_k|\mathbf{x}_{k-1}) = p(\mathbf{x}_0) \prod_{k=1}^K p_\eta[\mathbf{x}_k - \mathcal{M}_{k:k-1}(\mathbf{x}_{k-1})]. \quad (7)$$

By combining Eq. (6) and (7) using Bayes' rule, Eq. (3), we get the posterior distribution as a product

$$p(\mathbf{x}_{K:0}|\mathbf{y}_{K:1}) \propto p(\mathbf{x}_0) \prod_{k=1}^K p(\mathbf{y}_k|\mathbf{x}_k)p(\mathbf{x}_k|\mathbf{x}_{k-1}) = p(\mathbf{x}_0) \prod_{k=1}^K p_\epsilon[\mathbf{y}_k - \mathcal{H}_k(\mathbf{x}_k)]p_\eta[\mathbf{x}_k - \mathcal{M}_{k:k-1}(\mathbf{x}_{k-1})]. \quad (8)$$

Equation (8) is of central importance: it states that a new update can be obtained as soon as new data is available; it is called a hidden Markov chain in statistics.

Depending on which time period is needed for state estimation, it is possible to define *three estimation problems* (Wiener, 1949):

1. **Prediction:** estimate $p(\mathbf{x}_l|\mathbf{y}_{k:1})$ with $l > k$.
2. **Filtering:** estimate $p(\mathbf{x}_k|\mathbf{y}_{k:1})$.
3. **Smoothing:** estimate $p(\mathbf{x}_{K:0}|\mathbf{y}_{K:1})$, or selected marginals of this pdf, such as $p(\mathbf{x}_l|\mathbf{y}_{K:1})$, with $0 \leq l < K$.

A schematic illustration of the three problems is given in Fig. 1.

The *prediction problem* (Fig. 1 top panel) is formally addressed by integrating Eq. 4, i.e. by solving the Chapman-Kolmogorov equation for the propagation of a pdf by the model

$$p(\mathbf{x}_l|\mathbf{y}_{k:1}) = \int d\mathbf{x}_k p_\eta[\mathbf{x}_l - \mathcal{M}_{l:k}(\mathbf{x}_k)]p(\mathbf{x}_k|\mathbf{y}_{k:1}), \quad (9)$$

given the conditional pdf at time t_k , $p(\mathbf{x}_k|\mathbf{y}_{k:1})$.

The *filtering problem* (Fig. 1 mid panel) is the most common in geophysical applications, and is characterized by sequential processing, in which measurements are utilized as they become available (Jazwinski, 1970; Bengtsson et al., 1981). An *analysis step*, in which the conditional pdf $p(\mathbf{x}_k|\mathbf{y}_{k:1})$ is updated using the latest observation, \mathbf{y}_k , alternates with a forecast step which propagates this pdf forward until the time of a new observation. The analysis is based on the application of Bayes' Eq. (3), which becomes

$$p(\mathbf{x}_k|\mathbf{y}_{k:1}) = \frac{p_\epsilon[\mathbf{y}_k - \mathcal{H}_k(\mathbf{x}_k)]p(\mathbf{x}_k|\mathbf{y}_{k-1:1})}{\int d\mathbf{x}_k p_\epsilon[\mathbf{y}_k - \mathcal{H}_k(\mathbf{x}_k)]p(\mathbf{x}_k|\mathbf{y}_{k-1:1})}, \quad (10)$$

while in the *prediction step* one integrates the Chapman-Kolmogorov equation (9) from $k - 1$ to k . The process is then repeated, sequentially, with the outcome of the Chapman-Kolmogorov equation providing the prior distribution for the next analysis step.

Estimating the conditional pdf of the state at any time t_k , $0 \leq k \leq K$, based on all observations (past, present and future), is known as the *smoothing problem* (Fig. 1 bottom panel). This is relevant when one is interested in a retrospective analysis after the observations have been collected, and it is very useful in generating *reanalysis* as well as in the estimation of the parameters λ . Reanalysis programs offer an homogeneous reconstructed estimate of the system based on observations covering an extended period of time (up to a century), using state-of-the-art model and DA methods of the time when the reanalysis

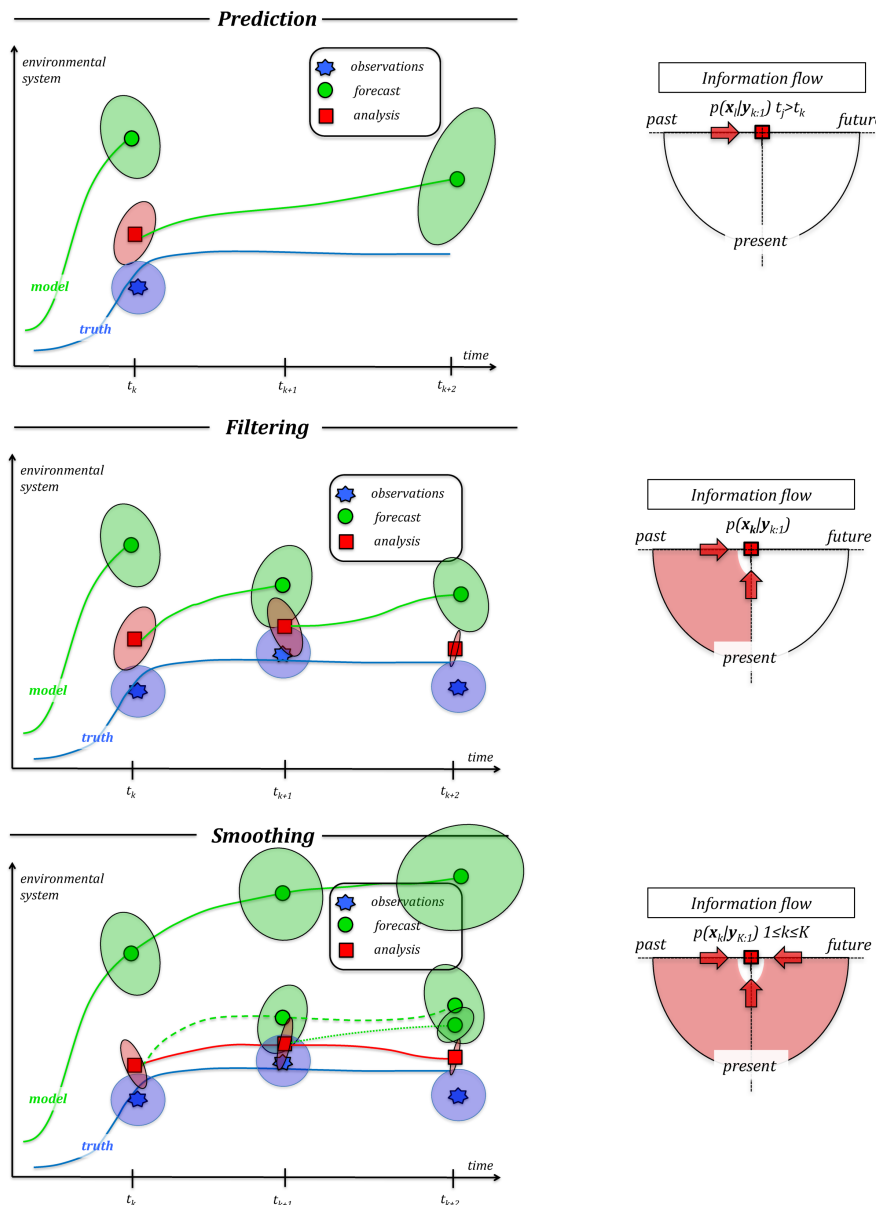


Figure 1: Caption next page

Figure 1: Illustration of the three estimation problems: *prediction* (top), *filtering* (middle) and *smoothing* (bottom). The true signal is displayed with the blue line, while the forecast and the analysis are in green and red, respectively. Observations are marked as blue 8-points stars and the analysis states with the red squares. Observational, forecast and analysis uncertainties are displayed with colored ellipsoids of proportional size, i.e. the smaller the ellipsoid the smaller the estimated uncertainty, so the larger the confidence in each of them. Note that in this illustration the observational error is assumed constant. In the *prediction* (top panel) an analysis is produced at time t_k by using the forecast at t_k and the observation at t_k ; the analysis (red square) is closer to the truth than the forecast (green circle). From the analysis a prediction is issued up to time t_{k+2} ; the prediction error (distance between the green and the blue lines between t_k and t_{k+2}) grows with time and the estimated forecast uncertainty at time t_{k+2} (the green ellipsoid) is correspondingly larger than the uncertainty in the analysis at time t_k (red ellipsoid). Information is thus only propagated forward from t_k as depicted in the information flow diagram (top right). In the *filter* case (mid panels) a prediction is issued from the analysis at t_k up to the next observations at t_{k+1} ; we see that the forecast uncertainty at t_{k+1} is larger than that of the analysis at t_k . At the analysis time, t_{k+1} , a new analysis performed by combining the forecast at t_{k+1} with the observation at the same time: the analysis is closer to the truth and its associated uncertainty (red ellipsoid) is smaller than the forecast and the observational uncertainty (green and blue ellipsoid/circle). From the analysis at t_{k+1} the process can then be repeated and a new forecast up to t_{k+2} is issued and a new analysis is performed at t_{k+2} using the new observation at t_{k+2} . Note that the analysis error (distance between the red squares and the blue line) decreases with time, as new observations are assimilated, and so does the estimated analysis uncertainty (red ellipsoids). The information flow diagram (mid right) illustrates how the information is both carried from the past (as in the prediction problem) and updated by current data. Finally, in the *smoother* (bottom panels), all observations between t_k and t_{k+2} contribute simultaneously to the analysis, which is now the entire trajectory within the smoothing interval $t_k - t_{k+2}$. The analysis solution is indeed smoother, and closer to the truth, than the sequences of analyses obtained with the filter (cf. mid and bottom left panels). At the final time, t_{k+2} , the smoother and filter have assimilated the same full amount of observations, so their analyses at t_{k+2} , and their associated estimated uncertainties, are approximately the same. However, the smoother provides a more accurate analysis at any other time in the assimilation window.

is produced. Reanalyses are paramount in climate diagnosis and several NWP, ocean and climate centers issue their own reanalysis products (e.g., among many others, *Dee et al.*, 2011; *Xie et al.*, 2017).

The joint smoothing pdf is given in Eq. (8), and is based on the recursive use of Bayes' formula for the update at each t_k , and the Chapman-Kolmogorov equation for the pdf propagation from t_{k-1} to t_k . To see this, the smoothing distribution at time t_k can be written using the subsequent state at time t_{k+1}

$$p(\mathbf{x}_k | \mathbf{y}_{K:1}) = \int d\mathbf{x}_{k+1} p(\mathbf{x}_k | \mathbf{x}_{k+1}, \mathbf{y}_{K:1}) p(\mathbf{x}_{k+1} | \mathbf{y}_{K:1}). \quad (11)$$

Furthermore, we note the following

$$p(\mathbf{x}_k | \mathbf{x}_{k+1}, \mathbf{y}_{K:1}) = p(\mathbf{x}_k | \mathbf{x}_{k+1}, \mathbf{y}_{k:1}) = \frac{p(\mathbf{x}_{k+1} | \mathbf{x}_k) p(\mathbf{x}_k | \mathbf{y}_{k:1})}{p(\mathbf{x}_{k+1} | \mathbf{y}_{k:1})}, \quad (12)$$

where we used again the fact that observations $\{\mathbf{y}_{k+1}, \dots, \mathbf{y}_K\}$ are independent of \mathbf{x}_k when \mathbf{x}_{k+1} is known (see Sect. 2.2), and $p(\mathbf{x}_k | \mathbf{y}_{k:1})$ is the filter solution (the analysis) at time t_k . Together, Eq. (11) and (12) suggest a forward-backward recursive algorithm, in which a forward filtering is followed by a backward smoothing. Starting from $p(\mathbf{x}_0)$, the forward phase consists of a sequential filter from t_1 to t_K which allows one to estimate, and to store, the sequence of filter pdfs $p(\mathbf{x}_k | \mathbf{y}_{k:1})$. In the backward phase, from t_{K-1} to t_1 , one evaluates Eq. (12) using the previously stored filter solutions, and finally estimates the smoothing pdf recursively via Eq. (11) using the smoothing pdf, $p(\mathbf{x}_{k+1} | \mathbf{y}_{K:1})$, from the previous iteration. We will see in Sect. 3.1.2 that the above recursion possesses an analytical solution when the dynamical and observational model are linear and all error pdfs are Gaussian.

We conclude the section with some comparative considerations between the filter and smoother. The filtering solution at an arbitrary t_k ($0 \leq k \leq K$) is obtained by sequential updating until t_k and it thus accounts for all observations before t_k . In contrast, the smoothing solution at the same time t_k also accounts for future observations until t_K , and it is thus generally more accurate than the filtering one. At the final time t_K both solutions have incorporated the same amount of data, so that in the absence of approximations, they will coincide (e.g., *Kalnay and Yang, 2010*).

3 A route to solutions: the Gaussian approximation

With the pdfs for smoother, filter and prediction, Eqs. (8-10), in hand, it still remains to be decided which estimator suits best a specific problem. Those pdfs, in fact, describe fully the probability of all possible states of the system but hardly make good targets for an estimation algorithm. Two “natural” options, the *mean* of the distribution or its *mode*, characterize two traditional approaches to state estimation. Methods designed targeting the mean are named *minimum squared error* estimators because, irrespective of the properties of the pdf (i.e., whether or not it is symmetric and unimodal), the mean is always the minimum squared error estimate (*Jazwinski, 1970*). The mode is the peak of the distribution, the most probable state, and methods targeting it are referred to as *maximum a posteriori* estimators. Other possible options are viable, such as the median, but they are generally more difficult to compute do not have the same wide range of applicability as the mean or the mode.

Despite its appealing and clear logic, the huge dimensions of typical models and datasets used in environmental science hamper the use of a fully Bayesian approach. The problem dimension renders it extremely difficult, or practically impossible, to define and to evolve the pdfs. To overcome this computational, albeit fundamental, issue it is usually assumed that the uncertainties of each piece of information (observations, model and prior) are Gaussian distributed. This hypothesis leads to a substantial simplification: the pdfs can be completely described by their first and second moments: the mean and the covariance matrix.

The Gaussian approximation is at the core of most DA procedures successfully used in the geosciences, and this overview will largely discuss methods that rely upon it to different

extents. This section presents two main approaches to the estimation problem in which DA in the geosciences is rooted: the minimum variance Kalman-like (Sect. 3.1) and the maximum a posteriori variational methods (Sect. 3.2). Section 3 is complemented by four Appendices (A-D) where interested readers can find additional details on the methods.

3.1 The linear and Gaussian case - The Kalman filter and smoother

The dynamical and observational models, Eqs. (1) and (2), are both assumed to be linear

$$\mathbf{x}_k = \mathbf{M}_{k:k-1}\mathbf{x}_{k-1} + \boldsymbol{\eta}_k, \quad \boldsymbol{\eta}_k \sim \mathcal{N}(\mathbf{0}, \mathbf{Q}_k), \quad (13)$$

$$\mathbf{y}_k = \mathbf{H}_k\mathbf{x}_k + \boldsymbol{\epsilon}_k, \quad \boldsymbol{\epsilon}_k \sim \mathcal{N}(\mathbf{0}, \mathbf{R}_k), \quad (14)$$

with $\mathbf{M}_{k:k-1}$ and \mathbf{H}_k being $m \times m$ and $d \times m$ matrices respectively. The observational and model noises are assumed to be mutually uncorrelated and in time, unbiased, and Gaussian distributed with covariance matrices $\mathbf{R}_k \in \mathbb{R}^{d \times d}$ and $\mathbf{Q}_k \in \mathbb{R}^{m \times m}$ respectively.

3.1.1 Kalman filter

Under the aforementioned hypotheses of all sources of errors being Gaussian and both the observational and dynamical models being linear, the Kalman filter is the exact (optimal) solution to estimate recursively the conditional mean and the associated uncertainty, the conditional covariance, of the filtering pdf $p(\mathbf{x}_k|\mathbf{y}_{k:0})$. The process is sequential, meaning that observations are assimilated in chronological order, and the KF alternates a *forecast step*, when the mean and covariance of the prediction conditional pdf, $p(\mathbf{x}_k|\mathbf{y}_{k-1:0})$, are evolved, with an *analysis step* in which the mean and covariance of the filtering conditional pdf, $p(\mathbf{x}_k|\mathbf{y}_{k:0})$, are updated. By virtue of the Gaussian assumption, the mean and covariance suffice to fully describe the pdfs and the KF provides an exact set of closed equations. The KF formulae are given below without their derivation, which goes beyond the scope of this overview, but the reader can find numerous alternative ways in classical books or reviews on filtering (*Jazwinski, 1970; Bengtsson et al., 1981; Cohn, 1997; Talagrand, 1997; Wikle and Berliner, 2007; Bain and Crisan, 2009*).

Let us indicate the forecast/analysis mean state and covariance as $\mathbf{x}^{\text{f/a}}$ and $\mathbf{P}^{\text{f/a}}$ respectively. The KF equations then read

$$\text{Forecast Step} \quad \mathbf{x}_k^{\text{f}} = \mathbf{M}_{k:k-1}\mathbf{x}_{k-1}^{\text{a}}, \quad (15)$$

$$\mathbf{P}_k^{\text{f}} = \mathbf{M}_{k:k-1}\mathbf{P}_{k-1}^{\text{a}}\mathbf{M}_{k:k-1}^{\text{T}} + \mathbf{Q}_k. \quad (16)$$

$$\text{Analysis step} \quad \mathbf{K}_k = \mathbf{P}_k^{\text{f}}\mathbf{H}_k^{\text{T}}(\mathbf{H}_k\mathbf{P}_k^{\text{f}}\mathbf{H}_k^{\text{T}} + \mathbf{R}_k)^{-1}, \quad (17)$$

$$\mathbf{x}_k^{\text{a}} = \mathbf{x}_k^{\text{f}} + \mathbf{K}_k(\mathbf{y}_k - \mathbf{H}_k\mathbf{x}_k^{\text{f}}), \quad (18)$$

$$\mathbf{P}_k^{\text{a}} = (\mathbf{I}_k - \mathbf{K}_k\mathbf{H}_k)\mathbf{P}_k^{\text{f}}. \quad (19)$$

Given as inputs the matrices \mathbf{Q}_k , \mathbf{R}_k , \mathbf{H}_k and \mathbf{M}_k , for $k \geq 1$, and the initial condition for the mean, $\mathbf{x}_0^{\text{a}} = \mathbf{x}_0$, and initial error covariance, $\mathbf{P}_0^{\text{a}} = \mathbf{P}_0$, Eqs. (15)–(19) estimate sequentially

the state, $\mathbf{x}_k^{f/a}$, and the associated error covariance, $\mathbf{P}_k^{f/a}$, at any time $k > 1$. The matrix $\mathbf{K}_k \in \mathbb{R}^{m \times d}$ is the Kalman gain and it contains the regression coefficients of the optimal linear combination between the prior (given here by the forecast \mathbf{x}_k^f) and the observations. The resulting state estimate, the analysis \mathbf{x}_k^a , has minimum error variance and is unbiased.

3.1.2 Kalman smoother

We discussed in Sect. 2.2 that a recursive estimate of the pdf of the system state at any arbitrary time in the observing window, conditioned on all observations in the window, i.e. the pdf $p(\mathbf{x}_k | \mathbf{y}_{K:1})$, can be obtained using a forward and backward recursions, in which a forward-in-time filter is followed by a backward-in-time smoother. Under the hypotheses of linear dynamical and observational models and Gaussian errors, this bi-directional recursion can be solved analytically and it is referred to as the *Kalman smoother* (KS, *Jazwinski*, 1970). Like for the KF, we describe the KS formulae in the following, but we do not provide their derivation which can be found, for instance, in *Jazwinski* (1970).

Assume that a forward in time KF has already been implemented using Eqs. (15–19) for $k = 1, \dots, K$, and the forecast and analysis means and covariances, $\mathbf{x}_k^{f/a}$ and $\mathbf{P}_k^{f/a}$, have been computed and stored. With the filtering solutions at disposal we can run the KS recursion backward in time, for $k = K - 1, \dots, 1$, to compute the smoothing mean and covariance, \mathbf{x}_k^{sm} and \mathbf{P}_k^{sm} , according to

$$\mathbf{S}_k = \mathbf{P}_k^a \mathbf{M}_{k+1:k}^T (\mathbf{M}_{k+1:k} \mathbf{P}_k^a \mathbf{M}_{k+1:k}^T + \mathbf{Q}_{k+1})^{-1} = \mathbf{P}_k^a \mathbf{M}_{k+1:k}^T \mathbf{P}_{k+1}^{-f}, \quad (20)$$

$$\text{KS Mean} \quad \mathbf{x}_k^{\text{sm}} = \mathbf{x}_k^a + \mathbf{S}_k (\mathbf{x}_{k+1}^{\text{sm}} - \mathbf{x}_{k+1}^f), \quad (21)$$

$$\text{KS Covariance} \quad \mathbf{P}_k^{\text{sm}} = \mathbf{P}_k^a + \mathbf{S}_k (\mathbf{P}_{k+1}^{\text{sm}} - \mathbf{P}_{k+1}^f) \mathbf{S}_k^T \quad (22)$$

with initial conditions, at time t_K , $\mathbf{x}_K^{\text{sm}} = \mathbf{x}_K^a$ and $\mathbf{P}_K^{\text{sm}} = \mathbf{P}_K^a$. As anticipated in Sect. 2.2, the KF and KS solutions are equivalent at final time t_K , but not at earlier times. The KS formulation given above is also known as *Rauch-Tung-Striebel* smoother; more details on the smoothing techniques can be found in *Cosme et al.* (2012).

Appendix A discusses in more details some key properties of the Kalman filter and smoother.

3.2 Variational approach

Variational methods are designed to estimate the model trajectory that “best fits” all the observations within a prescribed observing window $[t_0, t_K]$. Given that the model trajectory is adjusted globally to fit all observations simultaneously, the state estimate at an arbitrary time t_k , $t_0 \leq t_k \leq t_K$, is influenced by all observations within the window. The problem is formalized as the one of minimizing an appropriate scalar *cost function* that quantifies the model-to-data misfit, with the constraint given by the model equations (*Sasaki*, 1970). Assuming data are available at each time t_k in the window (this assumption can easily be relaxed without any major changes in the exposition that follows), the variational problem reads

$$\mathbf{x}_{K:0}^a = \operatorname{argmin}(\mathcal{J}(\mathbf{x}_{K:0})) \quad \text{subject to} \quad \mathbf{x}_k = \mathcal{M}_{k:k-1}(\mathbf{x}_{k-1}) + \boldsymbol{\eta}_k \quad k = 1, \dots, K. \quad (23)$$

where the notation *argmin* is used to signify that $\mathbf{x}_{K:0}^a$ is the solution for which the cost function, $\mathcal{J}(\mathbf{x}_{K:0})$, attains its minimum. Note that $\mathcal{J}(\mathbf{x}_{K:0})$ is a function of the entire model trajectory within the window and the variational analysis solution, the trajectory $\mathbf{x}_{K:0}^a$, provides the closest possible fit to the data, while being consistent with the model dynamics over the entire window. Note furthermore that, in formulating the variational problem in Eq. (23), we did not require the model being linear and we have not yet made any hypothesis on the statistical nature of the errors. The most common forms of the variational problem in the geosciences are discussed and derived in Sect. 3.2.1. For example, when both observational and model errors are uncorrelated in time, unbiased, and Gaussian distributed with covariances \mathbf{R}_k and \mathbf{Q}_k respectively, these errors are both penalized in the cost function as follows:

$$\mathcal{J}(\mathbf{x}_{K:0}) = \frac{1}{2} \sum_{k=0}^K \|\mathbf{y}_k - \mathcal{H}_k(\mathbf{x}_k)\|_{\mathbf{R}_k^{-1}}^2 + \frac{1}{2} \sum_{k=1}^K \|\mathbf{x}_k - \mathcal{M}_{k:k-1}(\mathbf{x}_{k-1})\|_{\mathbf{Q}_k^{-1}}^2 + \frac{1}{2} \|\mathbf{x}_0 - \mathbf{x}^b\|_{\mathbf{B}^{-1}}^2, \quad (24)$$

where the notation, $\|\mathbf{x}\|_{\mathbf{A}}^2 = \mathbf{x}^T \mathbf{A} \mathbf{x}$, is used to indicate the weighted Euclidean norm. In Eq. (24) we furthermore assumed to have a prior, commonly referred to as *background* in variational methods literature, for the initial state at the start of the window, in the form of a Gaussian pdf with mean, $\mathbf{x}^b \in \mathbb{R}^m$, and covariance, $\mathbf{B} \in \mathbb{R}^{m \times m}$, respectively. We will recall and derive Eq. (24) in Sect. 3.2.1.

The calculus of variations can be used to find the extremum of $\mathcal{J}(\mathbf{x}_{K:0})$ and leads to the corresponding Euler-Lagrange equations (see, e.g., *Le Dimet and Talagrand*, 1986; *Bennett*, 1992). These arise by searching for the solution of a constrained minimization problem in which the solution is required to follow the model dynamics by appending the model equations such that

$$\mathcal{L}(\mathbf{x}_{K:0}, \mathbf{\Gamma}) = \mathcal{J}(\mathbf{x}_{K:0}) + \sum_{k=1}^K \mathbf{\Gamma}_k^T (\mathbf{x}_k - \mathcal{M}_{k:k-1}(\mathbf{x}_{k-1}) - \boldsymbol{\eta}_k), \quad (25)$$

with $\mathbf{\Gamma}_k^T \in \mathbb{R}^m$ the Lagrange multiplier vector at time t_k . Although rigorous and formally appealing, solving the Euler-Lagrange equations for problems with the size and complexity of typical geophysical systems is practically impossible, unless drastic approximations are introduced. When the dynamics are linear and the amount of observations is not very large, the Euler-Lagrange equations can be solved with the *method of representers* which has been very successful in the early days of DA for the ocean (*Bennett*, 1992), and later extended to nonlinear dynamics by *Uboldi and Kamachi* (2000). A nice property of the representer method is that it reduces the dimension of the problem to the number of measurements (smaller than the whole model state at all times or the model state dimension; see *Bennett* (1992)).

Nevertheless, the representers method is still far from being applicable for realistic high-dimensional problems such as NWP. An attractive alternative is represented by the *descent methods*, which use the gradient vector of the cost function in an iterative minimization procedure (*Talagrand and Courtier*, 1987, see also Appendix B). This latter approach, in its many variants, is adopted in most of the operational NWP centers that employ variational assimilation (*Fisher and Andersson*, 2001). At the cost function minimum, its gradient must

vanish and its Hessian matrix be positive definite (this condition is the extension to vector functions of the classical condition for a minimum of a scalar function for which its first derivative, here the gradient, must vanish and its second derivative, here the Hessian, must be positive, here positive definite):

$$\nabla_{\mathbf{x}_{K:0}} \mathcal{J}(\mathbf{x}_{K:0}) = \mathbf{0}, \quad \nabla_{\mathbf{x}_{K:0}}^2 \mathcal{J}(\mathbf{x}_{K:0}) > 0, \quad (26)$$

where $\mathbf{0} \in \mathbb{R}^{m \times K}$ is a matrix with all entries equal to zero, and the second inequality stands for the positive definiteness of the Hessian matrix. The *control variable* with respect to which the minimization is performed is the entire model trajectory over the observing window. The variational problem defined by Eq. (23) is usually referred to as *weak-constraint* given that the model dynamics is affected by errors and it thus constitutes a weak constraint during the minimization (Sasaki, 1970).

An important particular case is given by the *strong-constraint* variational assimilation in which the model is assumed to be perfect (Lewis and Derber, 1985; Le Dimet and Talagrand, 1986) (i.e., $\boldsymbol{\eta}_k = 0$). In this case, the dynamical model is (assumed) purely deterministic and its solutions are uniquely determined by specifying the initial conditions. This transforms the problem from a constrained into an unconstrained one and the cost function into a function of the initial condition alone, $\mathcal{J}(\mathbf{x}_{K:0}) \Rightarrow \mathcal{J}(\mathbf{x}_0)$; its gradient with respect to the state at t_0 reads

$$\nabla_{\mathbf{x}_0} \mathcal{J}(\mathbf{x}_{K:0}) = \sum_{k=1}^K \mathbf{M}_{k:0}^T \nabla_{\mathbf{x}_k} \mathcal{J}(\mathbf{x}_k) + \nabla_{\mathbf{x}_0} \mathcal{J}(\mathbf{x}_0). \quad (27)$$

where we have used the fact that $\mathbf{x}_k = \mathcal{M}_{k:0}(\mathbf{x}_0)$, and applied the chain rule for differentiating compositions of functions. The matrix $\mathbf{M}_{k:0}^T$ is the *adjoint operator*, the adjoint of the tangent linear model, and implies a backward integration from t_k to t_0 . The gradient, Eq. (27), can be obtained through a set of operations involving both forward nonlinear and backward adjoint integration; see Appendix B for more details on the minimization procedures.

The drastic reduction of the number of control variables, from the entire trajectory $\mathbf{x}_{K:0}$ for the weak-constraint into the initial state alone \mathbf{x}_0 for the strong-constraint case, together with the use of the adjoint methods (Lions, 1971), have made possible the successful use and diffusion of strong-constraint variational methods, or some suitable approximation of them, in atmospheric and oceanic DA (see, e.g., Kalnay, 2002; Talagrand, 2010).

3.2.1 Statistical interpretation and 4DVar

The form the cost function reflects how we intend to balance the data and the model relative to each other and, again, statistics offers a natural framework to accomplish this task. A natural choice would be to set the cost function proportional to the conditional posterior pdf, $p(\mathbf{x}_{K:0} | \mathbf{y}_{K:0})$, for which a suitable functional form, desirably smooth and derivable, must be given.

This can be done, for instances, under the hypothesis of Gaussian errors, and it leads to a significant simplification. Recall the Gaussian assumptions made in formulating the Kalman filter (KF) and Kalman smoother (KS) in Sect. 3.1: the prior, model and observational errors are all Gaussian distributed. We can now substitute these Gaussian pdfs into Bayes's

Eq. (8), to obtain the desired posterior distribution; it is the product of three Gaussian pdfs and is thus itself Gaussian

$$\ln p(\mathbf{x}_{K:0}|\mathbf{y}_{K:0}) \propto - \left[\frac{1}{2} \sum_{k=0}^K \|\mathbf{y}_k - \mathcal{H}_k(\mathbf{x}_k)\|_{\mathbf{R}_k^{-1}}^2 + \frac{1}{2} \sum_{k=1}^K \|\mathbf{x}_k - \mathcal{M}_{k:k-1}(\mathbf{x}_{k-1})\|_{\mathbf{Q}_k^{-1}}^2 + \frac{1}{2} \|\mathbf{x}_0 - \mathbf{x}^b\|_{\mathbf{B}^{-1}}^2 \right], \quad (28)$$

$$= -\mathcal{J}^{\text{w4DVar}}(\mathbf{x}_{K:0}) \quad (29)$$

which provides the cost function already given in Eq. (24). Maximizing $\ln p(\mathbf{x}_{K:0}|\mathbf{y}_{K:0})$, i.e., finding the most likely trajectory (the analysis $\mathbf{x}_{K:0}^a$) is equivalent to minimizing the term between the squared brackets. Equation (29) defines the cost function of the *weak-constraint 4DVar* (e.g. *Zupanski, 1997; Vidard et al., 2004; Trémolet, 2006, 2007*). The minimization can be carried out iteratively using the gradient of the cost function as described in Appendix B. The control variable for the minimization is the entire trajectory, $\mathbf{x}_{K:0}$, and the estimate at each time t_k is influenced by all observations in the window, before and after t_k . The gradient (not shown; see *Trémolet, 2006; Carrassi and Vannitsem, 2010*) with respect to \mathbf{x}_k includes a term proportional to the innovation, $\mathbf{y}_k - \mathcal{H}_k(\mathbf{x}_k)$, because data are assumed to be available at each time step. In the general case, when the model time discretization is finer than the observational temporal density, the corresponding innovation term disappears. The model error being uncorrelated in time implies that the cost function requires only the model error spatial covariances at times t_k and not their temporal correlation, and the model error cost function term (the second one in the rhs of Eq. (28)) reduces to a single summation over the time steps weighted by the inverse of the model error covariances (*Trémolet, 2006*). Even in this case however, the size of the control variable is huge, $\mathbf{x}_{K:0} \approx \mathcal{O}(m \times K)$ (i.e. the state vector dimension times the temporal steps in the assimilation window), and it is difficult to estimate reliably the model error covariances, \mathbf{Q}_k (cf. Appendix A). The developments of specific solutions have thus been necessary to make the weak-constraint 4DVar feasible in the geosciences (see, e.g., *Griffith and Nichols, 2000; Vidard et al., 2004; Trémolet, 2007*), and its use in operational settings has only been very recent (*Lindskog et al., 2009; Fisher et al., 2011; Ngodock and Carrier, 2014*). The weak-constraint 4DVar in the presence of time correlated model error is described in *Carrassi and Vannitsem (2010)*, while its hybrid ensemble-variational formulation (cf. Sect. 4.5) has been studied recently by *Amezcuca et al. (2017)*. An interesting alternative conceptualization of the weak-constraint 4DVar is described in *Ye et al. (2015)* that uses path-integral and annealing methods to solve the problem.

In the more widely used *strong-constraint 4DVar* it is assumed that the model is perfect, which reduces the cost function to

$$\mathcal{J}^{\text{s4DVar}}(\mathbf{x}_0) = \frac{1}{2} \sum_{k=0}^K \|\mathbf{y}_k - \mathcal{H}_k \circ \mathcal{M}_{k:0}(\mathbf{x}_0)\|_{\mathbf{R}_k^{-1}}^2 + \frac{1}{2} \|\mathbf{x}_0 - \mathbf{x}^b\|_{\mathbf{B}^{-1}}^2, \quad (30)$$

with the \circ symbol representing the composition of operators and the control variable is now “only” the system’s state at the beginning of the window, \mathbf{x}_0 . The gradient can be obtained by applying Eq. (27) and reads

$$\nabla_{\mathbf{x}_0} \mathcal{J}^{\text{s4DVar}}(\mathbf{x}_0) = - \sum_{k=0}^K \mathbf{M}_{k:0}^T \mathbf{H}_k^T \mathbf{R}_k^{-1} [\mathbf{y}_k - \mathcal{H}_k \circ \mathcal{M}_{k:0}(\mathbf{x}_0)] - \mathbf{B}^{-1}(\mathbf{x}_0 - \mathbf{x}^b), \quad (31)$$

which reveals the effects of the adjoint operator, $\mathbf{M}_{k:0}^T$, to project backward the influence of the observation at any t_k . The final analysis is obtained using an iterative process starting by providing a first guess, $\mathbf{x}_0^{i=0}$, and evaluating $\mathcal{J}^{s4DVar}(\mathbf{x}_0^i)$ and the gradient at each iteration. As explained in Appendix B, the process is then repeated until the convergence criteria are met. Then using the final minimum state at \mathbf{x}_0^a the analyzed trajectory is obtained over the entire window, $\mathbf{x}_{K:0}^a$, by integrating the deterministic model from t_0 to t_K . This trajectory represents the most likely model solution fitting the observations within the window and given the prescribed initial condition and data uncertainty.

Appendix C discusses in more details some key properties of the variational methods, while three popular approximations of the Kalman filter and variational methods, namely the *extended Kalman filter*, the *incremental 4DVar* and the *3DVar* are described in Appendix D. Finally, a schematic illustration of the different problems tackled by the weak-constraint 4DVar, strong-constraint 4DVar, and 3DVar (cf. Appendix D) is given in Fig. 2.

4 Ensemble methods

A Monte Carlo approach is at the basis of a class of algorithms referred to as *ensemble-based methods* (Evensen, 2009b) of which the *ensemble Kalman filter*, EnKF, and the *ensemble Kalman smoother*, EnKS, are the most celebrated examples. The EnKF and EnKS are still based on the Gaussian hypothesis: their analysis update steps are only based on the mean and covariance. The transition density is, however, approximated using an ensemble of realizations of the prior $p(\mathbf{x}_k|\mathbf{x}_{k-1})$, in practice by running an ensemble of trajectories of the model dynamics. The EnKF and its variants (Evensen, 2009b; Asch et al., 2016, and cf. Sect. 4.1–4.2) are nowadays among the most popular approaches for DA in high-dimensional systems and have been successfully applied in atmospheric and oceanic contexts. Evidence has emerged that a small number of particles, typically 100, is sufficient in many applications, hence making EnKF feasible in situations where the forward step of the DA is computationally expensive. A version of the EnKF is operational for the atmospheric model at the Canadian Meteorological Centre, CMC (Houtekamer et al., 2005). Also, the EnKF is used in the ocean system TOPAZ (see Sect. 5.4) developed at NERSC (Sakov et al., 2012a). MET Norway is running an operational version of TOPAZ and produces operational forecasts for the Arctic Ocean, sea ice, and ecosystem, for the European Copernicus Marine Services (www.marine.copernicus.eu).

There have been numerous alternative EnKF-like methods, and we will not attempt here to discuss them all; a recent review of the EnKF for atmospheric DA is given by Houtekamer and Zhang (2016). However the many different formulations fall almost all into two main categories, namely the *stochastic* and the *square-root* (also called *deterministic*) ones, and this is the subject of the next sections. We shall then discuss the EnKS in Sect. 4.3 and devote Sect. 4.4 to the description of the important countermeasures that must be put in place to make the EnKF and EnKS work in realistic high-dimensional nonlinear cases. This part of the article closes by presenting an outlook of the current frontier of the hybrid ensemble-based and variational methods in Sect. 4.5.

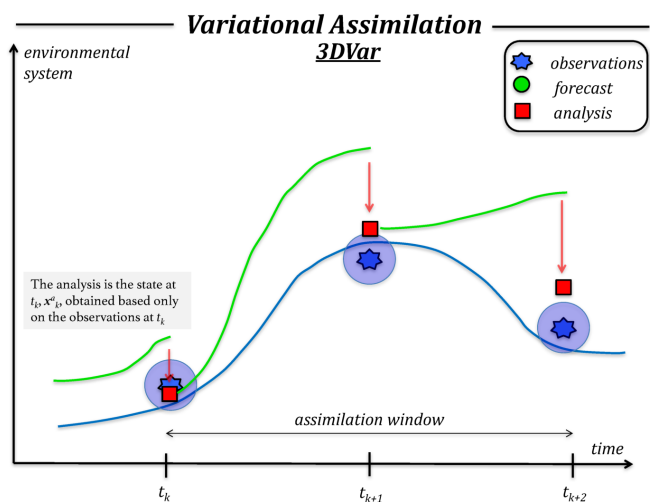
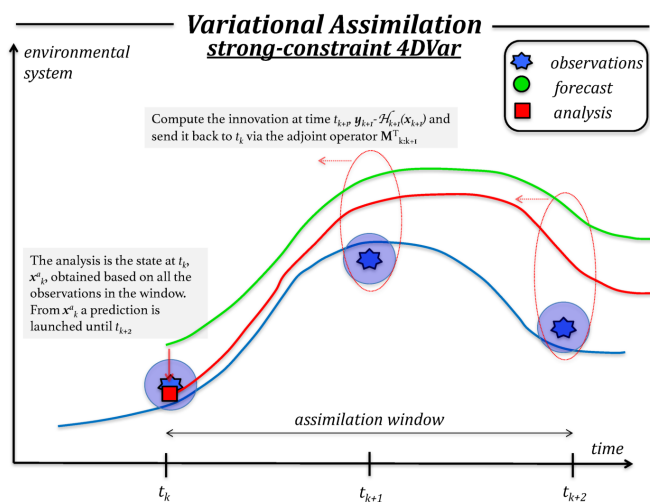
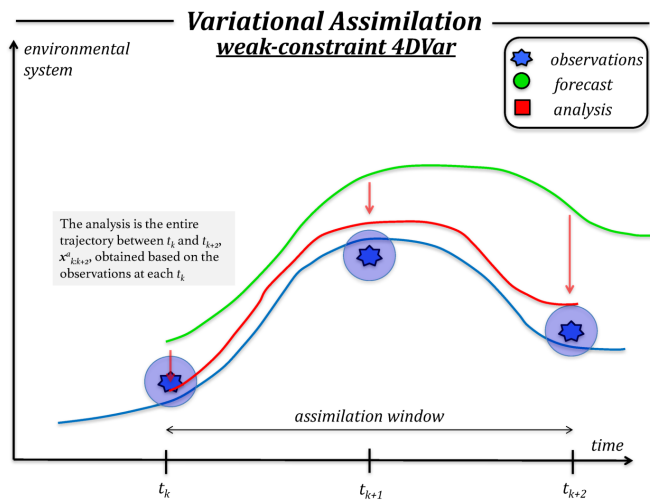


Figure 2: Caption next page

Figure 2: Illustration of the three variational problems: *weak-constraint 4DVar* (w4DVar, top panel), *strong-constraint 4DVar* (mid panel) and *3DVar* (bottom panel). In the w4DVar the control variable is the entire trajectory within the window (from t_k to t_{k+2} in Fig. 2), $\mathbf{x}_{k+2:k}$, so the corrections (continuous red arrow) are computed and utilized at the observation times. The analysis trajectory (red line) is moved toward the observations. In the s4DVar, the control variable is the state at the beginning of the window, \mathbf{x}_k , and the corrections (dotted red arrow) are computed at observation times but then propagated back to t_k using the adjoint model (see Eq. (31)): once the analysis at the initial time is computed, it is then used as initial condition to run a forecast until t_{k+2} . In the 3DVar the corrections are computed and utilized at each observation times t_k sequentially, so that the analysis at t_k , \mathbf{x}_k^a , takes into account only the observations at t_k and is then used as initial condition for a forecast until the next observations at t_{k+1} and so on.

4.1 Stochastic ensemble Kalman filter

The EnKF as introduced by *Evensen (1994); Burgers et al. (1998); Evensen (2003)* is based on the use of an ensemble representation for error statistics. Thus, instead of storing a full covariance matrix, we can represent the same error statistics using an appropriate ensemble of model states. Given an error covariance matrix, an ensemble of finite size provides an approximation of the error covariance matrix, and, as the size N of the ensemble increases, the errors in the Monte Carlo sampling decrease proportionally to $1/\sqrt{N}$.

The derivations that follow will assume a linear observation operator for the sake of simplicity. However ensemble-based methods can straightforwardly incorporate a nonlinear observation operator (*Evensen, 2009b*).

4.1.1 Representation of error statistics

Given an ensemble of model realizations at a certain time, it is convenient to introduce the ensemble matrix

$$\mathbf{E} = [\mathbf{x}_1, \dots, \mathbf{x}_N] \in \mathbb{R}^{m \times N}, \quad (32)$$

which contains the N ensemble members in its columns.

The error covariance matrices \mathbf{P}_k^f and \mathbf{P}_k^a for the predicted and analyzed estimate in the KF are defined in terms of the true state in the KF Eq. (16–19). However, since the true state is not known, we will instead define the ensemble-anomaly covariance matrices around the ensemble mean. Given the ensemble mean

$$\bar{\mathbf{x}} = \frac{1}{N} \sum_{n=1}^N \mathbf{x}_n, \quad (33)$$

we define the ensemble-anomaly matrix as

$$\mathbf{X} = \frac{1}{\sqrt{N-1}} [\mathbf{x}_1 - \bar{\mathbf{x}}, \dots, \mathbf{x}_N - \bar{\mathbf{x}}] \in \mathbb{R}^{m \times N}. \quad (34)$$

We can now write the ensemble-based error covariance matrices for the forecast and analysis ensembles as

$$(\mathbf{P}^e)^f = (\mathbf{X}^f)(\mathbf{X}^f)^T, \quad (35)$$

$$(\mathbf{P}^e)^a = (\mathbf{X}^a)(\mathbf{X}^a)^T, \quad (36)$$

where the superscript “e” denotes that the quantities (e.g., matrices in Eq. (35) and (36)) are estimated based on the ensemble. Having defined the ensemble members, mean, and covariance matrix, for both the forecast and the analysis, we now further simplify the notation by omitting the superscript “f”, so that for instance we have $\mathbf{X}_k^f = \mathbf{X}_k$, and the convention applies for \mathbf{E} , \mathbf{P}^e , \mathbf{x} , and $\bar{\mathbf{x}}$.

Equations (35) and (36) embed an interpretation where the ensemble mean is the best estimate, and the spread of the ensemble around the mean is a natural definition of the error in the ensemble mean. We can interpret an ensemble of model states as a Monte Carlo representation of the pdf $p(\mathbf{x}_0)$ in Eq. (7).

4.1.2 Prediction of error statistics

Given a pdf $p(\mathbf{x}_0)$ at time t_0 , the joint pdf from time t_0 to t_k is given by Eq. (7), which involves a multiplication by the transition density defined in Eq. (4). It was shown in *Evensen* (1994) that if the pdf $p(\mathbf{x}_0)$ at time t_0 is represented by an ensemble of model states, then the multiplication with the transition density is equivalent to integrating each realization of \mathbf{x} according to the model equations as defined in Eq. (1). Thus, from a finite ensemble of model states, we can compute an ensemble approximation of the joint pdf $p(\mathbf{x}_{k:0})$ for the time interval from t_0 to t_k .

4.1.3 Analysis scheme

The novel idea of *Evensen* (1994) was to design an alternative update scheme that could work directly on the ensemble and where it was not necessary to compute the full covariances as defined by Eq. (35) and (36). *Evensen* (1994) showed that, by updating each individual ensemble member according to the standard KF Eq. (17) and (18), the updated ensemble will have the correct mean and covariance matrix for the update in agreement with Eq. (19) in the standard KF. *Burgers et al.* (1998) further proved that, in order for the EnKF analysis error covariance, $(\mathbf{P}^e)^a$, to be consistent with that of the KF, it is essential to treat the observations as random variables having a distribution with mean equal to the observed value and covariance equal to \mathbf{R} . Thus, given a vector of observations, $\mathbf{y} \in \mathbb{R}^d$, we define an ensemble of perturbed observations

$$\mathbf{y}_n = \mathbf{y} + \boldsymbol{\epsilon}_n, \quad 1 \leq n \leq N, \quad (37)$$

which we store in the observation matrix

$$\mathbf{Y}_o = [\mathbf{y}_1, \dots, \mathbf{y}_N] \in \mathbb{R}^{d \times N}, \quad (38)$$

which columns are the perturbed measurements $\mathbf{y}_n \in \mathbb{R}^d$. Then we define the corresponding matrix of the normalized anomaly ensemble of the observations $\mathbf{Y}'_o \in \mathbb{R}^{d \times N}$ as

$$\begin{aligned} \mathbf{Y}'_o &= \frac{1}{\sqrt{N-1}}[\mathbf{y}_1 - \mathbf{y}, \dots, \mathbf{y}_N - \mathbf{y}] \\ &= \frac{1}{\sqrt{N-1}}[\boldsymbol{\epsilon}_1, \dots, \boldsymbol{\epsilon}_N]. \end{aligned} \quad (39)$$

By subtracting any nonzero mean from the N random draws $\boldsymbol{\epsilon}_n$, we ensure that the simulated random measurement errors have zero ensemble-mean and thus the random perturbations do not introduce any bias in the update. Next we define the ensemble covariance matrix of the measurement errors as

$$\mathbf{R}^e = \mathbf{Y}'_o (\mathbf{Y}'_o)^T. \quad (40)$$

In the limit, $N \rightarrow \infty$, of infinite ensemble size, this matrix converges to the prescribed error covariance matrix \mathbf{R} used in the KF.

The analysis step in the EnKF consists of updates performed on each of the ensemble members, as given by

$$\mathbf{x}_n^a = \mathbf{x}_n + \mathbf{P}^e \mathbf{H}^T \left(\mathbf{H} \mathbf{P}^e \mathbf{H}^T + \mathbf{R}^e \right)^{-1} \left(\mathbf{y}_n - \mathbf{H} \mathbf{x}_n \right), \quad 1 \leq n \leq N. \quad (41)$$

With a finite ensemble size, the use of the ensemble covariances introduces an approximation of the true covariances. Furthermore, if the number of measurements is larger than the number of ensemble members, then the matrices $\mathbf{H} \mathbf{P}^e \mathbf{H}^T$ and \mathbf{R}^e are singular, and we must use a pseudo-inversion.

Equation (41) implies the update of the ensemble mean

$$\bar{\mathbf{x}}^a = \bar{\mathbf{x}} + \mathbf{P}^e \mathbf{H}^T \left(\mathbf{H} \mathbf{P}^e \mathbf{H}^T + \mathbf{R}^e \right)^{-1} \left(\bar{\mathbf{y}} - \mathbf{H} \bar{\mathbf{x}} \right), \quad (42)$$

where $\bar{\mathbf{y}} = \mathbf{y}$ since the measurement perturbations have ensemble mean equal to zero. Thus, the relation between the analyzed and predicted ensemble mean is identical to the relation between the analyzed and predicted state in the standard KF, apart from the use of \mathbf{P}^e and \mathbf{R}^e instead of \mathbf{P}^f and \mathbf{R} .

If the ensemble updates \mathbf{x}_n^a and $\bar{\mathbf{x}}^a$ from Eqs. (41) and (42) are inserted back into the analyzed covariance Eq. (36), it was shown by *Evensen* (1994) and *Burgers et al.* (1998) that

$$(\mathbf{P}^e)^a = (\mathbf{I} - \mathbf{K}^e \mathbf{H}) \mathbf{P}^e, \quad (43)$$

with \mathbf{K}^e being the ensemble-based Kalman gain matrix (cf. Sect. 3.1.1 and Eq. (17)). The result in Eq. (43) proves a consistency between the original KF and the EnKF (cf. Eq. (19)).

Note that the EnKF analysis scheme is approximate since it does not correctly account for non-Gaussian contributions in the predicted ensemble. In other words, the EnKF analysis scheme does not solve the Bayesian update equation for a non-Gaussian pdf. On the other hand, the EnKF analysis scheme is not just a re-sampling of a Gaussian posterior distribution. Only the updates defined by the right-hand side of Eq. (41), which we add to the prior non-Gaussian ensemble, are linear. Thus, the updated ensemble inherits many of the non-Gaussian properties from the forecast ensemble. In summary, we have a computationally efficient analysis scheme where we avoid re-sampling of the posterior.

4.1.4 Formulation in terms of the ensemble

Evensen (2003) reformulated the EnKF analysis scheme in terms of the ensemble without reference to the ensemble covariance matrix, which allows for an efficient numerical implementation and alternative interpretation of the method. We follow the slightly updated formulation from *Evensen* (2009b).

The analysis equation (41), expressed in terms of the ensemble matrices, is

$$\mathbf{E}^a = \mathbf{E} + \mathbf{X}\mathbf{X}^T\mathbf{H}^T \left(\mathbf{H}\mathbf{X}\mathbf{X}^T\mathbf{H}^T + \mathbf{Y}'_o (\mathbf{Y}'_o)^T \right)^{-1} (\mathbf{Y}_o - \mathbf{H}\mathbf{E}), \quad (44)$$

where we replace all the error covariance matrices by their ensemble representations. *Evensen* (2003) showed that the analysis equation (44) could be written as

$$\mathbf{E}^a = \mathbf{E}\mathbf{T}, \quad (45)$$

with the transformation matrix $\mathbf{T} \in \mathbb{R}^{N \times N}$ defined as

$$\mathbf{T} = \mathbf{I}_N + \mathbf{Y}^T \mathbf{C}^{-1} (\mathbf{Y}_o - \mathbf{H}\mathbf{E}). \quad (46)$$

Here we have defined the observed ensemble-anomaly matrix

$$\mathbf{Y} = \mathbf{H}\mathbf{X} \in \mathbb{R}^{d \times N}, \quad (47)$$

and the matrix

$$\mathbf{C} = \mathbf{Y}\mathbf{Y}^T + \mathbf{Y}'_o (\mathbf{Y}'_o)^T \in \mathbb{R}^{d \times d}, \quad (48)$$

while $\mathbf{I}_N \in \mathbb{R}^{N \times N}$ is the identity matrix. In practical implementations, it is common also to use the full-rank exact measurement error covariance matrix \mathbf{R} as an alternative to the product of measurement perturbations $\mathbf{R}^e = \mathbf{Y}'_o (\mathbf{Y}'_o)^T$, although that comes at an additional computational cost unless one assumes \mathbf{R} to be diagonal (see also *Hoteit et al.*, 2015).

The significant result from Eq. (45) is that the EnKF update ensemble becomes a combination of the forecast ensemble members, and is searched within the space spanned by the forecast ensemble. It is clear that the formulation in Eq. (45) is a stochastic scheme due to the use of randomly perturbed measurements. The use of perturbed measurements allows for a natural interpretation of the EnKF as a Monte Carlo algorithm while making it easy to understand and implement. An illustration is provided in Fig. 3, which shows the EnKF mean solution and estimated error standard deviation, as a function of the model grid and for three successive analysis times.

An efficient and stable numerical implementation of the analysis scheme is discussed in *Evensen* (2009b), including the case in which \mathbf{C} is singular or of low rank, e.g., due to the number of measurements being larger than the number of realizations or if measurements are linearly dependent on each other.

In practice, the ensemble size is critical since the computational cost scales linearly with the number of realizations. That is, each realization needs to be integrated forward in time. The cost associated with the ensemble integration motivates the use of an ensemble with the minimum number of realizations that can provide acceptable accuracy. We will see in Sect. 5.1 how the optimal ensemble size to achieve satisfactory performance is also related to the dynamical properties, notably the degree of instabilities, of the model.

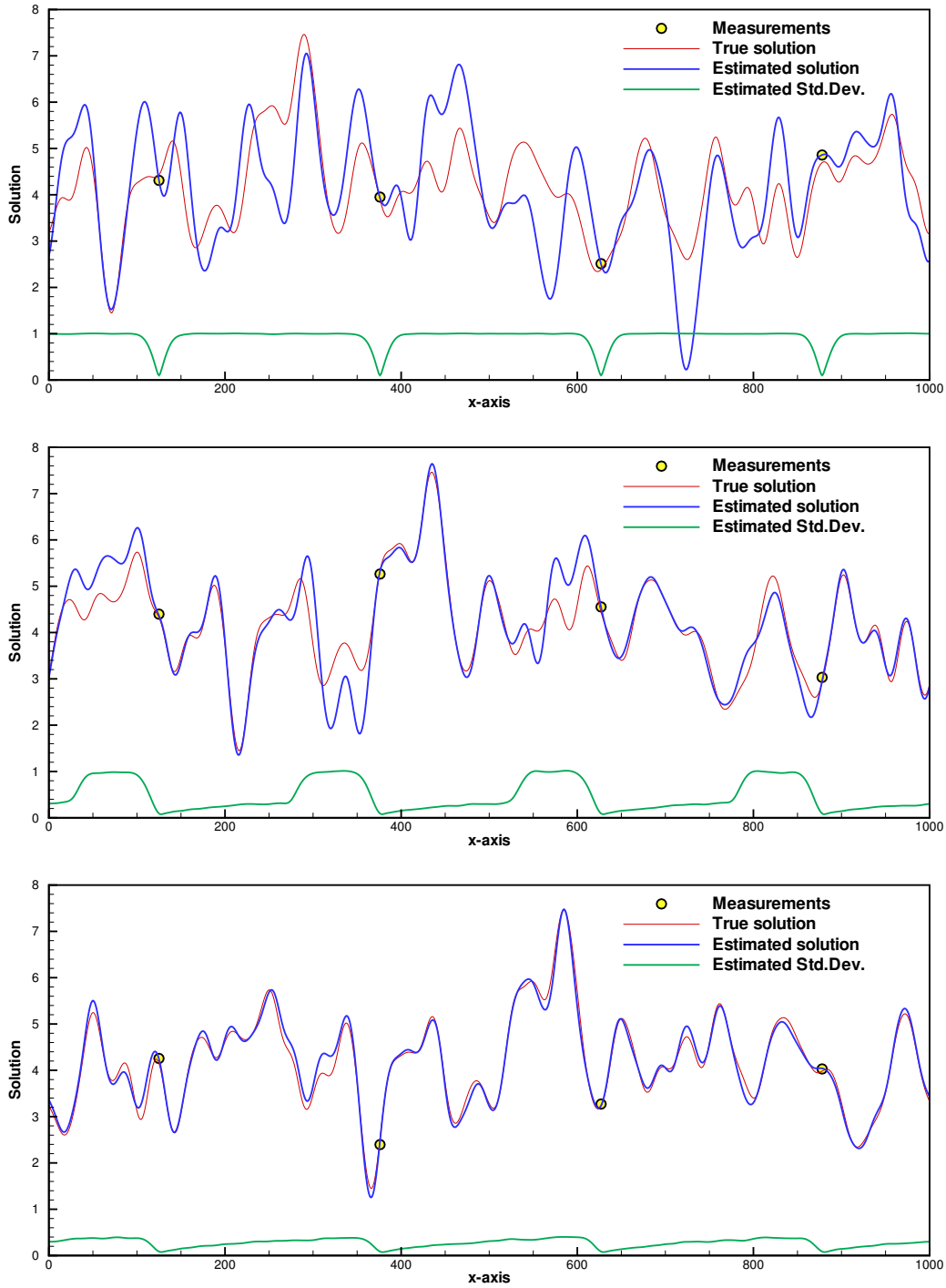


Figure 3: A linear advection equation on a periodic domain illustrates how the KF and/or EnKF estimates the state at three different times, namely, (top) $t = 5$, (middle) $t = 150$, and (bottom) $t = 300$. The plots show the reference solution, measurements, estimate, and standard deviation. The initial condition, observation and model error variance is 1.0, 0.01 and 0.0001 respectively, and the ensemble size is $N = 500$.

There are two significant sources of sampling errors in the EnKF, namely (i) the use of a finite ensemble of model realizations and (ii) the introduction of stochastic measurement perturbations (Evensen, 2004, 2009b). Besides, stochastic model errors influence the predicted error statistics, which are approximated by the ensemble. The stochastic perturbation of measurements used in EnKF can be avoided using a square-root implementation of the analysis scheme, which is the topic of the next Section.

4.2 Deterministic square-root schemes

The perturbation of measurements used in the EnKF standard analysis Eq. (44) is an additional source of sampling error. However, some papers have introduced methods alternative to the traditional EnKF, i.e., *square-root schemes*, which compute the analysis without perturbing the measurements and preserve precisely the posterior variance in the update. Examples include the Ensemble Transform Kalman Filter (ETKF) by Bishop *et al.* (2001); Whitaker and Hamill (2002), the Ensemble Adjustment Kalman Filter (EAKF) by Anderson (2001), and the Maximum Likelihood Ensemble Filter (MLEF) by Zupanski (2005).

4.2.1 Updating the mean

In a square-root scheme, the analyzed ensemble mean is computed from the standard KF analysis equation,

$$\bar{\mathbf{x}}^a = \bar{\mathbf{x}} + \mathbf{X}\mathbf{Y}^T\mathbf{C}^{-1}(\bar{\mathbf{y}} - \mathbf{H}\bar{\mathbf{x}}), \quad (49)$$

with the matrix \mathbf{C} defined in Eq. (48) but with $\mathbf{Y}'_o (\mathbf{Y}'_o)^T$ replaced by \mathbf{R} , i.e.,

$$\mathbf{C} = \mathbf{Y}\mathbf{Y}^T + \mathbf{R}. \quad (50)$$

The ensemble mean in the square-root formulation is thus computed without the use of perturbed observations.

4.2.2 Updating the ensemble perturbations

We derive the deterministic algorithm for updating the ensemble perturbations starting from the traditional analysis equation (19) for the covariance update in the KF but written in its ensemble-based representation in Eq. (43). We then insert the expression for the Kalman gain matrix to obtain

$$(\mathbf{P}^e)^a = \mathbf{P}^e - \mathbf{P}^e\mathbf{H}^T(\mathbf{H}\mathbf{P}^e\mathbf{H}^T + \mathbf{R})^{-1}\mathbf{H}\mathbf{P}^e. \quad (51)$$

Using the ensemble representation of the error covariance matrices, Eqs. (35) and (36), along with Eqs. (47) and (50), we can rewrite Eq. (51) as

$$(\mathbf{X}^a)(\mathbf{X}^a)^T = \mathbf{X}(\mathbf{I}_N - \mathbf{Y}^T\mathbf{C}^{-1}\mathbf{Y})\mathbf{X}^T = \mathbf{X}(\mathbf{I}_N + \mathbf{Y}^T\mathbf{R}^{-1}\mathbf{Y})^{-1}\mathbf{X}^T. \quad (52)$$

We obtain the second expression by making use of the Sherman-Morrison-Woodbury formula (see Golub and van Loan, 2013, their Sect. 2.1.4).

We can derive the square-root filters by factorizing the symmetric expression in Eq. (52). The simplest, but not a very efficient approach, is to compute the eigenvalue factorization of the matrix $\mathbf{I}_N - \mathbf{Y}^T \mathbf{C}^{-1} \mathbf{Y} = \mathbf{Z} \mathbf{\Lambda} \mathbf{Z}^T$, and then the update as

$$\mathbf{X}^a = \mathbf{X} \mathbf{Z} \sqrt{\mathbf{\Lambda}}, \quad (53)$$

which defines a symmetric factorization of Eq. (52). However, this update equation does not preserve the mean (it is biased). It was shown (Wang *et al.*, 2004; Sakov and Oke, 2008b; Livings *et al.*, 2008) that the *symmetric square root* preserves the zero mean in the updated perturbations. Accordingly, the update in Eq. (53) must be replaced by

$$\mathbf{X}^a = \mathbf{X} \mathbf{Z} \sqrt{\mathbf{\Lambda}} \mathbf{Z}^T, \quad (54)$$

which is another symmetric factorization of Eq. (52) (see, e.g., Hunt *et al.*, 2007). Consequently, if the predicted ensemble members have a non-Gaussian distribution, then the updated distribution retains the shape, although the variance is reduced (see the review in Raanes *et al.*, 2015, their Sect. 4). The importance of the symmetry in the square-root methods was first recognized by Ott *et al.* (2004) and then adopted by Hunt *et al.* (2007).

The operational use of the square-root schemes requires more focus on numerical stability and efficiency. Here we assumed that \mathbf{C}^{-1} exists, which is not always the case and particularly not so when the number of measurements is larger than the ensemble size nor when \mathbf{R} is not full rank. For a more elaborate derivation of numerically stable schemes, we refer to the initial publications by Anderson (2001); Whitaker and Hamill (2002); Bishop *et al.* (2001) and the reviews by Tippett *et al.* (2003) and Nerger *et al.* (2012). Evensen (2004, 2009a,b) derived a numerically efficient square-root filter that computes the inversion in the subspace spanned by the measured ensemble perturbations \mathbf{Y} . The scheme works equally well with a non-diagonal measurement error-covariance matrix and in the case when \mathbf{C} is of low rank.

Equation (52) is also known as *right transform* as it applies to the right-hand side of the anomalies, in the N -dimensional ensemble space (Asch *et al.*, 2016). Similarly, *left transform* expressions also exist, that apply to the m -dimensional state-space (see Asch *et al.*, 2016, their Sect. 6.4, for an extensive treatment of the subject).

A randomization of the analysis update can also be used to generate updated perturbations that better resemble a Gaussian distribution, see Evensen (2004). Thus, we write the symmetric square root solution Eq. (54) as

$$\mathbf{X}^a = \mathbf{X} \mathbf{Z} \sqrt{\mathbf{\Lambda}} \mathbf{Z}^T \mathbf{\Phi}^T, \quad (55)$$

where $\mathbf{\Phi}$ is a mean-preserving random orthogonal matrix, which can be computed using the algorithms from Pham (2001) or Sakov and Oke (2008a). Note again that the random rotation in the square-root filter, contrary to the measurement perturbation used in EnKF, eliminates all previous non-Gaussian structures from the forecast ensemble. Efficient means to account for stochastic model noise within square-root filters are discussed in Raanes *et al.* (2015).

4.3 Ensemble Kalman Smoother (EnKS)

The EnKS is a straightforward extension of the EnKF in which we use the output of the latter as a prior in the EnKS. Like the EnKF uses the ensemble covariances in space to

spread the information from the measurements, the EnKS uses the ensemble covariances to spread the information in both space and time (also backward). We need to reintroduce here the time index.

Assume we have measurements available at discrete times t_k , $k = 1, \dots, K$. We compute the EnKF solution recursively by assimilating the observations when they are available and then propagate the ensemble until the next measurements (cf. Sec. 4.1). The members of the EnKF can be stored at any time instant when we desire a smoother update.

The analysis update at a time t_k (which does not have to be an observation time) from measurements available at a later time t_j , $1 \leq k < j \leq K$, reads

$$\mathbf{E}_k^a = \mathbf{E}_k + \mathbf{X}_k \mathbf{Y}_j^T \mathbf{C}_j^{-1} (\mathbf{Y}_{o,j} - \mathbf{Y}_j) \quad 1 \leq k < j \leq K, \quad (56)$$

where \mathbf{Y}_j from Eq. (47), and \mathbf{C}_j from Eq. (48) are evaluated using the ensemble and measurements at t_j . From the right-hand side of Eq. (56) we recognize the product $\mathbf{X}_k \mathbf{Y}_j^T$ as the covariance between the predicted measurements at t_j and the model state at $t_k > t_j$.

The update at the time t_k uses precisely the same combination of ensemble members as was defined by \mathbf{T}_k in Eq. (46) for the EnKF analysis at the time t_k . Thus, we can compactly write the EnKS analysis as

$$\mathbf{E}_k^{a, \text{EnKS}} = \mathbf{E}_k^{a, \text{EnKF}} \prod_{j=\hat{k}}^K \mathbf{T}_j, \quad (57)$$

where \hat{k} corresponds to the first data time after t_k , and t_K is the last measurement time. It is then a simple exercise to compute the EnKS analysis as soon as the EnKF solution has been found. The computation requires only the storage of the transform matrices $\mathbf{T}_k \in \mathbb{R}^{N \times N}$, for $k = 1, \dots, K$, and the EnKF ensemble matrices for the times when we want to compute the EnKS analysis. Note that the EnKF ensemble matrices are large, but it is possible to store only specific variables at selected locations where the EnKS solution is needed. The equivalence between the formulation of the EnKS given above with the Rauch-Tung-Striebel smoother (cf. Sect. 3.1.2) even in the nonlinear, non-Gaussian, case is discussed in *Raanes* (2016).

An example of implementation of an ensemble smoother is represented by the "no cost smoother" (aka as *Running in place*, RIP) of *Kalnay and Yang* (2010) that provides explicitly the weights of the ensemble members at the end of the assimilation window, and then applies those same weights throughout the window. The RIP/no-cost smoother has been used to accelerate the spin up of the Local Ensemble Transform Kalman Filter (LETKF, *Hunt et al.*, 2007), to increase its accuracy and to allow longer time windows. The no cost smoother designed originally designed for the LETKF has been adapted to the Ensemble Square-Root Filter (EnSFR) by *Wang et al.* (2013) and is used operationally to accelerate the spinup of the EnSRF forecast of tornadoes and severe storms at the *Center for Analysis and Prediction of Storms* of the University of Oklahoma (www.caps.ou.edu). A recent study that analyses and compares ensemble smoothers for solving inverse problems can be found in *Evensen* (2018).

4.4 Making it work: Localization and Inflation

The reduction of dimensionality obtained through the Monte Carlo treatment of the KF that yielded the EnKF comes at a price. Indeed, with a limited number, N , of anomalies, the sample covariance matrix is severely rank-deficient. It would be surprising if such sample error covariance matrix could be a good substitute for the, possibly, full-rank true one.

Assume that the true error covariance matrix is \mathbf{B} . Further define \mathbf{P}^e as the sample covariance matrix meant to approximate \mathbf{B} and obtained from N samples, (as in Eq. (35)) of the normal distribution with covariance matrix \mathbf{B} . Then it can be shown that for two distinct entry indices i and j corresponding to distinct locations:

$$\mathbb{E}([\mathbf{P}^e - \mathbf{B}]_{ij}^2) = \frac{1}{N-1} ([\mathbf{B}]_{ij}^2 + [\mathbf{B}]_{ii}[\mathbf{B}]_{jj}), \quad (58)$$

with \mathbb{E} indicating the expectation (average) operator. In most spatial geophysical systems, $[\mathbf{B}]_{ij}$ is expected to vanish fast (often exponentially) with the distance between sites corresponding to i and j . By contrast, the $[\mathbf{B}]_{ii}$ are the variances and remain finite, so that

$$\mathbb{E}([\mathbf{P}^e - \mathbf{B}]_{ij}^2) \underset{|i-j| \rightarrow \infty}{\sim} \frac{1}{N-1} [\mathbf{B}]_{ii}[\mathbf{B}]_{jj}, \quad (59)$$

meaning that both expressions coincide when the sites separation is sufficiently large. Consequently, the right-hand-side arithmetically goes to 0 with the ensemble size N . Unfortunately, since $[\mathbf{B}]_{ij}$ is expected to vanish exponentially with the distance, we would have liked instead $\mathbb{E}([\mathbf{P}^e - \mathbf{B}]_{ij}^2)$ to also vanish exponentially with the distance. Hence, with N finite (and usually $N \ll m$) the sample covariance $[\mathbf{P}^e]_{ij}$ is potentially a bad approximation of the vanishing true covariance, especially for large distances $|i - j|$. This approximation generates spurious correlations between distant parts of the system, as a manifestation of the rank-deficiency of the sample error covariance matrix.

The errors committed with such an approximation are usually referred to as *sampling errors*. When taking \mathbf{P}^e as the forecast/background error covariance matrix, the accumulation of such errors over the EnKF data assimilation cycles can be detrimental to the stability of the EnKF. Without counter-measures, the divergence of the EnKF in high-dimensional geophysical systems is almost systematic. Fortunately, more or less *ad hoc* fixes meant to address the issue are known: *localization* and *inflation*. They are rather complementary and both of them are often required.

4.4.1 Localization

Localization fundamentally relies on the exponential decrease of the correlations with the distance in geophysical systems. Under this condition, one can assume that the interdependence of distant parts of a physical system is negligible. Hence, EnKF analyses could be made local (*Houtekamer and Mitchell, 2001; Hamill et al., 2001; Haugen and Evensen, 2002; Evensen, 2003; Ott et al., 2004*). Localization comes in two flavors that we describe in the following.

Covariance localization The first approach, named *covariance localization* (CL), seeks to regularize the sample error covariance matrix, with the goal to mitigate the rank-deficiency of \mathbf{P}^e and the appearance of spurious error correlations. A mathematical means to achieve this objective is to compute the Schur (or Hadamard) product of \mathbf{P}^e with a well chosen smooth correlation function $\boldsymbol{\rho}$. We assume $\boldsymbol{\rho}$ to have exponentially vanishing correlations for distant parts of the system and to be representative of such dampening of real geophysical systems. The Schur product of $\boldsymbol{\rho}$ and \mathbf{P}^e is defined by

$$[\boldsymbol{\rho} \circ \mathbf{P}^e]_{ij} = [\boldsymbol{\rho}]_{ij} [\mathbf{P}^e]_{ij}, \quad (60)$$

i.e., a point-wise matrix multiplication. The Schur product theorem (*Horn and Johnson*, 2012) ensures that this product is positive semi-definite, and hence still represents a proper covariance matrix. For sufficiently regular $\boldsymbol{\rho}$, $\boldsymbol{\rho} \circ \mathbf{P}^e$ turns out to be full-rank (hence positive definite). Moreover, the spurious correlations should be exponentially dampened as is obvious from Eq. (60).

To illustrate the CL principle, we consider a multivariate ($m = 100$) Gaussian distribution, with mean $\mathbf{x}^b = 0$. Its covariance matrix \mathbf{B} is given by $[\mathbf{B}]_{ij} = e^{-|i-j|/L}$, where $i, j = 1, \dots, m$ and $L = 10$ is the correlation length. An ensemble of $N = 20$ members $\{\mathbf{x}_n\}_{n=1, \dots, N}$ is drawn from this distribution from which we can compute the unbiased sample covariance matrix $\mathbf{P}^e = \frac{1}{N-1} \sum_{n=1}^N (\mathbf{x}_n - \bar{\mathbf{x}})(\mathbf{x}_n - \bar{\mathbf{x}})^T$, with the mean $\bar{\mathbf{x}} = \frac{1}{N} \sum_{n=1}^N \mathbf{x}_n$, which are approximations of \mathbf{B} and \mathbf{x}^b , respectively. The true and the sample covariance matrices are shown in Fig. 4. The spurious correlations are obvious in panel Fig. 4b, where \mathbf{P}^e is displayed. Let us define $\boldsymbol{\rho}$ through the Gaspari-Cohn (GC) function (*Gaspari and Cohn*, 1999),

$$G(r) = \begin{cases} \text{if } 0 \leq r < 1: & 1 - \frac{5}{3}r^2 + \frac{5}{8}r^3 + \frac{1}{2}r^4 - \frac{1}{4}r^5, \\ \text{if } 1 \leq r < 2: & 4 - 5r + \frac{5}{3}r^2 + \frac{5}{8}r^3 - \frac{1}{2}r^4 + \frac{1}{12}r^5 - \frac{2}{3r}, \\ \text{if } r \geq 2: & 0, \end{cases}$$

which is a fifth-order piece-wise rational function. The cutoff function is defined by $r > 0 \mapsto G(r/c)$ where c is a length scale which is called the localization radius. It mimics a Gaussian distribution but vanishes beyond $r \geq 2c$, which is numerically efficient (in mathematical terms, G is compactly supported). The Gaspari-Cohn cut-off function is shown in Fig. 4c. Hence, choosing $c = L$, we define $[\boldsymbol{\rho}]_{ij} = G(|i - j|/L)$. The regularized covariance matrix, $\boldsymbol{\rho} \circ \mathbf{P}^e$ is shown in Fig. 4d. As expected, the spurious correlations are tapered.

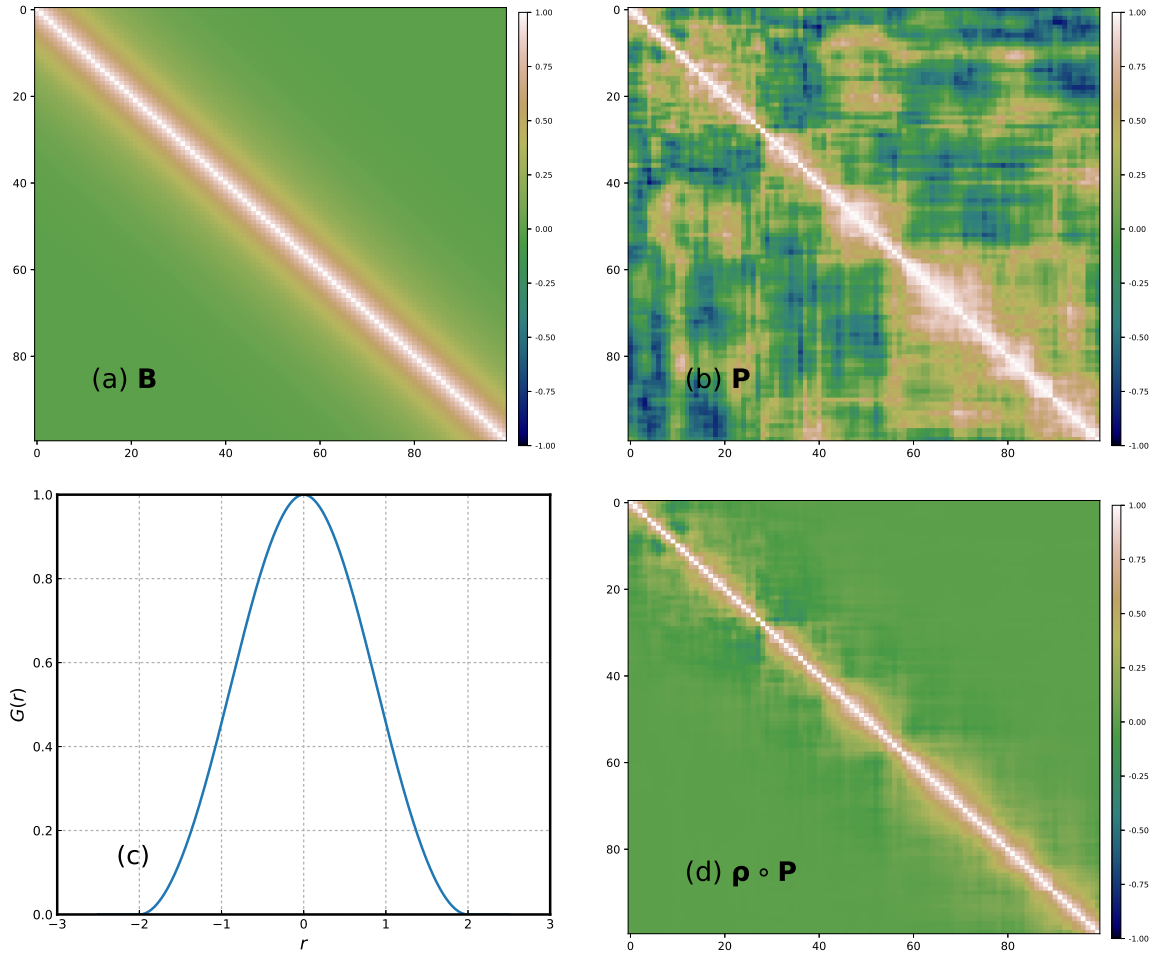


Figure 4: Panel a: True covariance matrix. Panel b: Sample covariance matrix. Panel c: Gaspari-Cohn correlation matrix used for covariance localization. Panel d: Regularized covariance matrix obtained from a Schur product.

One of the drawbacks of covariance localization is that it still uses huge regularized covariance matrices (a priori of size $m \times m$). Possible remedies are (i) avoiding the explicit computation and storage of $\rho \circ \mathbf{P}^e$, (ii) combining CL with domain localization (see below), (iii) or transferring the Schur product from state space to observation space for sparse in situ observations. Solution (iii) can for instance be used to compute the Kalman gain (cf. Eq. (17)) in a more efficient manner (Houtekamer and Mitchell, 2001; Ott et al., 2004; Greybush et al., 2011).

In a multivariate setting, variable localization was also proposed and tested by Kang et al. (2011), where cross-correlations between carbon dioxide concentration and meteorological variables other than wind variables are set to zero.

Domain localization An alternative to covariance localization is *domain localization* (DL). In DL, one performs the global EnKF analysis as a collection of independent local EnKF analyses, each of them assimilating a subset of the observations. Typically, one seeks

to update a state at location/grid-cell x . The EnKF analysis is locally carried out by assimilating observations contained in a disk of radius L centered on x . The number of observations in this local domain should be small enough so that the ensemble can accommodate the information content of these observations, *i.e.*, that \mathbf{P}^e is locally full rank. This is equivalent to setting the observation error covariance matrix \mathbf{R} to \mathbf{R}_x where all the entries associated to sites outside the disk are large or infinite, which rules out these outer observations. In DL, both the state vector and anomalies are locally updated. A global analysis is then recovered from this collection of local analyses. Because the subdomains overlap, one assumes that the transition between analyses is smooth enough so that the global updated ensemble remains physically balanced. A way to improve on these transitions, is to obtain \mathbf{R}_x by tapering (Schur product) \mathbf{R}^{-1} with a regularizing cut-off function, typically the GC, that decreases with the distance from x .

Because the number of local EnKF analyses to be carried out scales linearly with the size of the system m , the method may seem numerically doomed. However, on the one hand, all of the analyses can be performed in parallel and, on the other hand, their numerical complexity is significantly reduced as it is driven by the ensemble size and the number of local, not global, observations. The numerical feasibility of the approach has been demonstrated by *Ott et al.* (2004); *Hunt et al.* (2007).

Sakov and Bertino (2011) have shown that CL and DL are not mathematically equivalent in general but that they can become so in regimes where the analysis is dominated by the prior. Another important point to mention is the physical imbalance that may result from the gluing of local analyses and from the true long-distance correlations that have necessarily been discarded in the localization process (*Keptert*, 2009; *Greybush et al.*, 2011). For chaotic systems, it has been suggested (see Sect. 5.1) that the ensemble size below which localization is mandatory is equal to the dimension of the unstable and neutral subspace of the dynamics.

4.4.2 Inflation

Using localization addresses the rank-deficiency issue and gets rid of spurious correlations. Unfortunately, sampling errors are not entirely removed in the process. Residual errors are still often sufficient to make the EnKF diverge for long-term runs (see *Grudzien et al.*, 2018a, for a discussion on the need for inflation in reduced order filter). One very simple *ad hoc* means to account for this residual sampling error is to inflate the error covariance matrix by a multiplicative factor $\lambda^2 \geq 1$, $\mathbf{P}^e \rightarrow \lambda^2 \mathbf{P}^e$, which can also be implemented by inflating the anomalies $\mathbf{x}_n \rightarrow \bar{\mathbf{x}} + \lambda (\mathbf{x}_n - \bar{\mathbf{x}})$ (*Pham et al.*, 1998; *Anderson and Anderson*, 1999). Note that inflation is not only used to cure sampling errors (*Bocquet*, 2011; *Whitaker and Hamill*, 2012; *Bocquet et al.*, 2015b), but is also often used to counteract model error impact.

Inflation can also come in an additive, clearly non-equivalent, form: $\mathbf{x}_n \rightarrow \mathbf{x}_n + \boldsymbol{\epsilon}_n$ with $\mathbb{E} [\boldsymbol{\epsilon}_n (\boldsymbol{\epsilon}_n)^T] = \mathbf{Q}$.

As a drawback, inflation often needs to be tuned in order to obtain satisfactory performance of the EnKF, which is numerically costly. Hence, adaptive schemes have been developed to make the task more automatic (*Wang and Bishop*, 2003; *Anderson*, 2007; *Li et al.*, 2009; *Zheng*, 2009; *Brankart et al.*, 2010; *Bocquet*, 2011; *Miyoshi*, 2011; *Bocquet and Sakov*, 2012; *Liang et al.*, 2012; *Ying and Zhang*, 2015; *Bocquet et al.*, 2015b). For instance, a variant of the deterministic EnKF, the DEnKF from *Sakov and Oke* (2008b), was introduced as

an approximation of the EnKF with an implicit inflation.

4.5 Ensemble Variational methods

4DVar and the EnKF are now both used in operational meteorological centers as well as in academic studies (see, e.g., *Buehner et al.*, 2013; *Bauer et al.*, 2015). In spite of apparent similar performances in the context of synoptic scale meteorology, they are not equivalent. 4DVar allows for a nonlinear estimation of the maximum a posteriori of the underlying pdf using nonlinear optimization techniques, while the EnKF only performs a linear update (with the notable exception of the MLEF; *Zupanski*, 2005). The EnKF propagates the statistics of the errors, hence estimating the *errors of the day*, whereas the traditional 4DVar only relies on time-independent statistics of the errors. An important weakness of 4DVar, of technical nature, is the derivation of the adjoint models, which remains a computer sciences challenge, whereas the EnKF estimates the adjoint of the observation operator via the ensemble. These and other pros and cons of both approaches have been discussed by *Lorenc* (2003); *Kalnay et al.* (2007); *Yang et al.* (2009); *Bocquet and Sakov* (2013).

Hence, it is tempting to combine both approaches, for theoretical reasons (nonlinear analysis, errors of the day) and technical reasons (no adjoint models). The resulting algorithms are called *ensemble variational* methods (EnVar). They have been reviewed in chapter 7 of *Asch et al.* (2016) on theoretical grounds and with a focus on operational implementation by *Bannister* (2017), although the iterative ensemble Kalman smoother (see Sect. 4.5.4) is lacking in this latter review. A classification of these methods and the terminology has been proposed by *Lorenc* (2013).

Here, we distinguish between (i) the hybrid methods, (ii) the methods based on an ensemble of variational data assimilation (EDA), (iii) the so-called 4DEnVar, and (iv) full nonlinear four-dimensional EnVar methods, of which the IEnKS is a deterministic exemplar.

4.5.1 Hybrid methods

Hybrid can refer to any combination of a variational method and of an EnKF method. Yet, it quite often specifically refers to the hybridizing of a static error covariance matrix with a dynamical one sampled from an ensemble. The idea was first introduced by *Hamill and Snyder* (2000). The objective was to use the static covariance of a 3DVar and perform a variational analysis to be used for the analysis step of an EnKF. The effective covariance matrix used for the prior is:

$$\mathbf{B} = \alpha \mathbf{C} + (1 - \alpha) \mathbf{X}^f (\mathbf{X}^f)^T, \quad (61)$$

where \mathbf{C} is the static error covariance matrix (as used in 3DVar or optimal interpolation; *Kalnay*, 2002), \mathbf{X}^f is the matrix of the forecast ensemble anomalies, and $\alpha \in [0, 1]$ is a scalar that weights the static and dynamical contributions. The updated ensemble can be obtained within the framework of a stochastic EnKF (cf. Sect. 4.1) using several stochastically perturbed variational problems. On the other hand, if the mean is estimated in a deterministic EnKF framework (cf. Sect. 4.2), the anomalies update has to rely on an approximation due to the necessary reduction of the rank from the hybrid covariance to the new dynamical covariances. There are ways to improve this update, such as using a left-transform update

(Sakov and Bertino, 2011; Bocquet et al., 2015b), or Lanczos vectors (Auligné et al., 2016). Note that, as with the EnKF, it may be necessary to enforce localization of the sample covariances, which would be based on $\mathbf{B} = \alpha\mathbf{C} + (1 - \alpha)\boldsymbol{\rho} \circ [\mathbf{X}^f (\mathbf{X}^f)^T]$, using CL.

4.5.2 Ensemble of data assimilation

Methods known as *ensemble of data assimilations* (EDA) stem from meteorological prediction centers that operate a 4DVar, and in particular Météo-France and the European Centre for Medium-Range Weather Forecasts (ECMWF). The idea is to introduce dynamical errors that are absent in the traditional 4DVar. In order to build on the existing 4DVar systems, one considers an ensemble of N 4D-Var analyses. Each analysis, indexed by i , uses a different first guess \mathbf{x}_0^i , and observations perturbed with $\boldsymbol{\epsilon}_k^i \sim \mathcal{N}(\mathbf{0}, \mathbf{R}_k)$ to maintain statistical consistency. Hence, each analysis i carries out the minimization of (cf. Eq. (30))

$$\mathcal{J}_i^{\text{EDA}}(\mathbf{x}_0) = \frac{1}{2} \sum_{k=0}^K \|\mathbf{y}_k + \boldsymbol{\epsilon}_k^i - \mathcal{H}_k \circ \mathcal{M}_{k:0}(\mathbf{x}_0)\|_{\mathbf{R}_k}^2 + \frac{1}{2} \|\mathbf{x}_0 - \mathbf{x}_0^i\|_{\mathbf{B}^{-1}}^2. \quad (62)$$

The background covariance \mathbf{B} is typically a hybrid one as in Eq. (61) because it still uses the static covariances of the traditional 4DVar and incorporates the sampled covariances from the dynamical perturbations. The procedure yields an updated ensemble, from which it is possible to assess a dynamical part of the error covariance matrix. This is rather close to the idea of the hybrid EnKF-3DVar, but with a 4DVar scheme. The method has been implemented at Météo-France (Raynaud et al., 2009, 2011; Berre et al., 2015) and at the ECMWF (Bonavita et al., 2011, 2012). Like for the hybrid method, it may be necessary to localize the sampled part of the hybrid covariances, using for instance covariance localization (CL). In this context, it may be convenient to enforce CL via techniques such as the $\boldsymbol{\alpha}$ control variable trick (Lorenc, 2003; Buehner, 2005; Wang et al., 2007) – which is mathematically equivalent to CL – or using wavelet truncations (Berre et al., 2015).

4.5.3 4DEnVar

NWP centers which have been using 4DVar were also the ones to offer the most reliable forecasts. But the future of 4DVar as an operational tool is uncertain because of its poor scalability and of the cost of the adjoint model maintenance, although weak-constraint 4DVar has scalable implementations (Fisher and Gürol, 2017). The 4DEnVar method emerged in these centers as a way to circumvent the development of the adjoint of the dynamical model. The key idea is based on the ability of the EnKF to estimate the sensitivities of the observation to the state variables using the full observation model in place of the tangent linear one and of its adjoint in the computation of the Kalman gain.

Liu et al. (2008) essentially proposed to generalize this idea to the computation of the sensitivities of the observations within a data assimilation window (DAW) to the variables of the initial state. Hence, these sensitivities are associated to the composition $\mathcal{H} \circ \mathcal{M}$ defined over the DAW, rather than to observation operator \mathcal{H} as in the EnKF. As a consequence, the sensitivities with respect to the degrees of freedom of each anomaly can be approximated

with

$$\varepsilon^{-1} \mathcal{H}_k \circ \mathcal{M}_{k:0} (\bar{\mathbf{x}}_0 \mathbf{1}^\top + \varepsilon \mathbf{X}^f) \left(\mathbf{I}_m - \frac{\mathbf{1} \mathbf{1}^\top}{m} \right). \quad (63)$$

This formula first builds an ensemble of mean $\bar{\mathbf{x}}_0$ with anomalies \mathbf{X}^f scaled by ε ; then propagates this ensemble through $\mathcal{H}_k \circ \mathcal{M}_{k:0}$; rescales the output ensemble by ε^{-1} ; and finally generates an ensemble of centered perturbations. With $0 < \varepsilon \ll 1$, these perturbations can be seen as generated by the tangent linear of $\mathcal{H}_k \circ \mathcal{M}_{k:0}$ (using finite-differences), whereas with $\varepsilon = \sqrt{m-1}$ these perturbations account for the nonlinearity of $\mathcal{H}_k \circ \mathcal{M}_{k:0}$ as in the EnKF. The set of these sensitivity vectors form a basis for the analysis, an idea quite close to that of the reduced-rank 4DVar put forward in oceanography by *Robert et al.* (2005).

In 4DEnVar, the perturbations are usually generated stochastically, for instance resorting to a stochastic EnKF (*Liu et al.*, 2009; *Buehner et al.*, 2010a). Hence, in addition to avoiding the need for a model adjoint, flow-dependent error estimation is introduced. Given that 4DEnVar has been developed in NWP centers using 4DVar, which relies on building a sophisticated static background error covariance matrix, the background is usually of hybrid nature. If the perturbations are generated by a deterministic scheme, then the method could be seen as similar to the 4D-LETKF (*Hunt et al.*, 2007), where the linear analysis is carried out in a basis made of trajectories (the perturbations) over the DAW obtained from the previous deterministic analysis.

Because of the introduction of the limited set of perturbations, localization is again needed to mitigate the limited rank of the sample error covariance matrix. However, in a 4D ensemble context and in contrast with the synchronous EnKF, localization must be applied to covariances that are not only distant in space but also possibly in time within the DAW. Unfortunately localization and the dynamics do not commute in general (*Fairbairn et al.*, 2014; *Bocquet and Sakov*, 2014), yielding inconsistencies in the implementation of a static localization within the flow. A solution is to implement a *covariant* localization that changes in time with the dynamical flow (*Bocquet*, 2016; *Desroziers et al.*, 2016). For instance, if localization is enforced via domain localization (DL), one would pull-back the influential observations within the DAW using a surrogate, hyperbolic-like, model for the full evolution model and check in which local domains their antecedent would fall in (*Bocquet*, 2016). This type of solutions has also been put forward in a sensitivity analysis context (*Kalnay et al.*, 2012). Note, however, that this issue is circumvented if one possesses the adjoint of the dynamical model.

Many variants of the 4DEnVar are possible depending on the way the perturbations are generated, or if the adjoint model is available or not (*Buehner et al.*, 2010a,b; *Zhang and Zhang*, 2012; *Clayton et al.*, 2013; *Poterjoy and Zhang*, 2015; *Bocquet*, 2016). Full 4DEnVar operational systems are now implemented or are in the course of being so (*Buehner et al.*, 2013; *Gustafsson et al.*, 2014; *Desroziers et al.*, 2014; *Lorenc et al.*, 2015; *Kleist and Ide*, 2015; *Buehner et al.*, 2015a; *Bowler et al.*, 2017).

4.5.4 The iterative ensemble Kalman smoother

Most of these EnVar methods, with the noticeable exception of the more firmly grounded EDA ones (Sect. 4.5.2), have been designed heuristically blending theoretical insights and operational constraints. This led to many variants of the schemes, even when this is not

mathematically justified. Most of these ideas stemmed from the variational DA community, with the remarkable exception of the Running in Place (RIP), an EnKF with an outer loop (*Kalnay and Yang, 2010*). By contrast, the iterative ensemble Kalman smoother (IEnKS), is a four-dimensional EnVar method that is derived from Bayes’ rule and where all approximations are understood at a theoretical level. It comes from ensemble-based DA and, specifically, extends the iterative ensemble Kalman filter (*Sakov et al., 2012b*) to a full DAW as in 4DVar. The name *smoother* reminds us that the method smooths trajectories like 4DVar. However, it can equally be used for smoothing and filtering. The name also pays an homage to the iterative Kalman smoother of *Bell (1994)* which corresponds to the non-ensemble precursor of the method. Basically, the IEnKS can be seen as an EnKF, for which each analysis corresponds to a nonlinear 4DVar analysis but within the reduced subspace defined by the ensemble. Hence, the associated cost function is of the form

$$\mathcal{J}(\mathbf{w}) = \frac{1}{2} \|\mathbf{w}\|^2 + \sum_{k=L-S+1}^L \frac{1}{2} \|\mathbf{y}_k - \mathcal{H}_k \circ \mathcal{M}_{k:0}(\bar{\mathbf{x}}_0 + \mathbf{X}_0 \mathbf{w})\|_{\mathbf{R}_k}^2, \quad (64)$$

where L is the length of the DAW, and S is the length of the forecast in between cycles (in units of $t_{k+1} - t_k$). Because the IEnKS catches the best of 4DVar (nonlinear analysis) and EnKF (flow-dependence of the error statistics), both parameters could be critical.

The minimization of \mathcal{J} can be performed in the ensemble subspace using any nonlinear optimization method, such as Gauss-Newton (cf. Appendix B), Levenberg-Marquardt or trust-region methods (*Bocquet and Sakov, 2012; Mandel et al., 2016; Nino Ruiz and Sandu, 2016*). The required sensitivities (derivative of the observation with respect to the initial state) are computed using an ensemble forecast within the DAW, as in 4DEnVar. Hence, it does not require the tangent and adjoint models but emulates them, similarly to 4DEnVar. The anomalies update is computed using an approximate Hessian of this cost function, using again these sensitivities. The ensemble forecast step is similar to the EnKF but over S time units.

The parameters L and S are constrained to satisfy $1 \leq S \leq L + 1$ if all observations are to be assimilated. In the case $S = L + 1$, with a single iteration of the minimization and further less important restrictions, the IEnKS identifies with the 4D-ETKF (*Hunt et al., 2004*). In the case $S = 1$ and $L = 0$, it coincides with the MLEF (*Zupanski, 2005*), which can be seen as a precursor to the IEnKF and IEnKS. The IEnKS represents an ideal tool to study deterministic four-dimensional EnVar methods and test new strategies.

In chaotic systems, the IEnKS outperforms any reasonably scalable DA method in terms of accuracy. By construction, it outperforms the EnKF, the EnKS and 4DVar for smoothing but also filtering. This has been checked numerically on several low-order models (Lorenz models; *Lorenz, 1963; Lorenz and Emanuel, 1998; Lorenz, 2005*), 2D turbulence and quasi-geostrophic models (*Bocquet and Sakov, 2014; Bocquet, 2016*). Figure 5 compares the performance of the IEnKS with that of optimally tuned 4DVar, EnKF and EnKS for filtering and smoothing on the 40-variable Lorenz-95 model (*Lorenz, 1996*). As for the other EnVar methods, localization needs to be used in high-dimensional systems. It can be implemented using covariant DL or CL (*Bocquet, 2016*).

To conclude this brief review of the EnVar set of techniques, the simplified table 1 summarizes some key properties of a selection of the methods we described.

Table 1: Comparison of EnVar data assimilation techniques. This table answers the following questions: (i) Is the analysis based on a linear or nonlinear scheme? (ii) Is the adjoint of the evolution model required? (iii) Is the adjoint of the observation operator required? (iv) Is the background flow-dependent? (v) Are the updated perturbations stochastic or deterministic? (vi) Are the updated perturbations fully consistent with the analysis, i.e., are they a faithful representation of the analysis uncertainty? (vii) Is localization of the ensemble analysis required? (viii) Is a static background used? To some extent, all algorithms can accommodate a static background; the answer tells whether the published algorithm has a static background. Blank answers correspond to irrelevant questions.

algorithm	<i>analysis type</i>	<i>evol. model adjoint required?</i>	<i>obs. operator adjoint required?</i>	<i>background flow-dependence?</i>	<i>sto. or det. perturbations?</i>	<i>consistent perturbations?</i>	<i>localization required?</i>	<i>static background</i>
EnKF	linear	no	yes	both	yes	yes	no ⁴	
3D-Var	nonlinear	yes	no				yes	
4D-Var	nonlinear	yes	yes	no			yes	
EDA with 4D-Var	nonlinear	yes ¹	yes ¹	yes	sto.	yes	part.	yes ³
4DEnVar	linear	no	no	yes	sto.	no ²	yes	yes ³
IEnKS	nonlinear	no	no	yes	det.	yes	yes	no ⁴
MLEF	nonlinear	no	no	yes	det.	yes	yes	no ⁴
4D-ETKF	linear	no	no	yes	det.	yes	yes	no ⁴

¹ The adjoint models could be avoided considering an EDA of 4DEnVar.

² It depends on the implementation of 4DEnVar; the perturbation are often generated by a concomitant EnKF.

³ With an hybridization of the covariances.

⁴ But possible with an hybridization of the covariances.

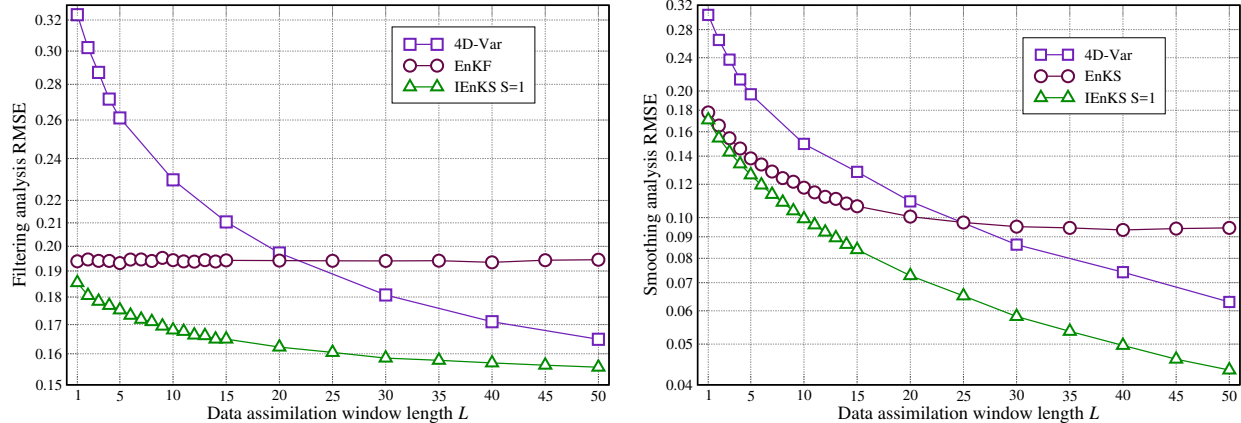


Figure 5: Average root mean square error of several DA methods computed from synthetic experiments with the Lorenz-95 model. The left panel shows the filtering analysis root mean square error of optimally tuned EnKF, 4DVar, IEnKS assimilation experiments, as a function of the length of the DAW. The right panel shows the smoothing analysis root mean square error of optimally tuned EnKS, 4DVar and IEnKS as a function of the length of their data assimilation window. The optimal RMSE is chosen within the window for 4DVar and it is taken at the beginning of the window for the IEnKS. The EnKF, EnKS and IEnKS use an ensemble of $N = 20$, which avoids the need for localization but requires inflation. The length of the DAW is $L \times \Delta t$, where $\Delta t = 0.05$.

5 Special topics

This section discusses four selected topics related to the application of DA to the geosciences. The issues for the DA and the countermeasures connected to the chaotic nature of the atmosphere and ocean are the content of Sect. 5.1. Section 5.2 discusses the techniques that allow to deal with non-Gaussian variables in the framework of DA methods originally devised to tackle with Gaussian quantities. The DA for chemical species is the subject of Sect. 5.3: the topic is of great relevance (pollutant dispersion, accidental nuclear release etc.) and has received much attention in recent years. Finally Sect. 5.4 describes one example of operational DA, the TOPAZ system for ocean prediction.

5.1 Dealing with chaotic dynamics

Many natural systems, including atmosphere and ocean, are examples of chaotic dissipative dynamics (*Dijkstra*, 2013). Among the characteristic features of this class of system, the one having the largest impact on prediction, is the extreme sensitivity to initial conditions (*Lorenz*, 1963). Infinitesimal errors are bound to grow exponentially in the short time (and later saturate), and the rate and directions of such a growth are themselves highly state-dependent (*Trevisan and Palatella*, 2011b). Forecasters have been long aware of this flow-dependent behavior of the forecast uncertainty and “prediction of predictability” (i.e., the prediction of the uncertainty) has become an important issue in NWP (*Kalnay and Dalcher*, 1987; *Lorenz*, 1996). The difficulties inherent to the chaotic nature of the climate on the one

hand, and the social pressure to deliver reliable forecast with associated prediction of the uncertainty, on the other, have motivated a huge bulk of research on predictability (see the review by *Vannitsem*, 2017, and references therein). In forecasting practice, the problem of predicting uncertainty, thus moving from a "single-realization deterministic forecast" to a "multi-realizations probabilistic forecast", has been tackled by ensemble prediction schemes (*Leutbecher and Palmer*, 2008).

Dealing with such a flow-dependent error growth is obviously also a challenge for DA: one must in fact be able to properly track and incorporate this dependency in the DA description of the state estimation error. A situation that is further complicated by the large size of the geophysical models ($m = \mathcal{O}(10^9)$). Nevertheless, the dissipative character (due to friction) of the dynamics, induces an effective dimensional reduction, in the sense that the error dynamics, in deterministic systems, is often confined to a subspace of much smaller dimension, $n_0 \ll m$. This subspace, referred to as the *unstable-neutral subspace*, is defined as the vector space generated by the backward Lyapunov vectors with non-negative Lyapunov exponents, i.e., the space of the small perturbations that are not growing exponentially under the action of the backward dynamics (see *Legras and Vautard*, 1996, for a topical review). The full phase-space can thus be seen as split in a (usually much smaller) unstable-neutral subspace and a stable one (*Kuptsov and Parlitz*, 2012). For instance, *Carrassi et al.* (2007) have shown how a quasi-geostrophic atmospheric model of $O(10^5)$ degrees of freedom possesses an unstable-neutral subspace of dimension as small as $n_0 = 24$.

The existence of this underlying splitting of the phase-space has enormous impact on the skill of DA with chaotic models. In EnKF-like methods, *Carrassi et al.* (2009); *Ng et al.* (2011); *Bocquet and Sakov* (2014) have studied the relation between the properties of the model dynamics and the performance of DA, and revealed how the knowledge about the former can be used in the design of the square-root EnKF and EnKS: for purely deterministic models, the minimum ensemble size required to achieve good performance must be at least as big as the number, n_0 , of non-negative Lyapunov exponents (*Carrassi et al.*, 2009; *Bocquet and Sakov*, 2014). Along similar lines, but for variational DA, *Pires et al.* (1996) showed that the relative projection of the state estimation error on the stable and unstable subspaces depend on the length of the DAW (see Sect. 4.5.3): for long DAW the stable components are all dampened and the error is essentially confined on the unstable subspace.

These results have recently been corroborated by a proper mathematical understanding of the behavior of the KF and KS (cf. Sect. 3.1.1 and 3.1.2) for linear unstable systems in the absence of model noise. It has been proven analytically that the span of the error covariance matrices of the KF and KS tends asymptotically to the unstable-neutral subspace (*Gurumoorthy et al.*, 2017), independently from the initial condition (*Bocquet et al.*, 2017), and that the rate of such convergence is faster for the KS (*Bocquet and Carrassi*, 2017). Remarkably, *Bocquet and Carrassi* (2017) have shown that, even in the case of a four-dimensional EnVar method (the IEnKS, cf. Sect. 4.5.4) applied to a noiseless nonlinear system, the full alignment of the ensemble anomaly subspace with the unstable-neutral subspace is accompanied by the maximum reduction of the state estimation error. Figure 6 illustrates this mechanism for the EnKF using the L95 model (*Lorenz and Emanuel*, 1998).

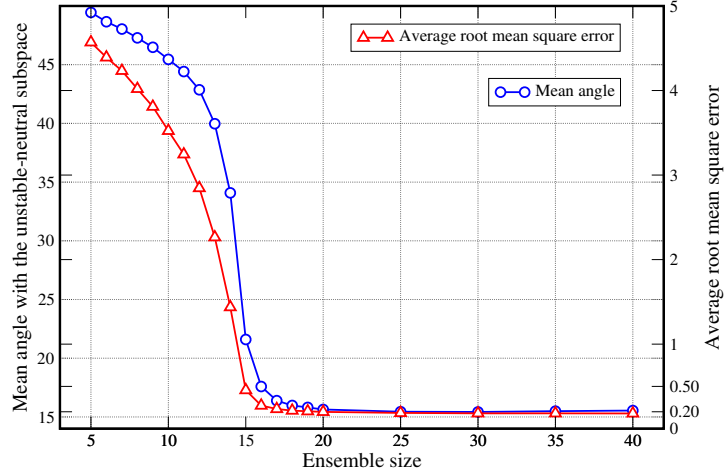


Figure 6: Time- and ensemble- averaged angle (in degree) between an anomaly from the EnKF ensemble and the unstable-neutral subspace as a function of the ensemble size N (left y-axis) and corresponding time-averaged root mean square error of the EnKF (right y-axis). The numerical experiments are performed on the L95 model with $m = 40$ variables (Lorenz and Emanuel, 1998) and the DA setup is $\mathbf{H} = \mathbf{I}_d$, $\mathbf{R} = \mathbf{I}_d$, observational frequency $\Delta t = 0.05$ and error variance $\sigma = 1$.

These results indicate that, in deterministic chaotic systems, the unstable-neutral subspace fully describes (in an average, asymptotic, sense) the uncertainty in the state estimate. This fact is at the basis of a class of DA algorithms known as *assimilation in the unstable subspace* (AUS) pioneered by Anna Trevisan and collaborators (Trevisan and Uboldi, 2004; Palatella et al., 2013a), in which the unstable-neutral subspace (or a suitable numerical approximation of it) is explicitly used in the DA scheme to parametrize the description (both temporally and spatially) of the uncertainty in the state estimate. Given that usually $n_0 \ll m$, AUS represents an interesting alternative to operate DA efficiently on high-dimensional system (large m) by monitoring only n_0 unstable-neutral directions. Applications to large atmospheric (Carrassi et al., 2008b) and oceanic models (Uboldi and Trevisan, 2006) have confirmed its capabilities. The AUS paradigm has been successfully incorporated in both the EKF (Trevisan and Palatella, 2011a) and the 4DVar (Trevisan et al., 2010) and its extension to cope with the deviations from the linear error dynamics and perfect model assumptions on which it relies, has been studied recently by Palatella and Trevisan (2015) and Grudzien et al. (2018b) respectively.

5.2 Dealing with non Gaussian variables

There are cases for which the linear analysis is sub-optimal. These arise when either the state variables, observations or model parameters are not Gaussian distributed. We consider first the case in which the distribution of at least one variable is not Gaussian, for example it exhibits a clear skewness or kurtosis, but the pdf remains continuous.

Ignoring the non-Gaussian nature of a variable will normally make the least-squares estimator sub-optimal (cf. Appendix A): either by systematic biases, by under-estimating

the correlation length scales (*Brankart et al.*, 2012), or more visibly by returning nonphysical values (for example negative concentrations of tracer variables). In a DA framework, the state variables (called the "control variable" in this context) need not be exactly defined as in the forward model: nonlinear transformations are allowed and will change the outcomes of the minimization problem (*Bertino et al.*, 2003).

Transformations of the variables have been practiced extensively in the geostatistical literature under the term *Gaussian anamorphosis* (also known as "normal-score transform"): a nonlinear function is applied to the cumulative pdf in order to make it Gaussian (*Chilès and Delfiner*, 2012). In DA, the Gaussian anamorphosis function can either be applied to the state variables $\tilde{\mathbf{x}} = \phi(\mathbf{x})$ or to the observations $\tilde{\mathbf{y}} = \varphi(\mathbf{y})$ or the model parameters or to all of them at the same time. The prerequisite is that the transformed variables $\tilde{\mathbf{x}}$ and $\tilde{\mathbf{y}}$ should be "more Gaussian" and better suited to a linear analysis update than the original ones. The anamorphosis function must be strictly increasing so that backward transformations from the Gaussian values to the "natural" pdf can be given by ϕ^{-1} and φ^{-1} . Since $\mathbf{E}(\phi^{-1}(\tilde{\mathbf{x}})) \neq \phi^{-1}(\mathbf{E}(\tilde{\mathbf{x}}))$, Monte Carlo techniques are often employed to obtain unbiased statistics. This makes the anamorphosis particularly convenient to apply in conjunction with ensemble techniques (*Bertino et al.*, 2003).

In practice, the stochastic models (13) and (14) are valid for the transformed $\tilde{\mathbf{x}}$ and $\tilde{\mathbf{y}}$, so that the EnKF and EnKS equations can be re-used with $\tilde{\mathbf{x}}$ and $\tilde{\mathbf{y}}$ in replacement of \mathbf{x} and \mathbf{y} . Equations (32) and (38) become

$$\mathbf{E}^{f/a} = (\tilde{\mathbf{x}}_{[1]}^{f/a}, \tilde{\mathbf{x}}_{[2]}^{f/a}, \dots, \tilde{\mathbf{x}}_{[N]}^{f/a}) \in \mathbb{R}^{m \times N}, \quad (65)$$

$$\mathbf{Y}^o = (\tilde{\mathbf{y}}_{[1]}, \tilde{\mathbf{y}}_{[2]}, \dots, \tilde{\mathbf{y}}_{[N]}) \in \mathbb{R}^{d \times N}. \quad (66)$$

The observations are preferably transformed before perturbing the observations, since the perturbations are more conveniently applied in the Gaussian space (even when using a deterministic version of the EnKF, the \mathbf{R} matrix characterizes more adequately Gaussian observation errors). After the analysis, the inverse transformation ϕ^{-1} is applied to each member of the analyzed ensemble $\mathbf{x}_i^a = \phi^{-1}(\tilde{\mathbf{x}}_i^a)$ before the next propagation step. If one variable is both an observation and a model state variable, then the same transformation should be applied to both so that the observation operator \mathbf{H} keeps a simple form (*Amezcuca and Van Leeuwen*, 2014). Alternatively, using independent transformations can be a practical way to correct for biases (*Lien et al.*, 2016a,b).

There are infinitely many of strictly increasing functions: choosing a good anamorphosis function is therefore an open question. When a set of observations is available or a free model run, it is possible to approximate the anamorphosis function based on the histogram of available data, using for example a piece-wise linear fit (*Simon and Bertino*, 2009). Adaptive types of anamorphosis functions have also then been explored (*Simon and Bertino*, 2012), in which the anamorphosis function is fitted to the values present in the ensemble forecast at the assimilation time. These have proven advantageous in twin experiments (*Simon and Bertino*, 2012; *Li et al.*, 2012), but their stability remains to be tested in real cases, where the true density is unknown and the results can become excessively sensitive to the choice of the tails of the distribution (*Simon and Bertino*, 2012). In practical cases, simple analytical functions are sometimes preferred like the exponential, gamma or logit functions, which can be supported theoretically knowing the nature of the problem at hand (*Simon et al.*, 2015;

Gharamti et al., 2017a).

One immediate benefit of the Gaussian anamorphosis is the ability to impose positivity constraints in the EnKF which is useful for example in ecosystem models (*Simon and Bertino*, 2009). The use of an anamorphosis function has been demonstrated with the EnKF in hydrological models (*Li et al.*, 2012; *Zhou et al.*, 2012), NWP models (*Lien et al.*, 2013, 2016a,b; *Kotsuki et al.*, 2017), in joint parameter-state estimation in ocean ecosystem models (*Simon and Bertino*, 2012; *Gharamti et al.*, 2017a,b), for the evaluation of covariance length scales in various ocean modeling applications (*Brankart et al.*, 2012) and with moderate success in a coupled ice-ocean model (*Barth et al.*, 2015). It has been as well introduced in a snow model with an ensemble smoother (*Aalstad et al.*, 2018).

One limitation of the Gaussian anamorphosis as described above is that it does not consider the multi-Gaussian case: only the marginal distributions of the variables are transformed independently from each other. Although this does not guarantee that the joint distributions become multi-Gaussian, the experience still shows that the multi-Gaussian properties are generally improved after transforming the marginals (*Wackernagel*, 2003; *Amezcuca and Van Leeuwen*, 2014). The anamorphosis framework can however be further extended by the use of copulas (*Schölzel and Friederichs*, 2008).

A more serious limitation in many practical cases is that the Gaussian anamorphosis does not lend itself to discontinuous pdf. These are better addressed in the framework of truncated Gaussians: a threshold is defined on the Gaussian distribution, and all values exceeding the threshold are reset to its precise value, generating an atom of probability distribution. Truncated Gaussians were first applied in optimal interpolation, by introducing a Lagrange parameter in the minimization (*Thacker*, 2007), only in the cases when assimilated values exceeded the threshold, leading to a two-step interpolation process (detect and constrain). The issue of sampling a multivariate truncated Gaussian in the framework of an EnKF was then explored applying a Gibbs sampler (*Lauvernet et al.*, 2009), under the simplifying assumption of small truncations. Another approach is the use of Quadratic Programming (*Janjić et al.*, 2014), more general in the sense that it can accommodate nonlinear constraints. An alternative and inexpensive approach is to "moderate" the strength of DA in order to avoid reaching the discontinuities of the distribution. This has been proposed for assimilation into an ocean model in isopycnic coordinates, for which the values of layer thickness must be positive (*Wang et al.*, 2016). Combinations of Gaussian anamorphosis and truncations have been successfully tested by (*Lien et al.*, 2013, 2016b) by setting the Gaussian value of the threshold to the median of the out-of-range Gaussian pdf (zero precipitations in their case).

The above examples are extending the Gaussian framework introduced in Sect. 3.1 and extend as well the use of the EnKF and EnKS methods. The Gaussian anamorphosis can be included at almost no additional costs, but the costs of the truncated Gaussian methods are potentially a limitation in realistic cases (a 500% increase of the analysis step is reported with the Gibbs sampler; *Lauvernet et al.*, 2009). Still, these methods benefit from the advantages of the Gaussian framework in high dimensions and represent attractive alternatives to more general Bayesian methods that suffer from the curse of dimensionality (see Sect. 6.1).

5.3 Data assimilation for chemicals

There is a huge literature on the use of DA for chemical constituents of the atmosphere. There are several quasi exhaustive reviews about the advances in this field, such as *Carmichael et al.* (2008); *Zhang et al.* (2012); *Bocquet et al.* (2015a). We here briefly explain what chemical DA is, what the motivations for using DA in this field are, and, finally, which methods are used.

The specific set of chemical reactions that prevails in the atmosphere depends on the species but also on the considered spatial and temporal scales. For instance, one typically distinguishes between global atmospheric chemistry and air quality. The former is concerned with species transported and reacting over long distances and within the whole column of the atmosphere, whereas the latter is more concerned with the complex chemistry within the boundary layer (about 1 km from the ground) at regional scales. As an example of species, greenhouse gases are global pollutants with long life spans considered in the first type of study, even though regional studies of their transport are also of interest. Another example is ozone, which, in the lower troposphere, is studied and forecast in air quality as a harmful pollutant whereas, in the stratospheric layer, or when transported in between continents, is the focus of global studies. Besides the global and regional scales, DA is also nowadays used for chemical studies at urban scale.

Chemistry and transport models are fundamentally multivariate with many species to be accounted for (about a hundred for gaseous species, hundreds when considering aerosols). This also significantly increases the dimensionality of the models compared to atmospheric and ocean models independently. That is why the choice of the control variables (cf. Sect. 3.2) is critical in the feasibility of chemical DA.

One also distinguishes between online and offline models. Offline models (also called CTM for *chemical transport model*) only consider emissions and uptakes, chemistry, loss processes and transport driven by meteorological fields that are supposed to be provided. Online models (also called CCMM for *coupled chemistry meteorology model*) couple meteorology with chemistry and transport. CCMMs are therefore much more costly but allow for two-way coupling between meteorology and chemistry. Most of chemical DA studies are performed offline.

One major difference with atmospheric and ocean models is that the dynamics of CTMs are mostly stable. In practice two model trajectories with distinct initial conditions will coalesce, quite differently from chaotic geofluid dynamics (*Haussaire and Bocquet, 2016; Vannitsem, 2017*). Hence, the initial conditions are rarely the most important control variables in chemical DA. Quite often, the species emissions are the most influential input parameters, if not control variables. More generally, model error is more influential for chemical DA than for geofluids DA. One consequence of this dynamical stability is that air quality forecast are rarely useful beyond 48 hours, even with the help of DA. Another consequence is the importance of all other parameters and input of these models and their uncertainty and hence of model error.

For these many reasons, but also to serve the enforcement of regulations, chemical DA is used for (i) chemical forecast, nowcasting and possibly reanalysis, (ii) inverse modeling of species emission and uptake, and (iii) parameter estimation, such as the boundary conditions, constants of the physical and chemical parametrizations.

The methods used in chemical DA are largely inspired by meteorological DA. Optimal interpolation (*Kalnay, 2002*) has been largely used from the very beginning. Since the beginning of the 2000s, 4DVar has also been used, which can advantageously be adopted for the simultaneous estimation of inputs and model parameters (*Elbern et al., 2007*). Methodological advances in chemical DA also had some influence, with the early development of reduced Kalman and ensemble methods in the 90s' (*Hanea et al., 2007; Constantinescu et al., 2007a,b; Wu et al., 2008*). Four-dimensional ensemble variational methods have also been tested in this field (*Haussaire and Bocquet, 2016; Emili et al., 2016*).

5.4 An example of operational data assimilation and reanalysis: the TOPAZ integrated ice-ocean system

The concept of operational oceanography has gradually arisen in the 1990's under the joint pressure from its users in the navy, the authorities in charge of emergency response (oil spills, search and rescue operations) and the offshore oil and gas industry. Ocean monitoring was becoming possible from remote sensing and increasing in-situ observations to fulfill the needs of both the operational and the climate research communities and the development of ocean models was accelerated. The conditions for ocean DA were then ripe and a community was formed around the international Global Ocean Data Assimilation Experiment (GODAE, now GODAE-OceanView, www.godae-oceanview.org). The EnKF, originally introduced in a QG model, was then extended to a multi-layer isopycnal model (Miami Isopycnal Coordinate Model, MICOM) and then its offspring in generalized vertical coordinates HYCOM (HYbrid Coordinate Ocean model *Bleck, 2002*). The EnKF (*Evensen, 2009b*), SEEK filter (*Pham et al., 1998*) as well as the EnKS (*Evensen, 2009b*) were applied successfully to this model to assimilate ocean remote sensing observations from satellite altimeters and sea surface temperatures in a North Atlantic configuration called DIADEM (*Brusdal et al., 2003*). In parallel, the assimilation of sea ice concentrations in a coupled ice-ocean model was demonstrated (*Lisæter et al., 2003*) as well as the assimilation of remotely sensed ocean color in a coupled physical-ecosystem model (*Natvik and Evensen, 2003*), both with the EnKF. These experiments were all using similar settings of the EnKF: same number of members, same sources and statistics of model errors and were therefore encouraging signs that a single integrated system could monitor the ocean, the sea ice and the ocean ecosystem consistently, with the uncertainties of the three components represented by the same ensemble. Such an integrated system for the North Atlantic and the Arctic Oceans was then built and named TOPAZ, including downscaling capabilities to forecast the coastal zones at higher resolution. An illustration showing a typical output from the TOPAZ system is given in Figure 7.

The TOPAZ system has been set in near real-time forecasting mode in January 2003, initially using the perturbed-observations EnKF (*Evensen, 2003*) (cf. Sect. 4.1), and then moved on to the DEnKF (*Sakov and Oke, 2008b*) (cf. Sect. 4.4.2) in January 2010.

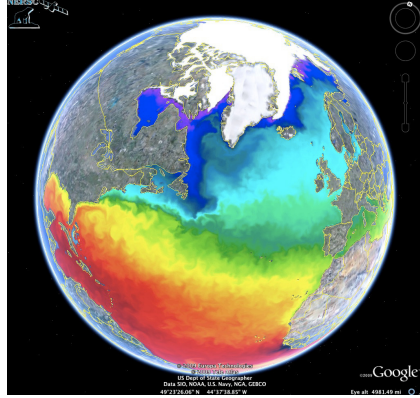


Figure 7: Example of sea surface temperature (in color) and sea ice concentration (in white) real-time analysis by the TOPAZ system on the 28th November 2009.

The HYCOM ocean model uses isopycnic coordinates in the deep stratified ocean, the following state vector is then the closest possible to the original model prognostic variables¹:

- 3-dimensional variables, defined for each hybrid vertical layer: layer thickness, u- and v-components of the current velocity, temperature and salinity
- 2-dimensional variables: barotropic pressure, u- and v-components of the barotropic velocity, sea ice characteristics (ice concentration, ice thickness, snow depth).
- Static parameters, 2-dimensional bias fields for mean SLA and mean SST.
- If the ecosystem module is coupled:
 - 3-dimensional nutrients concentrations (nitrate, phosphate and silicates in North Atlantic and Arctic regions)
 - 3-dimensional phytoplankton (diatoms and flagellates) and zooplankton species (meso- and microzooplankton).
 - 3-dimensional detritus variable, as well as oxygen and biogenic silicate.
 - 2-dimensional maps of model parameters (different plankton loss rates).

Recalling that the EnKF analysis is conserving linear equilibrium, the above definition of the state vector in generalized (isopycnic) vertical coordinates is advantageous for preserving the geostrophic balance, which relates linearly the velocity vector averaged over one ocean layer to the gradient of the layer thickness (*Evensen, 2003*). The use of isopycnic coordinates in the state vector has also the advantage of reducing diapycnal mixing during the linear update in Eq. (45) or (55) since the analyzed temperature and salinity tracers are the results of combinations of forecast temperature and salinity from different members but at the same density. The application of the EnKF in the MICOM isopycnic model has also proven to make the assimilation of surface temperature properties more efficient in the context of a climate reanalysis (*Counillon et al., 2016*).

¹A prognostic variable is necessary for carrying out the model calculations.

On the downside, not all the above state variables are Gaussian distributed, so according to the discussion in Sect. 5.2, biological variables are log-transformed (*Simon et al.*, 2015). However variables with discontinuous distributions (sea ice variables, ocean layer thickness) are simply post-processed (*Sakov et al.*, 2012a), and TOPAZ is thus exposed to assimilation biases. Yet, the experience has not revealed strong biases.

TOPAZ has used a local analysis (cf. Sect. 6.1.5) ever since its inception, a global analysis having proven utterly incapable of controlling millions of state variables with only 100 members. The inflation is implicit in the formulation of the DEnKF (*Sakov and Oke*, 2008b) and additionally in the form of a factor applied to the \mathbf{R} matrix, used only in the update of the anomalies (*Sakov et al.*, 2012a). The use of a constant multiplicative inflation (cf. Sect. 4.4.2) of the forecast anomalies has proven problematic in the case of the Arctic due to the inhomogeneous observation coverage, even with a small inflation of 1%.

The present TOPAZ4 physical system with its horizontal resolution of about 12 km and 28 hybrid vertical layers counts about 80 million unknowns. The data assimilated in a weekly cycle count the along-track sea level anomalies from satellite altimeters, the interpolated sea surface temperatures and sea ice concentrations from satellites as well, the Lagrangian sea ice drift from continuous maximum cross-correlation of scatterometer data, and the temperature and salinity profiles from various in-situ platforms, including the Argo autonomous buoys and Ice-Tethered Profilers. This amounts to about 400 thousands observations after super-obing. The altimeter and the sea ice drift data are assimilated asynchronously (*Sakov et al.*, 2010), accounting for time-delayed covariances.

The computer costs of the TOPAZ4 system are mainly related to the propagation of the 100 members (1200 CPU hours per week, but embarrassingly parallel as the 100 members are submitted independently and the HYCOM model is itself parallel, running on 144 CPUs), the analysis step takes 20 hours only, and is also parallelized because all local analysis updates are independent from each other.

The TOPAZ4 reanalysis (*Xie et al.*, 2017) has been conducted over 24 years (covering the altimeter era 1991-2015) and thus 1250 assimilation steps. During this time, the Arctic observing system has undergone large changes with for example the International Polar Year (IPY, 2007-2009) during which several Ice-Tethered Profilers have been deployed in the Central Arctic, measuring temperature and salinity profiles in areas previously unobserved. The large increase of observations during the IPY is visible in the time series of Fig. 8 and does, as expected, reduce the bias and root mean square error, but the latter increases again during the 6 months that follow the end of the IPY. This implies that the special observation efforts done on the occasion of the IPY should be the rule rather than the exception for the sake of monitoring the Arctic Ocean. The diagnostics shown for other variables indicate that the reanalysis is stable all through the 1250 assimilation cycles (*Xie et al.*, 2017) and how much each observation type contributes to the minimization.

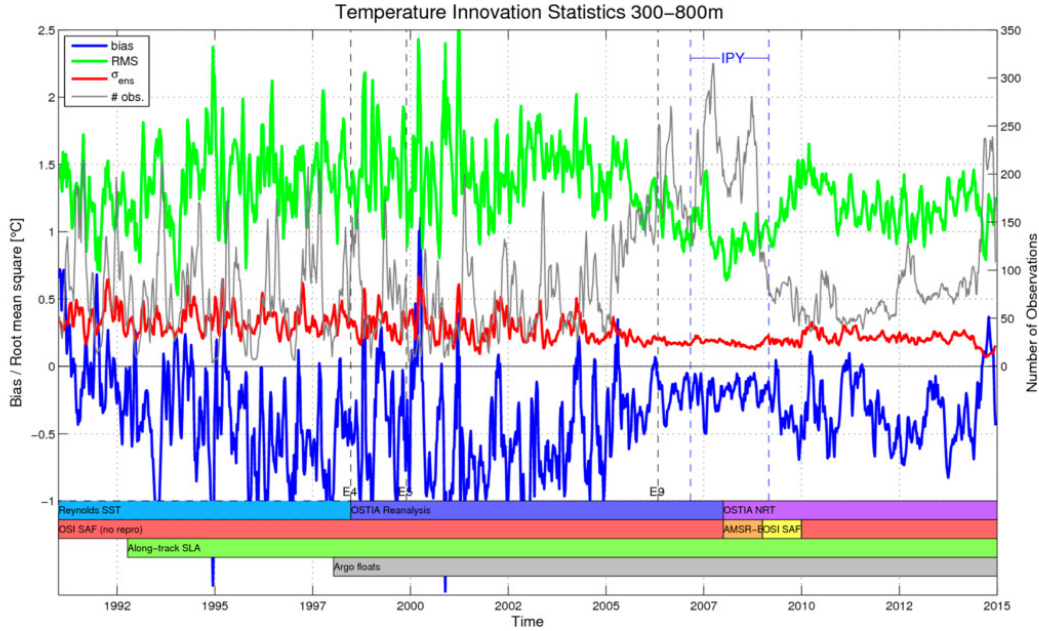


Figure 8: Time series of data assimilation diagnostics across the 24-years reanalysis for all temperature profiles in the depths 300 m to 800 m in the whole Arctic. The blue line is the average of all innovations, the green line is the related standard deviation (Root Mean Square Error), the red line is the ensemble spread of \mathbf{S} and the grey line is the number of observations. Vertical dashed lines indicate changes applied to the assimilation system during the reanalysis. The bars in the bottom indicate the succession of input data products assimilated, from top to bottom: SST, sea ice concentrations, SLA and Argo data.

The coupled physical-biological reanalysis with assimilation of surface chlorophyll estimates from remotely-sensed ocean color data is a much more difficult endeavor than the physical reanalysis, both on technical and scientific levels (*Simon et al.*, 2015).

6 Where we are and where we go: a look at the perspectives

Data assimilation is nowadays a key ingredient of the atmospheric and oceanic prediction machinery and substantial computational power and economical resources are allocated to its maintenance and updates. What are the challenges DA is facing at this present time? Which solutions are being proposed to cope with the requirements of present days climate research? Figure 9 illustrates this quest by displaying the required DA approach as a function of the model resolution (x-axis) and of the prediction horizon (y-axis).

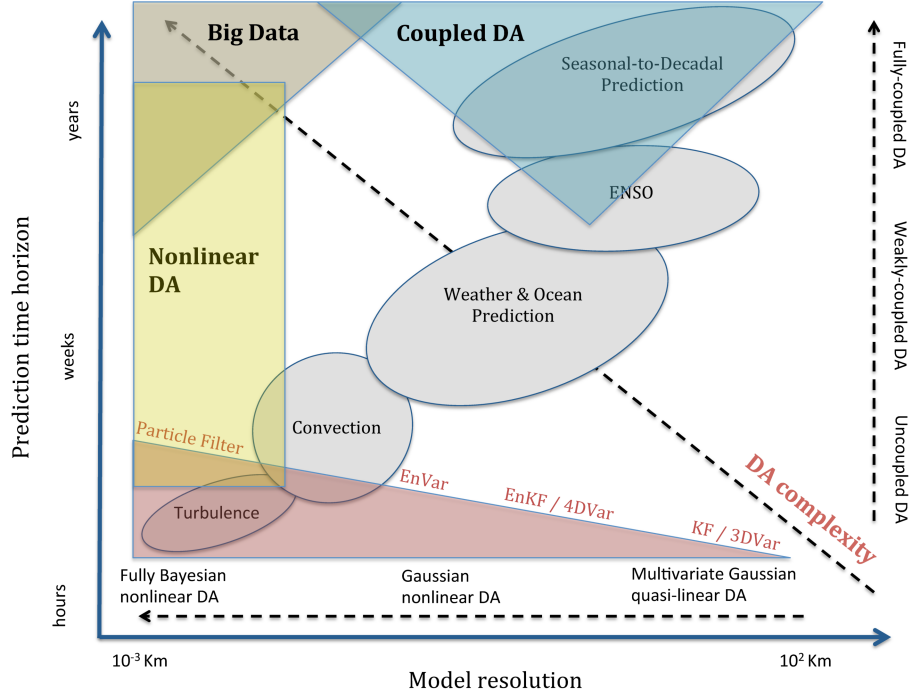


Figure 9: Required DA method versus model resolution and prediction time horizon; examples of corresponding natural phenomena are also shown for illustrative purposes. The degree of sophistication of the DA grows commensurately with the increase in prediction time horizon and the decrease of the model grid size.

The constant increase of the numerical model resolution, i.e., reducing the model grid size, implies resolving more and more small scale processes (e.g., convection or turbulence) that are often inherently nonlinear and non-Gaussian. The transition toward high-resolution models must thus be accompanied by corresponding DA developments where the Gaussian and linear assumptions are relaxed (see, e.g., *Yano et al.*, 2017). This identifies one of the more challenging and active lines of research in DA at the current time: fully Bayesian methods. The horizontal dashed line in Fig. 9 illustrates the DA method required features as a function of the model grid size; particle filters, the subject of Sect. 6.1, are fully Bayesian and nonlinear methods and are placed at the top of the algorithms hierarchy in Fig. 9.

Together with the increase in model resolution, the current era is also characterized by a growing interest in long-term forecasts. Indeed, beyond the meteorological time horizon of two weeks, predictions over seasonal-to-decadal (s2d) time scales potentially bear higher societal relevance: they can guide adaptation to near-term climate change and related risks (*Doblas-Reyes et al.*, 2013). Such long-term predictability arises from the interactions between the atmosphere and the more slowly varying components of the climate system, like the ocean, land surface and cryosphere, so that predictions are issued using fully coupled models (Earth System Models, ESMs). The fruitful use of DA with coupled models necessitates the development of adequate coupled DA (CDA) methods that allow for a consistent and balanced propagation of the informational content of the observations across all model components (see vertical dashed line in Fig. 9). As will be discussed in Sect. 6.2, this is

not straightforward with standard DA methods and substantial efforts are currently being undergone to develop CDA strategies.

In addition to the increase in numerical model resolution and of the prediction time horizon, we are also experiencing a dramatic growth and refinement of the observations suppliers. The Earth is now observed over a wide range of spatial and temporal scales, thanks to an increasingly wider variety of sustained observing systems, which includes satellites, but also new, not stationary, ocean measurements such as floats, drifters and more recently gliders (see, e.g., *Kuznetsov et al.*, 2003). The assimilation of data derived from instruments that are not stationary has come to be known as *Lagrangian DA* (see, e.g., *Ide et al.*, 2002; *Nodet*, 2006). These methods have gained popularity as they offer a suitable way to consistently incorporate modern observation of the ocean, and have experienced a flourishing stream of improvements in the last decade, driven by addressing two main challenges: the use of indirect measurements of the state variables (see, e.g., *Salman et al.*, 2006) and the inherent nonlinear character of the underlying dynamics (*Apte and Jones*, 2013). More recently, the Lagrangian dimension of the DA problem has also involved the model component, and not just the data, with the appearance of numerical models discretised on a spatio temporal varying mesh (see, e.g., *Rampal et al.*, 2016, for an example of Lagrangian sea-ice model). This feature represents another methodological challenge for DA, which is no longer only demanded to update the value of the physical variables on the grid points, but also the physical location of grid itself (see, e.g., *Bonan et al.*, 2017).

6.1 Bayesian data assimilation: particle filters

From the Bayesian standpoint, the state estimation problem is best formulated as Eq. (3):

$$p(\mathbf{x}|\mathbf{y}) = \frac{p(\mathbf{y}|\mathbf{x})p(\mathbf{x})}{p(\mathbf{y})}. \quad (67)$$

We have seen in Sect. 2.2 how to exploit and formulate the sequential estimation problem through the conjunction of Bayes' rule and the Chapman-Kolmogorov equations.

Yet, these formulae were claimed to be impractical, at least for high-dimensional models, and we moved on to solutions based on Gaussian approximations. The algebra involved with these approximations is numerically demanding with inversions of covariance matrices in the analysis step, which contrasts with the apparent simplicity of Eq. (67).

A direct and brute force approach to the DA problem would be to use Monte Carlo methods and draw N samples from Eq. (3). The hope is that in the asymptotic limit, i.e., $N \rightarrow \infty$, one would properly estimate the conditional density $p(\mathbf{x}|\mathbf{y})$. In a sequential context, this approach is called the particle filter (PF), or sequential Monte Carlo. In the following we show how to justify and implement such simple algorithm but that it unfortunately comes with its own drawbacks.

6.1.1 Bootstrap particle filter and resampling

As a first step, let us see how to solve the filtering problem sequentially with the PF. The forecast pdf $p_{k|k-1}$ from t_{k-1} to t_k is assumed – and this is the main approximation at finite

N , i.e. with a limited ensemble – to be of the form

$$p_{k|k-1}(\mathbf{x}_k|\mathbf{y}_{k-1:}) = \sum_{n=1}^N \omega_{k-1}^n \delta(\mathbf{x}_k - \mathbf{x}_k^n), \quad (68)$$

which is an empirical distribution with delta-Dirac masses δ , each one centered on an \mathbf{x}_k^n . The $\{\mathbf{x}_k^n\}_{n=1,\dots,N}$ are the particles (i.e., the ensemble members or the samples) and the $\{\omega_k^n\}_{n=1,\dots,N}$ are positive weights attached to the particles; \mathbf{x}_k^n is a shortcut for the particle \mathbf{x}_n , as denoted in Sect. 4, at time t_k . Since $p_{k|k-1}$ is a pdf, the weights need to be normalized to one, $\sum_{n=1}^N \omega_{k-1}^n = 1$. Hence, those weights tell how probable a particle is.

The analysis at t_k consists in the assimilation of \mathbf{y}_k using Bayes' rule:

$$\begin{aligned} p_{k|k}(\mathbf{x}_k|\mathbf{y}_{k:}) &= \frac{p_k(\mathbf{y}_k|\mathbf{x}_k)}{p(\mathbf{y}_{k:})} p_{k|k-1}(\mathbf{x}_k|\mathbf{y}_{k-1:}) \\ &= \sum_{n=1}^N \omega_{k-1}^n \frac{p_k(\mathbf{y}_k|\mathbf{x}_k)}{p(\mathbf{y}_{k:})} \delta(\mathbf{x}_k - \mathbf{x}_k^n) \\ &\propto \sum_{n=1}^N \omega_{k-1}^n p_k(\mathbf{y}_k|\mathbf{x}_k^n) \delta(\mathbf{x}_k - \mathbf{x}_k^n). \end{aligned} \quad (69)$$

This suggests to define the updated weights as

$$\omega_k^n \propto \omega_{k-1}^n p_k(\mathbf{y}_k|\mathbf{x}_k^n), \quad (70)$$

where the proportionality factor can be determined afterwards by the condition that the normalized updated weights should sum up to 1. Hence, the analysis elegantly sums up to a simple multiplication of the weights by the likelihood of each particle.

The forecast step amounts to applying Chapman-Kolmogorov Eq. (9):

$$\begin{aligned} p_{k+1|k}(\mathbf{x}_{k+1}|\mathbf{y}_{k:}) &= \int d\mathbf{x}_{k+1} p(\mathbf{x}_{k+1}|\mathbf{x}_k) p_{k|k}(\mathbf{x}_k|\mathbf{y}_{k:}) \\ &= \sum_{n=1}^N \int d\mathbf{x}_{k+1} p(\mathbf{x}_{k+1}|\mathbf{x}_k) \omega_k^n \delta(\mathbf{x}_k - \mathbf{x}_k^n) \\ &= \sum_{n=1}^N \omega_k^n p(\mathbf{x}_{k+1}|\mathbf{x}_k^n). \end{aligned} \quad (71)$$

If the model, defined by its transition density $p(\mathbf{x}_{k+1}|\mathbf{x}_k)$, as in Eq. (4), is deterministic, the forecast pdf $p_{k+1|k}$ is, as the update pdf $p_{k|k}$, in the form of a delta-Dirac density; otherwise it is not so. To obtain $p_{k+1|k}$ as a delta-Dirac pdf, which would be necessary in order to cycle the algorithm, we need to sample from Eq. (71).

One solution to obtain a delta-Dirac pdf from Eq. (71) consists, for each particle n , in sampling \mathbf{x}_{k+1}^n from the density $p(\mathbf{x}_{k+1}|\mathbf{x}_k^n)$ by simply forecasting \mathbf{x}_k^n from t_k to t_{k+1} using the (possibly stochastic) model associated with the transition density $p(\mathbf{x}_{k+1}|\mathbf{x}_k)$, which yields:

$$p_{k+1|k}(\mathbf{x}_{k+1}|\mathbf{y}_{k:}) \approx \sum_{n=1}^N \omega_k^n \delta(\mathbf{x}_{k+1} - \mathbf{x}_{k+1}^n). \quad (72)$$

Alternatively, one can sample particle n from Eq. (71) by randomly selecting one of the particles, say n' , with a probability proportional to its importance weight. Once $\mathbf{x}_k^{n'}$ is selected, one can forecast it and define \mathbf{x}_{k+1}^n using, as in the previous case, the model associated with the transition density $p(\mathbf{x}_{k+1}|\mathbf{x}_k^{n'})$, which yields

$$p_{k+1|k}(\mathbf{x}_{k+1}|\mathbf{y}_{k:}) \approx \frac{1}{N} \sum_{n=1}^N \delta(\mathbf{x}_{k+1} - \mathbf{x}_{k+1}^n). \quad (73)$$

The first option corresponds to the *bootstrap* PF (Gordon et al., 1993) or sequential importance sampling (SIS) PF. The second option adds, before forecasting, a *resampling* step that uniformly resets the weights to N^{-1} ; it is called sequential importance resampling (SIR) PF and is depicted in Fig. 10. There are several ways to resample the particles given their weights. Popular resampling schemes include multinomial resampling, residual resampling, and stochastic universal (or systematic) resampling, the latter minimizing the sampling noise introduced in the procedure (Douc and Cappé, 2005).

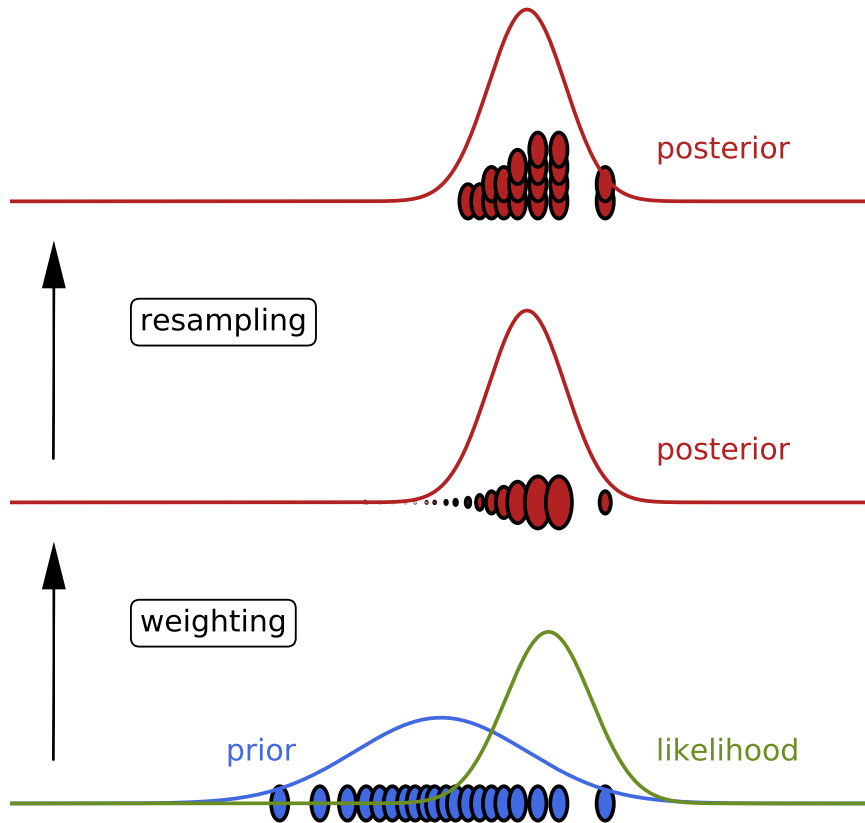


Figure 10: Principle of the SIR particle filter (here $N = 19$). The lower panel curves are the pdfs of the prior and the observation. The initial equal-weight particles are also displayed. The middle panel shows the weighing of the particles by the likelihood yielding unequal weights. The upper panel shows the outcome of resampling with multiple copies of several of the initial particles.

6.1.2 Importance sampling with a proposal

In statistics, most smart sampling strategies usually come with the possibility to draw samples from an ancillary, more accessible, distribution, naturally called the *proposal* distribution. However, the weights of these drawn particles must be corrected so that their empirical distribution is an unbiased estimator of the targeted distribution. Particle filters can also crucially benefit from this approach. Since this subject is more technical, the reader not interested in the details of its implementation is invited to move on to the next subsection Sec. 6.1.3.

A richer class of particle filters can be formalized if we consider a density of trajectories $p_{k|k}(\mathbf{x}_{k:}|\mathbf{y}_{k:})$ in place of model states (i.e., the density $p_{k|k}(\mathbf{x}_k|\mathbf{y}_{k:})$), a pdf which is usually associated to a smoothing problem (cf. Sect. 2.2). Now, we assume the existence of a smoothing density $q(\mathbf{x}_{k:}|\mathbf{y}_{k:})$ from which it is easier to sample, instead of the "desired" $p_{k|k}(\mathbf{x}_{k:}|\mathbf{y}_{k:})$. It has the following delta-Dirac representation:

$$q(\mathbf{x}_{k:}|\mathbf{y}_{k:}) = \sum_{n=1}^N \omega_k^n \delta(\mathbf{x}_{k:} - \mathbf{x}_{k:}^n). \quad (74)$$

We can exploit this *proposal* density, which is auxiliary to the conditional pdf under study, to compute any statistical moment of the conditional probability $p_{k|k}(\mathbf{x}_{k:}|\mathbf{y}_{k:})$. If ϕ is a generic test function, we have

$$\mathbb{E}[\phi(\mathbf{x}_{k:})] = \int d\mathbf{x}_{k:} \phi(\mathbf{x}_{k:}) p_{k|k}(\mathbf{x}_{k:}|\mathbf{y}_{k:}) \quad (75)$$

$$= \int d\mathbf{x}_{k:} \phi(\mathbf{x}_{k:}) \frac{p_{k|k}(\mathbf{x}_{k:}|\mathbf{y}_{k:})}{q(\mathbf{x}_{k:}|\mathbf{y}_{k:})} q(\mathbf{x}_{k:}|\mathbf{y}_{k:}) \quad (76)$$

$$= \sum_{n=1}^N \omega_k^n \phi(\mathbf{x}_{k:}^n) \frac{p_{k|k}(\mathbf{x}_{k:}^n|\mathbf{y}_{k:})}{q(\mathbf{x}_{k:}^n|\mathbf{y}_{k:})}. \quad (77)$$

Hence, the conditional pdf can be represented using weighted samples:

$$p_{k|k}(\mathbf{x}_{k:}|\mathbf{y}_{k:}) \approx \sum_{n=1}^N \frac{p_{k|k}(\mathbf{x}_{k:}^n|\mathbf{y}_{k:})}{q(\mathbf{x}_{k:}^n|\mathbf{y}_{k:})} \omega_k^n \delta(\mathbf{x}_{k:} - \mathbf{x}_{k:}^n). \quad (78)$$

We further assume that the proposal density factorizes according to

$$q(\mathbf{x}_{k:}|\mathbf{y}_{k:}) = q(\mathbf{x}_k|\mathbf{x}_{k-1:}, \mathbf{y}_{k:}) q(\mathbf{x}_{k-1:}|\mathbf{y}_{k-1:}) \quad (79)$$

such that it is easy to sample \mathbf{x}_k^n from $q(\mathbf{x}_k|\mathbf{x}_{k-1:}^n, \mathbf{y}_{k:})$.

The particle trajectories $\{\mathbf{x}_{k-1:}^n, \omega_{k-1}^n\}_{n=1, \dots, N}$ can then be extended to t_k by sampling \mathbf{x}_k^n from $q(\mathbf{x}_k|\mathbf{x}_{k-1:}^n, \mathbf{y}_{k:})$ so as to obtain $\{\mathbf{x}_{k:}^n, \omega_{k-1}^n\}_{n=1, \dots, N}$. Hence, the smoothing conditional pdf at t_k is

$$p_{k|k}(\mathbf{x}_{k:}|\mathbf{y}_{k:}) = \sum_{n=1}^N \frac{p_{k|k}(\mathbf{x}_{k:}^n|\mathbf{y}_{k:})}{q(\mathbf{x}_{k:}^n|\mathbf{y}_{k:})} \omega_{k-1}^n \delta(\mathbf{x}_{k:} - \mathbf{x}_{k:}^n). \quad (80)$$

Assuming Markovian dynamics, the sequential evolution of the smoothing pdf decomposes as

$$p_{k|k}(\mathbf{x}_{k:}|\mathbf{y}_{k:}) \propto p(\mathbf{y}_k|\mathbf{x}_k)p(\mathbf{x}_k|\mathbf{x}_{k-1})p_{k-1|k-1}(\mathbf{x}_{k-1}|\mathbf{y}_{k-1:}), \quad (81)$$

which, together with Eq. (79), yields

$$p_{k|k}(\mathbf{x}_{k:}|\mathbf{y}_{k:}) \propto \sum_{n=1}^N \frac{p(\mathbf{x}_k^n|\mathbf{x}_{k-1}^n)p(\mathbf{y}_k|\mathbf{x}_k^n)}{q(\mathbf{x}_k^n|\mathbf{x}_{k-1:}, \mathbf{y}_{k:})} \omega_{k-1}^n \delta(\mathbf{x}_{k:} - \mathbf{x}_{k:}^n). \quad (82)$$

By comparison with the generic Eq. (78), the weights should be updated at t_k according to

$$\omega_k^n \propto \frac{p(\mathbf{x}_k^n|\mathbf{x}_{k-1}^n)p(\mathbf{y}_k|\mathbf{x}_k^n)}{q(\mathbf{x}_k^n|\mathbf{x}_{k-1:}, \mathbf{y}_{k:})} \omega_{k-1}^n, \quad (83)$$

up to a normalization to 1 of the updated weights. The filtering solution of the estimation problem is simply obtained without further computation from $\{\mathbf{x}_{k:}^n, \omega_k^n\}_{n=1, \dots, N}$ by marginalization, i.e., keeping the states at t_k with the same weights: $\{\mathbf{x}_k^n, \omega_k^n\}_{n=1, \dots, N}$.

Importantly, if we choose $q(\mathbf{x}_k|\mathbf{x}_{k-1:}, \mathbf{y}_{k:}) \equiv p(\mathbf{x}_k|\mathbf{x}_{k-1})$, then we obtain $\omega_k^n \propto p(\mathbf{y}_k|\mathbf{x}_k^n)\omega_{k-1}^n$ and recover the bootstrap PF (cf. Eq. (70)). Furthermore, if we choose $q(\mathbf{x}_k^n|\mathbf{x}_{k-1:}, \mathbf{y}_{k:}) \equiv p(\mathbf{x}_k|\mathbf{y}_k, \mathbf{x}_{k-1})$, then we obtain $\omega_k^n \propto p(\mathbf{y}_k|\mathbf{x}_{k-1}^n)\omega_{k-1}^n$. This corresponds to the *optimal importance proposal* PF (Doucet et al., 2000). It is optimal only in the sense that it minimizes the theoretical variance of each weight ω_k^n conditional on $\mathbf{x}_{k-1:}^n$ and $\mathbf{y}_{k:}$; over the realizations of \mathbf{x}_k^n . This variance is actually 0.

6.1.3 Degeneracy of the particle filter

The algebra required by these PFs is very simple and elegant, and in principle offers a nice and asymptotically exact alternative to the Gaussian approximations to DA. Unfortunately, the PF is plagued by the *curse of dimensionality* as the dimensionality of the model is increased. In a sequential scheme, this curse manifests itself by the degeneracy of the weights: one weight will be close to 1, while the others essentially vanish (Kong et al., 1994). That is to say, the ensemble of particles collapses onto one single particle, while updating the weights via Eq. (70) or Eq. (83). This collapse is very inefficient as far as state estimation is concerned. Resampling does help by resetting to uniform weights, but it is, quite often, not enough to counteract this curse. Moreover, this trend essentially grows exponentially with the dimension of the system. More precisely, it has been shown in very simple but instructive Gaussian models that the particle numbers required to avoid degeneracy should scale like the variance of the likelihood (Snyder et al., 2008):

$$\ln(m) \propto \text{Var}[\ln(p(\mathbf{y}|\mathbf{x}))]. \quad (84)$$

Equation (84) has the merit to show that m could scale exponentially with the size of simple systems, but the derivation of such scaling is not straightforward in general. A carefully designed proposal, such as the optimal proposal mentioned in Sec. 6.1.2, and which can be shown to minimize the variance of the weights, does not change this exponential trend. Yet, it does reduce the constant in the exponent (MacKay, 2003; Snyder et al., 2015). Numerical investigations confirm this trend (Bocquet et al., 2010; Slivinski and Snyder, 2016).

6.1.4 Smarter particle filters for the geosciences

Particle filtering is a well developed field of statistics and engineering (*Doucet et al.*, 2001; *Arulampalam et al.*, 2002; *Chen*, 2003). It is very successful with low-dimensional models (such as object tracking). The number of contributions to the topic has substantially grown in geophysical DA in recent years (*van Leeuwen*, 2009; *Bocquet et al.*, 2010). Yet, the curse of dimensionality remains a major obstacle. That is why appealing schemes have been proposed to reduce its impact.

The implicit particle filter (*Chorin and Tu*, 2009; *Morzfeld et al.*, 2012) combines smoothing and particle filtering over a DAW, similarly to 4DVar or the IEnKS. It stands as a possible extension of the optimal proposal particle filter but over a several-step long DAW.

In order to circumvent the curse of dimensionality, one can restrict the full Bayesian analysis to a limited number of degrees of freedom, while the rest of the control variables are estimated via a Gaussian-based method, typically the EnKF. This strategy has been developed in Lagrangian DA (*Slivinski et al.*, 2015).

Another strategy relies on mitigating the degeneracy of the PF by hybridizing with the EnKF (*Santitissadeekorn and Jones*, 2015). A family of algorithm can be created and parametrized by a mixing coefficient, which can be tuned or adaptively selected (*Stordal et al.*, 2011; *Frei and Künsch*, 2013; *Chustagulprom et al.*, 2016).

The equal weight PF and variants thereof (*Ades and van Leeuwen*, 2015; *Zhu et al.*, 2016) build a proposal such that the particles effectively get the same numerical weight out of the analysis, a procedure which is obviously meant to avoid the degeneracy.

6.1.5 Localization

Similarly to the EnKF, a strategy to mitigate the curse of dimensionality that plagues the PF is to reduce the number of degrees of freedom by making local analyses. However, its implementation is trickier than with the EnKF. Indeed, considering a local domain localization, a particle will be given distinct local weights, even though they might vary smoothly in space. Hence, there is no natural updated particle that could emerge from the former if the local weights are unequal, as opposed to the local EnKF. One should devise a gluing of local parts of particles through resampling and try to avoid nonphysical discontinuities at the intersections of the local domains. Such strategies have recently been proposed and implemented (*Reich*, 2013; *Poterjoy*, 2016; *Penny and Miyoshi*, 2016; *Robert and Künsch*, 2017; *Beskos et al.*, 2017). Their success is mitigated by the still large number of particles required in each local domain. As a consequence, the size of such domain (localization radius) is generally diagnosed to be significantly smaller than with the local EnKF. Yet, localization is thought to be a necessary ingredient of a successful particle filter in high-dimensional geophysical systems.

6.2 Coupled data assimilation

Data assimilation algorithms have been conceived mainly for NWP applications and have been usually designed for state estimation in systems with a single dominant dynamical scale and/or for an observational network having a dominant spatio-temporal density. The sustained increase of model resolutions, the deployment of more and more observation platforms

and the use of coupled ESMs for seasonal to decadal (s2d) predictions, altogether bind to a deep re-thinking of the DA procedures. The design of efficient CDA methods, able to keep simultaneously control of all resolved scales and propagate adequately information across the climate system components, has been recently recognized to have primary importance.

Several research groups and institutions, including weather and climate services, are currently studying and developing CDA (see *Penny and Hamill, 2017*, for an updated report on these efforts). Early attempts include the case of sparsely observed flow possessing a wide range of scales with a KF-like procedure (*Harlim and Majda, 2010*), or a study of the performance of the EnKF in a prototypical nonlinear dynamics possessing two scales of motion (*Ballabrera-Poy et al., 2009*). On the side of variational methods, *Lorenz and Payne (2007)* have nicely illustrated a modification of the 4DVar which might be successfully applied to global high-resolution coupled models.

Seasonal-to-decadal prediction spans time horizons of up to approximately 10 years, falling between NWP and centennial projections (*Doblas-Reyes et al., 2013*). Correct initialization of the model is known to improve forecast quality on horizons of several years (*Carrassi et al., 2016*), and for a long time predictions have been initialized with observations of the present climatic state using either the full field (FFI) or the anomaly initialization (AI) (see, e.g., *Carrassi et al., 2014*). FFI makes use of the best possible available estimate of the real state: it reduces the initial error, but the unavoidable presence of model deficiencies causes the model trajectory to drift away from the observations (see, e.g., *Stockdale, 1997*). Anomaly initialization assimilates the observed climate anomalies on top of an estimate of the model mean climate. This initial state, at the expense of an initial error of the size of the model bias, is expected to be closer to the model attractor (see, e.g., *Smith and Murphy, 2007*), so that drift is reduced. Comparisons between FFI and AI have revealed respective advantages and drawbacks, the strong regional and model-dependency of the results (see, e.g., *Magnusson et al., 2013; Smith et al., 2013; Hazeleger et al., 2013; Carrassi et al., 2014*), and the fact that AI is a viable option only when the model and the observed statistics differ largely on their first moments alone (i.e., the bias) (*Weber et al., 2015*).

However it was made clear that such a decoupled initialization approach induced problems, particularly imbalances at the boundary between the ocean and the atmosphere. To cope with this issue, a solution has shown some success: the *weakly coupled data assimilation (wCDA)*. In the wCDA, a coupled model is used to run the predictions but the observations of the different model compartments (atmosphere, ocean, land and sea-ice) are used independently, so that each component is subject to a separate analysis. A first attempt to create a weakly coupled reanalysis has been done in the USA at the National Center for Environmental Prediction (NCEP) (*Saha et al., 2010*) and at the Japanese Agency for Marine-Earth Science and Technology (JAMSTEC) (*Sugiura et al., 2008*), based on global ESMs and using 3DVar and 4DVar respectively. The wCDA reanalysis showed a marked improvement over the standard uncoupled formulation. In the JAMSTEC implementation the control variable includes the ocean initial conditions plus a set of parameters related to the air-sea fluxes. The approach acted as a proof-of-concept for successfully producing balanced initial conditions for the coupled system and optimal coupling parameters, and enhancing the skills of the s2d prediction. The UK MetOffice has designed a weakly coupled atmosphere-ocean assimilation using the incremental 4DVar (*Laloyaux et al., 2016*) (cf. Appendix D) and the global coupled model, but the corrections for atmosphere and ocean are calculated indepen-

dently. Similarly, the ECMWF has produced a 20-th century reanalysis based on wCDA (Poli *et al.*, 2016). The EnKF in a wCDA setting has been recently used to assimilate ocean observations to initialize s2d predictions with the Norwegian Earth System Model (NorESM) (Counillon *et al.*, 2014).

Atmosphere and ocean are constrained independently using the ensemble-based approach at the Geophysical Fluid Dynamics Laboratory (GFDL) using the EAKF (Zhang *et al.*, 2007). Using the same framework, Lu *et al.* (2015) have achieved some success in a controlled simulated scenario using *strongly CDA (sCDA)*, in which the different model compartments are coupled together also at the analysis times, so that observations on one compartment, say the atmosphere, impact on another, say the ocean. The assimilation reconstructed successfully relevant climate fields over the period of interest and provides automatically the initial conditions to run an ensemble of forecasts. One of the first attempts of sCDA for a coupled ocean and sea-ice model has been used operationally in TOPAZ (cf. Sect. 5.4), demonstrating that successful assimilation of sea ice concentrations requires a coupled, multivariate and time-dependent assimilation method (Sakov *et al.*, 2012a). A recent interesting result using sCDA is due to Sluka *et al.* (2016) that shows improvements over wCDA in using only atmospheric observations in a coupled atmosphere-ocean model. Coupled data assimilation with the EnKF to recover the Atlantic meridional overturning circulation with simulated observations in a low-order coupled atmosphere-ocean model has been studied by Tardif *et al.* (2014), and subsequently with data from a millennial-scale simulation of a comprehensive coupled atmosphere-ocean climate model in Tardif *et al.* (2015). These studies suggest that atmospheric observations alone, albeit frequent, do not suffice to properly recover the slowly evolving AMOC. Interestingly, it was shown that, in the lack of enough observations in the ocean, CDA of time-averaged atmospheric measurements can successfully track the AMOC.

A comparison of different CDA approaches in the context of incremental 4DVar (cf. Appendix D) using an idealized single-column atmosphere ocean model is given in Smith *et al.* (2015), and revealed the benefit of CDA as being able to produce more balanced analysis fields than its uncoupled counter-part, thus reducing initialization shock and the subsequent predictions. The same idealistic model setup has been used to investigate the impact of the model error and of the window length of the 4DVar showing that while uncoupled DA may reduce the analysis error more than the CDA, the latter better reduces the imbalances and thus reduces the forecasts error.

Coupled data assimilation is one of the main areas of research at present time and more advancements can be expected in the coming years; a review on the current status of the field can be found in Penny and Hamill (2017).

7 CONCLUSIONS

From its origin in the context of numerical weather prediction, data assimilation (DA) has later expanded to the broad areas of environmental prediction, including seasonal, interannual and decadal time-scales. The current efforts toward the implementation of seamless predictions, where the same high-resolution coupled models are used from short to long term forecasts, is also accompanied by advancements in DA so as to tackle the nonlinearities emerging from the increase in resolution and the coupling mechanisms giving rise to long

term predictability.

Nevertheless, the range of applications of DA have not remained confined to the state (and/or parameters) estimation to initialize prediction, but are progressively involving other problems. A notable example is the detection and attribution of climate change, or climate related events (*Stott et al.*, 2013), which is the issue of providing evidence for either the existence or the non-existence of a causal relationship between a hypothetical external forcing (e.g., anthropogenic emission) to a system (e.g., the climate) and an observed response (e.g., increase of temperature), for which novel methods based on DA have proven to be very efficient (*Hannart et al.*, 2016). More generally, DA can be efficiently used to estimate the marginal likelihood of the data, the so called model evidence (*Carrassi et al.*, 2017), which is a key statistical metric to perform model selection (see, e.g., *Carson et al.*, 2017, for an application in the context of glacial-interglacial cycle) and calibration or parameter estimation (see, e.g., *Winiarek et al.*, 2011, for the estimation of a radiological plume), or *Tandeo et al.* (2015) for the optimization of a subgrid-scale parametrization. DA has been used to reconstruct the climate of the past based on observations proxies (see, e.g., *Dubinkina and Goosse*, 2013), and, in the solid Earth science, for seismology applications (see, e.g., *Fichtner et al.*, 2006).

In general the use of DA has proven that the consistent data-to-model fusion provides a more insightful view on the phenomena of interest, than any of the two components, the model or the data, independently. Future applications of DA within the geosciences and beyond, are expected to be numerous, and to naturally arise by the improvement of our modelling capabilities, as a result of the increased computational power and physical understanding, on the one hand, and by the progresses of the observing facilities (such as, but not only, satellite) on the other. Data assimilation is nowadays spreading to many emerging disciplines such as neurosciences, genetics, biology, medicine or even in sociology-demography and traffic managements just to mention a few (see, e.g., *Palatella et al.*, 2013b; *Kadakia et al.*, 2016, for an example of applications for traffic flow and biology respectively). This expansion exposes DA to the need of new theoretical principles and novel methodological solutions and provide new contexts for challenging its effectiveness and robustness. Data assimilation is thus expected to continue playing a central role to bridge model with data, to maximally exploit their respective informational content.

We hope that this overview may be a first guide for scientists who are confronting with the use of DA methods, and provide them with a complete first outlook of the approaches and of their foundations. The present work is thus to be intended as a detailed introduction to the topic from where interested readers and researchers may later expand their knowledge.

Appendix A: Some properties of the Kalman filter and smoother

Although the straightforward use of the Kalman filter (KF) and Kalman smoother (KS) in geosciences is obviously hampered by the computational limitations and by the inconsistency of their statistical/dynamical hypotheses (Gaussianity and linearity), yet they represent the backbone of many practical DA algorithms. The history of the use of KF-like methods in geosciences is the one of a never-ending search for suitable approximations that, even if sub-optimal, can still work satisfactorily in a nonlinear, non-Gaussian, and high dimensional setting. We have seen in Sect. 4 how the KF has served as a key conceptual and factual

framework upon which several successful operational DA methods have been built. This appendix reviews some of the key properties and issues of the KF and KS. Our discussion here mainly pertains to the KF, but most of the conclusions apply to the KS too.

Time dependent prior

The KF analysis will be closer to either the observations or the prior depending on their respective accuracy, i.e., on our belief about them as estimated via the covariances \mathbf{R}_k and \mathbf{P}_k^f respectively. In the geosciences, the number of observations, albeit large, is usually insufficient to fully cover the state space ($d \ll m$) so that much of how the information is spread from observed to unobserved areas is controlled by the prior. Having an informative, accurate, and reliable prior is thus of great importance. As mentioned at the end of Sect. 2.1, the situation $d \ll m$ is endemic in NWP, and the use of a short-range numerical forecast in a cyclic DA procedure has been key to the success of DA in that context (see, e.g., Daley, 1993; Kalnay, 2002). The KF recursion provides a time-dependent estimate of the prior (its mean, \mathbf{x}_k^f , and covariance, \mathbf{P}_k^f) that is highly desirable in environmental systems that are usually chaotic, so that the actual error associated with \mathbf{x}_k^f is itself strongly time-dependent. We have seen in Sect. 5.1 that this property of the chaotic dynamics, while representing a challenge to the state estimation process, can also be exploited explicitly in the design of DA algorithms for this class of systems.

Filter divergence

Filter divergence is the name used to refer to the situation in which the solution of the KF deviates dramatically from the true signal that it was supposed to track, and the KF is not longer able to pull back its solution close to the truth (Fitzgerald, 1971; Harlim et al., 2010). Filter divergence is often the result of progressive and repeated under-estimation of the actual error, $\mathbf{P}_k^a < \mathbf{P}_k^{\text{truth}}$ (the matrices order relationship is that of the cone of the positive semi-definite matrices, Bocquet et al., 2017). Under the action of the dynamics, Eq. (16), the analysis error covariance, \mathbf{P}_{k-1}^a , is transformed into the forecast one at the next time, \mathbf{P}_k^f . If the dynamical model is chaotic (or just unstable) then at least one of the eigenvalues of $\mathbf{M}_{k:k-1}$ is larger than one and $\mathbf{P}_k^f \geq \mathbf{P}_{k-1}^a$: the estimated error grows during the forecast phase. However, for generic stable dynamics such an error growth is not guaranteed. At the analysis times, the term $(\mathbf{I}_k - \mathbf{K}_k \mathbf{H}_k)$ in Eqs. (18) and (19) represents the forcing due to the observations, and it has a stabilizing effect since its eigenvalues are bounded to be lower or equal to one (Carrassi et al., 2008a). This implies that the estimated analysis error covariance is always smaller or equal to the forecast (prior) error covariance, $\mathbf{P}_k^a \leq \mathbf{P}_k^f$. The overall fate of the KF error covariance comes by the balances between the (possible) growth during the forecast phases and the (certain) decrease at analysis times. If the dynamics is not able to counteract the covariance decrease occurring at analysis times, the KF error covariance will progressively decrease, and once $\mathbf{H}_k \mathbf{P}_k^f \mathbf{H}_k^T \ll \mathbf{R}_k$ the filter solution may start to ignore the observations. This is not an issue in itself, as long as the actual error is also decreasing and the KF solution is properly tracking the desired signal. Nevertheless, when this is not the case, i.e., when the KF error estimates decrease but the actual error does not, the KF solution starts to deviate from the observations, eventually diverging completely from the true signal.

Several factors may be at the origin of filter divergence, notably in the misspecification in the DA setup, such as a too strong influence from the measurements (from wrongly specified error statistics, neglected measurement error covariances, etc.), or wrongly specified or neglected model errors. Filter divergence also occurs in ensemble-based DA (see Sect. 4) and we have seen in Sect. 4.4 which countermeasures, inflation and localization, have been placed in order to deal with this issue in real applications.

A diagnostic tool

A remarkable property of the KF, originating from the linear and Gaussian assumptions, is that the error covariances, \mathbf{P}_k^f and \mathbf{P}_k^a do not depend on the observation values: they are thus unconditional covariances. This is a direct consequence of the first and second moments of the system’s state pdf being independent from each other (and uncoupled with higher order moments); a behavior that no longer holds in nonlinear, non-Gaussian, scenarios. Another peculiar feature, which serves as a measure of the filter deviations from optimality, is that the innovation vector sequence, $\mathbf{v}_k = \mathbf{y}_k - \mathbf{H}_k \mathbf{x}_k^f$, is Gaussian and uncorrelated in time (*Jazwinski, 1970*): one can thus keep monitoring the innovations to assess the KF optimality and, possibly, to implement corrections (*Daley, 1993*).

Bias and covariance estimation

The optimality of the KF relies upon the veracity of its assumptions: the linearity of the model and observational operator, and the Gaussianity of the true error pdfs. Any mismatch between the real conditions on which the KF operates and its working hypotheses will negate its optimality. Nevertheless, even when the hypotheses are correct, the KF will still depend on the correct specification of its statistical inputs: the model and observational error covariances. The initial conditions, \mathbf{x}_0^a and \mathbf{P}_0^a , are also input but their impact on the filter performance is discussed separately in the following paragraph.

Recall from Eqs. (13–14) that the model and observational error are assumed unbiased and Gaussian, $\boldsymbol{\eta}_k \sim \mathcal{N}(\mathbf{0}, \mathbf{Q}_k)$ and $\boldsymbol{\epsilon}_k \sim \mathcal{N}(\mathbf{0}, \mathbf{R}_k)$. If either the actual model or observational errors are biased (or both), the KF analysis will be biased too, unless those biases are removed from the forecast before the analysis update, Eqs. (18–19). These biases can be estimated recursively in time, along with the system’s state, using an approach known as *state augmentation* in which the state is formally augmented with the bias term (e.g. *Dee, 2005*). The state augmentation strategy is also the classical choice to deal with the simultaneous model state and parameter estimation (*Jazwinski, 1970*).

Likewise, discrepancies can also be present between the actual model and observation error covariances and those stipulated in the filter setup. In contrast to the bias, the covariances cannot be corrected using the state augmentation approach, and an additional procedure is required. A possibility is again on the use of the innovations: when all error covariances entering the KF are correct, the innovations are distributed according to $\mathbf{v}_k \sim \mathcal{N}(\mathbf{0}, \boldsymbol{\Sigma}_k)$, with $\boldsymbol{\Sigma}_k = \mathbf{H}_k(\mathbf{M}_{k:k-1} \mathbf{P}_{k-1}^a \mathbf{M}_{k:k-1}^T + \mathbf{Q}_k) \mathbf{H}_k^T + \mathbf{R}_k$ (*Cohn, 1997*). It is then possible, in principle, to estimate the “best” \mathbf{Q}_k and/or \mathbf{R}_k as those maximizing the conditional probability, $p(\mathbf{v}_k | \mathbf{Q}_k, \mathbf{R}_k)$, where the innovation is treated as a random variable (*Dee, 1995*). Given the large dimension of \mathbf{Q}_k and \mathbf{R}_k , such a maximum likelihood approach can only be feasible if \mathbf{Q}_k and \mathbf{R}_k are parametrized based on a very small number of parameters.

In any case, suitable parametrizations of the covariance matrices are necessary, partic-

ularly for model error, given the huge size of the geophysical models and the wide range of possible error sources. The former problem implies the need to estimate large matrices based on a limited number of available observations. The second is related to the multiple sources of model error, such as incorrect parametrization, numerical discretization, and the lack of description of some relevant scale of motion, which makes it difficult to set a unified parametrization. Recent works have proposed efficient combinations of Bayesian estimation procedures with Monte Carlo approximation to estimate both the observational and model error covariances (*Ueno and Nakamura, 2014, 2016; Dreano et al., 2017; Liu et al., 2017; Pulido et al., 2018*).

The computation of the Kalman gain, Eq. (17), requires the inversion of the matrix $(\mathbf{H}_k \mathbf{P}_k^f \mathbf{H}_k^T + \mathbf{R}_k)^{-1} \in \mathbb{R}^{d \times d}$. To make it computationally tractable, \mathbf{R}_k is often assumed to be diagonal and full rank, i.e., observations are assumed to be spatially uncorrelated. The estimation of \mathbf{R}_k is reduced to the task of specifying only its diagonal. It can also negatively affect the filter's performance when observations are spatially correlated, which is typically for remotely sensed data. The impact of neglecting observational error correlations, as well as approaches to include them efficiently in the DA setup, have been studied in several works (see, e.g., *Stewart et al., 2008; Miyoshi et al., 2013*).

Dependence on the initial condition

The criticality of the choice of the initial error covariance, \mathbf{P}_0 , is related to the filter's stability, intended as the convergence of its solutions to an asymptotic sequence, independently of the initial conditions (*Gelb, 1974*). Stability is a very desirable practical property: a stable filter will always tend to a steady solution and all unwanted errors in the specification of the initial conditions, \mathbf{x}_0 and \mathbf{P}_0 , do not alter the its final output. Nevertheless, optimality of the filter alone does not guarantee stability but, for a stochastically-driven dynamical system as in Eq. (13), it also requires the filter to be (uniformly) *observable* and *controllable* (see, e.g., *Kalman, 1960; Jazwinski, 1970; Cohn and Dee, 1988*). Roughly, observability is the condition that, given sufficiently many observations, the initial state of the system can be reconstructed by using a finite number of observations (*Quinn and Abarbanel, 2010*). To see this, let consider the case of a discrete, autonomous (i.e., constant, $\mathbf{M}_k = \mathbf{M}$), and deterministic dynamical model $\mathbf{x}_k = \mathbf{M}\mathbf{x}_{k-1}$ of dimension n , that is observed n -times, without error, with scalar measurements and a linear operator, so that $y_k = \mathbf{H}\mathbf{x}_k$ (the operator \mathbf{H} is in this case a n -dimensional row vector). Starting from the initial condition at t_0 , we have $y_0 = \mathbf{H}\mathbf{x}_0$, $y_1 = \mathbf{H}\mathbf{x}_1 = \mathbf{H}\mathbf{M}\mathbf{x}_0$, and so on until, $y_{n-1} = \mathbf{H}\mathbf{x}_{n-1} = \mathbf{H}\mathbf{M}^{n-1}\mathbf{x}_0$, that can be written compactly as

$$\begin{bmatrix} y_0 \\ y_1 \\ \cdot \\ \cdot \\ y_{n-1} \end{bmatrix} = \begin{bmatrix} \mathbf{H} \\ \mathbf{H}\mathbf{M} \\ \cdot \\ \cdot \\ \mathbf{H}\mathbf{M}^{n-1} \end{bmatrix} \mathbf{x}_0 = \boldsymbol{\Psi}^T \mathbf{x}_0.$$

We see therefore that, if one wants to determine uniquely the initial state, \mathbf{x}_0 , based on the observations, the $n \times n$ matrix $\boldsymbol{\Psi}$ must be invertible, that is to say its rank must be equal to n , or equivalently its determinant must be nonzero. In this case the system is said to be observable by the sequence of observations $y_0 \dots y_{n-1}$. As an example consider the simple

2×2 system

$$\mathbf{M} = \begin{pmatrix} 2 & 1 \\ 0 & 1 \end{pmatrix}$$

such that the dynamics of the first component depends on both the first and second components, while the second component depends only on itself. It is easy to show that observing the first component alone (i.e., $\mathbf{H} = [1 \ 0]$, a 2-dimensional row vector), the corresponding 2×2 matrix Ψ has determinant equal to 1, is therefore invertible, and the system is observable. On the other hand, if it is second component to be observed (i.e. $\mathbf{H} = [0 \ 1]$), the determinant of Ψ is zero and the system is not observable. This result is physically interpretable such that, given that the first component carries also information about the second, but not vice-versa, its observation is more effective in informing about the full 2-dimensional system. Similarly to observability, controllability can be described as the ability to move the system from any initial state to a desired one over a finite time interval, and is related to the properties of the system noise, \mathbf{Q}_k (see *Gelb, 1974*, for a complete discussion on observability and controllability with several examples).

The KF stability and convergence for purely deterministic systems (i.e., like in Eq. (13) but with $\mathbf{Q}_k = \mathbf{0}$), under the sole condition of uniform observability has been recently proved by *Ni and Zhang (2016)* and further characterized in terms of the stability properties of the dynamics by *Carrassi et al. (2008a)*; *Gurumoorthy et al. (2017)*. The generalization to the case of degenerate (rank deficient) initial condition error covariance is given in *Bocquet et al. (2017)*, thus corroborating reduced-rank formulations of the KF based on the system's unstable modes (*Trevisan and Palatella, 2011a*).

Appendix B: Minimization process in variational methods

With the gradient, Eq. (27), in hand, the minimization is iteratively solved searching for the state vector, \mathbf{x}_0^i , at the i -th iteration that satisfies $\mathcal{J}(\mathbf{x}_0^i) < \mathcal{J}(\mathbf{x}_0^{i-1})$ (i.e. the amplitude of the cost function decreases from iteration $i - 1$ to i), and the process is repeated until a prespecified convergence criteria (a threshold on the amplitude of the cost function) is verified. The new state at each iteration is updated as $\mathbf{x}_0^i = \mathbf{x}_0^{i-1} + \gamma^{i-1} \mathbf{v}^{i-1}$, with \mathbf{v}^i being the searching direction and γ^{i-1} the step size.. Moreover, the various minimization algorithms differ on how \mathbf{v}^i and the step size along it are chosen. When the searching direction is chosen to have an angle greater than 90 degrees with respect to the gradient (i.e., $(\mathbf{v}^i)^T \nabla_{\mathbf{x}} \mathcal{J}(\mathbf{x}^i) < 0$), the minimization procedures are referred to as *descent methods*. The most common and straightforward descent methods are the *steepest* and the *Newton* method.

In the former, \mathbf{v}^i is taken as opposite to the gradient. This strategy works very well when the cost function is uniformly strictly convex (i.e., it has a global quadratic dependence on the control variable), in which case the gradient at any arbitrary point always heads to the absolute (and unique) minimum of the cost function, and the rate of convergence is linear. The computational cost of each iteration is relatively low, but the linear convergence can be so slow that the difference, $\mathbf{x}_0^i - \mathbf{x}_0^{i-1}$, becomes smaller than computer precision. Furthermore, the assumption of a globally convex cost function is critical in geosciences applications (*Miller et al., 1994*; *Pires et al., 1996*).

To cope with this, Newton’s method assumes that the cost function can be locally approximated by a quadratic expansion around the state point, \mathbf{x}^i , $\mathcal{J}(\mathbf{x}) \approx \mathcal{J}^{Newt}(\mathbf{x}) = \mathcal{J}(\mathbf{x}^i) + \nabla_{\mathbf{x}}\mathcal{J}(\mathbf{x}^i)(\mathbf{x} - \mathbf{x}^i) + \frac{1}{2}(\mathbf{x} - \mathbf{x}^i)^T \nabla_{\mathbf{x}}^2 \mathcal{J}(\mathbf{x}^i)(\mathbf{x} - \mathbf{x}^i)$. The state at i -th iteration is found by setting the gradient of this approximation to zero, which gives $\mathbf{v}^i = -\nabla_{\mathbf{x}}^{-2} \mathcal{J}^{Newt}(\mathbf{x}^i) \nabla_{\mathbf{x}} \mathcal{J}^{Newt}(\mathbf{x}^i)$; the search direction is equal to the opposite of the Hessian matrix of the cost function multiplied by its gradient. At the minimum the Hessian of the cost function is positive definite so that the search direction verifies the condition of being oriented with an angle greater than 90 degrees from the gradient. In practice, and in contrast to steepest descent, the Newton method uses also the local information about the curvature of the cost-function in order to better point toward its minimum. Although the convergence of the Newton’s method is quite rapid, its operational use in geophysical DA is rendered difficult by the need to invert the Hessian matrix, which is usually huge size and ill conditioned.

Minimization algorithms used operationally are a trade-off between efficiency and computational limitation and have features that mimic those of the two main algorithms just described. A throughout description of the state-of-art minimization methods goes beyond the scope of this article but interested readers can find more details in, e.g., *Fisher and Andersson* (2001) or *Asch et al.* (2016).

Appendix C: Comments on the variational methods

The Gaussian hypothesis has not just allowed to get an analytic expression for the cost function, Eq. (29) or (30), but it also offered a statistical, and physically plausible, interpretation of the analyzed trajectory. Given the unimodality of the Gaussian pdf, the most likely state is also the mean of the pdf, that is to say the minimum variance estimate. Without unimodality the mean state, while still having minimum variance, may well be of scarce relevance (it may fall in very low probability region) or not have physical plausibility at all.

In deriving the 4DVar, either in the weak or strong constraint formulations, no assumptions have been made about the characteristics of the dynamical and observational models: they can be assumed nonlinear and so they are in many real applications. Nevertheless, whether or not the latter is actually the case it has enormous consequences on the accuracy of the 4DVar analysis, as well as on the complexity of the algorithms used to solve it. When both models are linear and all errors are Gaussian, mutually uncorrelated and white-in-time, the 4DVar cost-function is quadratic and the gradient, that will depend linearly on the control variable, will correctly point to its global minimum. In this linear case, the 4DVar solution will match exactly the mean solution of a Kalman smoother (KS), Eq. (21), to which the same input statistics are provided, and it will thus represent an alternative way to get the best mean estimate without the explicit need to compute inverse matrices as in the KS (*Fisher et al.*, 2005).

In the general nonlinear case however an exact solution cannot be obtained. The approximate analysis will be the outcome of the minimization process and the degree of its accuracy will strongly depend on the degree of nonlinearity in the dynamical and observational models, even if the initial condition and observational error are Gaussian. The cost function will not longer be quadratic and it may possess multiple minima to which the minimization procedure can wrongly be trapped. A number of fixes have been proposed and put in place

to overcome this issue, so as to render the cost-function "more quadratic", notably by the use of a preconditioner under the form of a suitable invertible control variable transformation (Zupanski, 1996). It is beyond our scopes to expand further on this subject, but the readers can find more details in the literature (Talagrand, 2010; Asch et al., 2016).

The variational approach does not automatically solve the complete Gaussian estimation problem: it does not provide the two moments, the mean and the covariance, of the posterior distribution, but only the first one. It is possible to show that the analysis error covariance is indeed given, exactly/approximately for the linear/nonlinear case respectively, by the inverse Hessian matrix of the cost function; at its minimum the (inverse) Hessian must be positive definite (see Appendix B), consistently with a feature of a covariance matrix. Nevertheless, estimating the Hessian matrix for a realistic geophysical applications is extremely difficult, and usually the same (fixed in time) error covariance matrix is used to characterize the background errors at the beginning of each DA cycle. When solving the s4DVar the background error covariance is implicitly evolved within the window so that, effectively, a dynamically evolved estimate of the prior error is used at the observation times (Pires et al., 1996), but such an updated covariance is not explicitly accessible to initialize the next cycle.

This inherent limitation of the variational approach marks a key distinction with respect to sequential methods like the Kalman filter or smoother, that provide a time-dependent description of the uncertainty associated to the state estimate. This aspect has largely, but not solely, contributed to the popularity of KF-like approaches for DA with chaotic models (Vannitsem, 2017) where a time dependent description of the estimation error is highly desirable (cf. Sect. 5.1). We have seen in Sect. 4.5 that the recent promising efforts toward hybrid variational-ensemble methods are also aiming to cope with this issue, thus endowing the 4DVar with a flow-dependent estimate of the error covariance (Lorenc et al., 2015; Kleist and Ide, 2015; Buehner et al., 2015b).

Appendix D: Some popular approximations

We describe briefly some of the early successful approximations of the Kalman filter and of the variational approach that have made their implementation possible in the geosciences.

Extended Kalman filter

The *extended Kalman filter* (EKF) represents a first-order expansion of the Kalman filter (KF) and extends its use to nonlinear dynamics (Jazwinski, 1970). Like KF, it is sequential: the systems state and associated error covariance are updated at discrete observation times and evolved in between them. In the EKF, the mean state estimate is propagated by the full nonlinear model, but the error covariance evolution is approximated using the tangent linear one. The linearization is taken around the nonlinear model solution, so that the Jacobian of the model is evaluated upon it and it is thus state dependent.

As with the standard KF for linear dynamics, the EKF also assumes that errors are all Gaussian distributed. Nevertheless, under the action of the nonlinear dynamics, even a possible initial Gaussian error covariance will not stay Gaussian, and the EKF will only provide an approximate description of the actual estimation error distribution. In general, the accuracy of the EKF scales with the degree of nonlinearity in the model (Miller et al.,

1994). For instance, *Evensen* (1992) implemented the EKF with a multilayer ocean model finding that the tangent linear operator led to unbounded error growth since the nonlinear saturation that should occur at climatological level is contained in higher order moments of the error covariance equations, and those are all neglected in the closure used in the EKF.

The EKF has been successful in a number of pioneering applications of DA for meteorology (*Ghil et al.*, 1981; *Dee et al.*, 1985) and oceanography (*Ghil and Malanotte-Rizzoli*, 1991). It has also been used in one of the early study of coupled DA (cf. Sect. 6.2) with an atmosphere-ocean model of intermediate complexity (*Sun et al.*, 2002). The joint state and parameter estimation is possible with the EKF using the state-augmentation approach and its efficiency for this purpose has been demonstrated in the context of DA for seasonal forecasts (*Kondrashov et al.*, 2008) or land surface DA (see, e.g., *de Rosnay et al.*, 2014). A formulation of the EKF for parameter estimation in the presence of time correlated model error has been proposed by *Carrassi and Vannitsem* (2011) and later applied to a soil model (*Carrassi et al.*, 2012).

Along with the linear assumption on which it is built, another limitation of the EKF is due to the enormous computational requirements of the error covariance propagation. This involves the storage of full covariance matrices, the derivation of the tangent linear model, and its application a number of times twice the state vector dimension (*Asch et al.*, 2016).

Incremental 4DVar and 3DVar

The *incremental formulation* (*Courtier et al.*, 1994) employs a linearization of the problem around the background trajectory: both the dynamical and observational models are linearized and the cost function of the incremental (strong-constraint) 4DVar reads

$$\mathcal{J}^{\text{s4DVar-Incr}}(\delta\mathbf{x}_0) = \frac{1}{2} \sum_{k=0}^K \|\mathbf{v}_k - \mathbf{H}_k \mathbf{M}_{k:0} \delta\mathbf{x}_0\|_{\mathbf{R}_k}^2 + \frac{1}{2} \|\delta\mathbf{x}_0\|_{\mathbf{B}}^2, \quad (85)$$

where the increment, $\delta\mathbf{x}_0 = \mathbf{x}_0 - \mathbf{x}^b$, is now the control variable for the minimization, and $\mathbf{v}_k = \mathbf{y}_k - \mathcal{H}_k(\mathbf{x}_k) = \mathbf{y}_k - \mathcal{H}_k \circ \mathcal{M}_{k:0}(\mathbf{x}_0)$ is the innovation vector (cf. Appendix A).

The cost function is now quadratic, it possesses a unique absolute minimum, and it can be minimized much more easily. The minimization can be carried out by first computing the innovations (outer loop) using the nonlinear models, \mathcal{H} and \mathcal{M} . In the inner loop, Eq. (85) is evaluated using the linearized models, \mathbf{H} and \mathbf{M} , and then the gradient using the adjoint \mathbf{M}^T . This procedure returns the analysis increment, $\delta\mathbf{x}_0$, to be used for the next outer loop and so on until convergence. The incremental 4DVar allows thus to deal with small nonlinearities in an incremental way, given that the linearized models are cyclically updated when a new outer loop trajectory is computed. Usually a simplified version of the model (coarser resolutions, simplified physics, etc.) is used in the inner loop (*Lawless et al.*, 2008), and this feature along with the quadratic form of the cost function, have been pivotal for the operational implementation of the incremental 4DVar (see, e.g., *Courtier et al.*, 1994).

3DVar is a special case of the 4DVar where the time dimension is removed and only the observations at the analysis time are assimilated (see Fig. 2 and *Kalnay* (2002)). In this case the control variable is the state at t_0 , \mathbf{x}_0 , like for the strong-constraint 4DVar, however in contrast to it only the observations at t_0 are used in the update.

ACKNOWLEDGEMENTS

The authors wish to thank Eugenia Kalnay and another anonymous reviewer for their detailed, deep and critical reviews of the original version of this work. Their comments and suggestions have substantially improved its readability to a wider audience and have also helped in clarifying the discussion in many instances. The authors are thankful to P. N. Raanes (NERSC), A. Farchi (ENPC) and C. Grudzien (NERSC) for their comments, suggestions and insightful discussions and to J. Xie (NERSC) for providing Figure 8. Finally, the authors also wish to thank R. Davy (NERSC) who provided a critical review of the second version of the manuscript that helped to smooth further the mathematics and to make the work more accessible to the geosciences community at large. A. Carrassi has been funded by the project REDDA (#250711) of the Norwegian Research Council. G. Evensen has been partly funded by the project Embla of Nordforsk. CEREA is a member of Institut Pierre-Simon Laplace (IPSL).

References

- Aalstad, K., S. Westermann, T. Chuler, J. Boike, and L. Bertino, Ensemble-based assimilation of fractional snow-covered area satellite retrievals to estimate the snow distribution at Arctic sites, *The Cryosphere*, *12*, 247–270, 2018.
- Ades, M., and P. J. van Leeuwen, The equivalent-weights particle filter in a high-dimensional system, *Q J Roy. Meteor. Soc.*, *141*, 484–503, 2015.
- Amezcuca, J., and P. J. Van Leeuwen, Gaussian anamorphosis in the analysis step of the EnKF: a joint state-variable/observation approach, *Tellus A*, *66*, 1–18, 2014.
- Amezcuca, J., M. Goodliff, and P. J. van Leeuwen, A weak-constraint 4DEnsembleVar. Part I: formulation and simple model experiments, *Tellus A*, *69*, 1271,564, 2017.
- Anderson, J. L., An ensemble adjustment Kalman filter for data assimilation, *Mon. Weather Rev.*, *129*, 2884–2903, 2001.
- Anderson, J. L., An adaptive covariance inflation error correction algorithm for ensemble filters, *Tellus A*, *59*, 210–224, 2007.
- Anderson, J. L., and S. L. Anderson, A Monte Carlo implementation of the nonlinear filtering problem to produce ensemble assimilations and forecasts, *Mon. Weather Rev.*, *127*, 2741–2758, 1999.
- Apte, A., and C. K. Jones, The impact of nonlinearity in Lagrangian data assimilation, *Nonlinear Proc. Geoph.*, *20*, 329–341, 2013.
- Arulampalam, S., S. Maskell, N. Gordon, and T. Clapp, A tutorial on particle filters for online nonlinear non-Gaussian Bayesian tracking, *IEEE Trans. on Signal Processing*, *50*, 174–188, 2002.
- Asch, M., M. Bocquet, and M. Nodet, *Data Assimilation: Methods, Algorithms, and Applications*, Fundamentals of Algorithms, SIAM, Philadelphia, 2016.
- Auligné, T., B. Ménérier, A. C. Lorenc, and M. Buehner, Ensemble-variational integrated localized data assimilation, *Mon. Weather Rev.*, *144*, 6773696, 2016.
- Auroux, D., and J. Blum, A nudging-based data assimilation method: the back and forth nudging (bfn) algorithm, *Nonlin. Processes Geophys.*, *15*, 305–319, 2008.
- Bain, A., and D. Crisan, *Fundamentals of stochastic filtering*, vol. 3, Springer, 2009.

- Ballabrera-Poy, J., E. Kalnay, and S.-C. Yang, Data assimilation in a system with two scales combining two initialization techniques, *Tellus A*, *61*, 539–549, 2009.
- Bannister, R. N., A review of operational methods of variational and ensemble-variational data assimilation, *Q J Roy. Meteor. Soc.*, *143*, 607–633, 2017.
- Barth, A., M. Canter, B. van Schaeybroeck, S. Vannitsem, F. Massonnet, V. Zunz, P. Mathiot, A. Alvera-Azcarate, and J.-M. Beckers, Assimilation of sea surface temperature, ice concentration and ice drift in a model of the Southern Ocean, *Ocean Modell*, *93*, 22–39, 2015.
- Bauer, P., A. Thorpe, and G. Brunet, The quiet revolution of numerical weather prediction, *Nature*, *525*, 47–55, 2015.
- Bell, B. M., The iterated Kalman smoother as a Gauss-Newton method, *SIAM J. Optim.*, *4*, 626–636, 1994.
- Bengtsson, L., M. Ghil, and E. Källén (Eds.), *Dynamic Meteorology: Data Assimilation Methods*, Springer-Verlag, New York/Heidelberg/Berlin, 1981.
- Bennett, A. F., *Inverse methods in physical oceanography*, Cambridge university press, 1992.
- Berre, L., H. Varella, and G. Desroziers, Modelling of flow-dependent ensemble-based background-error correlations using a wavelet formulation in 4D-Var at Météo-France, *Q J Roy. Meteor. Soc.*, *141*, 2803–2812, 2015.
- Bertino, L., G. Evensen, and H. Wackernagel, Sequential data assimilation techniques in oceanography, *International Statistical Review*, *71*, 223–241, 2003.
- Beskos, A., D. Crisan, A. Jasra, K. Kamatani, and Y. Zhou, A stable particle filter for a class of high-dimensional state-space models, *Advances in Applied Probability*, *49*, 24–48, 2017.
- Bishop, C. H., B. J. Etherton, and S. J. Majumdar, Adaptive sampling with the ensemble transform Kalman filter. Part I: Theoretical aspects, *Mon. Weather Rev.*, *129*, 420–436, 2001.
- Bleck, R., An oceanic general circulation model in pressure coordinates, *Ocean Modell*, *37*, 55–88, 2002.
- Bocquet, M., Ensemble Kalman filtering without the intrinsic need for inflation, *Nonlinear Proc. Geoph.*, *18*, 735–750, 2011.
- Bocquet, M., Localization and the iterative ensemble Kalman smoother, *Q J Roy. Meteor. Soc.*, *142*, 1075–1089, 2016.
- Bocquet, M., and A. Carrassi, Four-dimensional ensemble variational data assimilation and the unstable subspace, *Tellus A*, *69*, 1304,504, 2017.
- Bocquet, M., and P. Sakov, Combining inflation-free and iterative ensemble Kalman filters for strongly nonlinear systems, *Nonlinear Proc. Geoph.*, *19*, 383–399, 2012.
- Bocquet, M., and P. Sakov, Joint state and parameter estimation with an iterative ensemble Kalman smoother, *Nonlinear Proc. Geoph.*, *20*, 803–818, 2013.
- Bocquet, M., and P. Sakov, An iterative ensemble Kalman smoother, *Q J Roy. Meteor. Soc.*, *140*, 1521–1535, 2014.
- Bocquet, M., C. Pires, and L. Wu, Beyond Gaussian Statistical Modeling in Geophysical Data Assimilation, *Mon. Weather Rev.*, *138*, 2997–3023, 2010.
- Bocquet, M., H. Elbern, H. Eskes, M. Hirtl, R. Zabkar, G. R. Carmichael, J. Flemming, A. Inness, M. Pagowski, J. L. Pérez Camaño, P. E. Saide, R. San Jose, M. Sofiev, J. Vira, A. Baklanov, C. Carnevale, G. Grell, and C. Seigneur, Data assimilation in atmospheric chemistry models: Current status and future prospects for coupled chemistry meteorology models, *Atmos. Chem. Phys.*, *15*, 5325–5358, 2015a.
- Bocquet, M., P. N. Raanes, and A. Hannart, Expanding the validity of the ensemble Kalman filter without the intrinsic need for inflation, *Nonlinear Proc. Geoph.*, *22*, 645–662, 2015b.

- Bocquet, M., K. S. Gurumoorthy, A. Apte, A. Carrassi, C. Grudzien, and C. K. Jones, Degenerate Kalman filter error covariances and their convergence onto the unstable subspace, *SIAM/ASA J. Uncertainty Quantification*, 5, 304–333, 2017.
- Bonan, B., N. K. Nichols, M. J. Baines, and D. Partridge, Data assimilation for moving mesh methods with an application to ice sheet modelling, *Nonlinear Proc. Geoph.*, 24, 515–534, 2017.
- Bonavita, M., L. Raynaud, and L. Isaksen, Estimating background-error variances with the ECMWF ensemble of data assimilation system: some effects of ensemble size and day-to-day variability, *Q J Roy. Meteor. Soc.*, 137, 423–434, 2011.
- Bonavita, M., L. Isaksen, and E. Hólm, On the use of EDA background error variances in the ECMWF 4D-Var, *Q J Roy. Meteor. Soc.*, 138, 1540–1559, 2012.
- Bowler, N. E., A. M. Clayton, M. Jardak, E. Lee, A. C. Lorenc, C. Piccolo, S. R. Pring, M. A. Wlasak, D. M. Barker, G. W. Inverarity, and R. Swinbank, Inflation and localization tests in the development of an ensemble of 4D-ensemble variational assimilations, *Q J Roy. Meteor. Soc.*, n/a, n/a–n/a, 2017.
- Brankart, J.-M., E. Cosme, C.-E. Testut, P. Brasseur, and J. Verron, Efficient adaptive error parameterization for square root or ensemble Kalman filters: application to the control of ocean mesoscale signals, *Mon. Weather Rev.*, 138, 932–950, 2010.
- Brankart, J.-M., C.-E. Testut, D. Béal, M. Doron, C. Fontana, M. Meinvielle, P. Brasseur, and J. Verron, Towards an improved description of ocean uncertainties : effect of local anamorphic transformations on spatial correlations, *Ocean Sci.*, 8, 121–142, 2012.
- Brusdal, K., J. Brankart, G. Halberstadt, G. Evensen, P. Brasseur, P. J. van Leeuwen, E. Dombrowsky, and J. Verron, An evaluation of ensemble based assimilation methods with a layered OGCM, *J. Marine. Sys.*, 40-41, 253–289, 2003.
- Buehner, M., Ensemble-derived stationary and flow-dependent background-error covariances: Evaluation in a quasi-operational NWP setting, *Q J Roy. Meteor. Soc.*, 131, 1013–1043, 2005.
- Buehner, M., P. L. Houtekamer, C. Charette, H. L. Mitchell, and B. He, Intercomparison of variational data assimilation and the ensemble Kalman filter for global deterministic NWP. Part I: Description and single-observation experiments, *Mon. Weather Rev.*, 138, 1550–1566, 2010a.
- Buehner, M., P. L. Houtekamer, C. Charette, H. L. Mitchell, and B. He, Intercomparison of variational data assimilation and the ensemble Kalman filter for global deterministic NWP. Part II: One-month experiments with real observations, *Mon. Weather Rev.*, 138, 1567–1586, 2010b.
- Buehner, M., J. Morneau, and C. Charette, Four-dimensional ensemble-variational data assimilation for global deterministic weather prediction, *Nonlinear Proc. Geoph.*, 20, 669–682, 2013.
- Buehner, M., R. McTaggart-Cowan, A. Beaulne, C. Charette, L. Garand, S. Heilliette, E. Lapalme, S. Laroche, S. R. Macpherson, J. Morneau, and A. Zadra, Implementation of deterministic weather forecasting systems based on ensemble-variational data assimilation at Environment Canada. Part I: The global system, *Mon. Weather Rev.*, 143, 2532–2559, 2015a.
- Buehner, M., R. McTaggart-Cowan, A. Beaulne, C. Charette, L. Garand, S. Heilliette, E. Lapalme, S. Laroche, S. R. Macpherson, J. Morneau, et al., Implementation of deterministic weather forecasting systems based on ensemble-variational data assimilation at environment canada. part i: The global system, *Mon. Weather Rev.*, 143, 2532–2559, 2015b.
- Burgers, G., P. J. van Leeuwen, and G. Evensen, Analysis scheme in the ensemble Kalman filter, *Mon. Weather Rev.*, 126, 1719–1724, 1998.
- Carmichael, G. R., A. Sandu, T. Chai, D. Daescu, E. Constantinescu, and Y. Tang, Predicting air quality: Improvements through advanced methods to integrate models and measurements, *J. Comput Phys*, 227, 3540–3571, 2008.

- Carrassi, A., and S. Vannitsem, Accounting for model error in variational data assimilation: A deterministic formulation, *Mon. Weather Rev.*, *138*, 3369–3386, 2010.
- Carrassi, A., and S. Vannitsem, State and parameter estimation with the extended Kalman filter: an alternative formulation of the model error dynamics, *Q J Roy. Meteor. Soc.*, *137*, 435–451, 2011.
- Carrassi, A., and S. Vannitsem, Deterministic treatment of model error in geophysical data assimilation, in *Mathematical Paradigms of Climate Science*, pp. 175–213, Springer, 2016.
- Carrassi, A., A. Trevisan, and F. Uboldi, Adaptive observations and assimilation in the unstable subspace by breeding on the data-assimilation system, *Tellus A*, *59*, 101–113, 2007.
- Carrassi, A., M. Ghil, A. Trevisan, and F. Uboldi, Data assimilation as a nonlinear dynamical systems problem: Stability and convergence of the prediction-assimilation system, *Chaos*, *18*, 023,112, 2008a.
- Carrassi, A., A. Trevisan, L. Descamps, O. Talagrand, and F. Uboldi, Controlling instabilities along a 3DVar analysis cycle by assimilating in the unstable subspace: a comparison with the EnKF, *Nonlinear Proc. Geoph.*, *15*, 503–521, 2008b.
- Carrassi, A., S. Vannitsem, D. Zupanski, and M. Zupanski, The maximum likelihood ensemble filter performances in chaotic systems, *Tellus A*, *61*, 587–600, 2009.
- Carrassi, A., R. Hamdi, P. Termonia, and S. Vannitsem, Short time augmented extended Kalman filter for soil analysis: a feasibility study, *Atmos. Sci. Lett.*, *13*, 268–274, 2012.
- Carrassi, A., R. Weber, V. Guemas, F. Doblas-Reyes, M. Asif, and D. Volpi, Full-field and anomaly initialization using a low-order climate model: a comparison and proposals for advanced formulations, *Nonlinear Proc. Geoph.*, *21*, 521–537, 2014.
- Carrassi, A., V. Guemas, F. Doblas-Reyes, D. Volpi, and M. Asif, Sources of skill in near-term climate prediction: generating initial conditions, *Clim. Dyn.*, *47*, 3693–3712, 2016.
- Carrassi, A., M. Bocquet, A. Hannart, and M. Ghil, Estimating model evidence using data assimilation, *Q J Roy. Meteor. Soc.*, *143*, 866–880, 2017.
- Carson, J., M. Crucifix, S. Preston, and R. D. Wilkinson, Bayesian model selection for the glacial–interglacial cycle, *J. R. Stat. Soc. C-Appl.*, 2017.
- Chekroun, M., E. Simonnet, and M. Ghil, Stochastic climate dynamics: random attractors and time-dependent invariant measures, *Physica D*, *240*, 1685–1700, 2011.
- Chen, Z., Bayesian filtering: From Kalman filters to particle filters, and beyond, *Statistics*, *182*, 1–69, 2003.
- Chilès, J. P., and P. Delfiner, *Geostatistics: Modeling Spatial Uncertainty*, Wiley, New York, 2012.
- Chorin, A. J., and X. Tu, Implicit sampling for particle filters, *PNAS*, *106*, 17,249–17,254, 2009.
- Chustagulprom, N., S. Reich, and M. Reinhardt, A hybrid ensemble transform particle filter for nonlinear and spatially extended dynamical systems, *SIAM/ASA J. Uncertainty Quantification*, *4*, 592–608, 2016.
- Clayton, A. M., A. C. Lorenc, and D. M. Barker, Operational implementation of a hybrid ensemble/4D-Var global data assimilation system at the Met Office, *Q J Roy. Meteor. Soc.*, *139*, 1445–1461, 2013.
- Cohn, S. E., An Introduction to Estimation Theory (Special Issue — Data Assimilation in Meteorology and Oceanography: Theory and Practice), *J. Meteorol. Soc. Jpn.*, *75*, 257–288, 1997.
- Cohn, S. E., and D. P. Dee, Observability of discretized partial differential equations, *SIAM J. Numer. Anal.*, *25*, 586–617, 1988.
- Constantinescu, E. M., A. Sandu, T. Chai, and G. R. Carmichael, Ensemble-based chemical data assimilation. I: General approach, *Q J Roy. Meteor. Soc.*, *133*, 1229–1243, 2007a.

- Constantinescu, E. M., A. Sandu, T. Chai, and G. R. Carmichael, Ensemble-based chemical data assimilation. II: Covariance localization, *Q J Roy. Meteor. Soc.*, *133*, 1245–1256, 2007b.
- Cosme, E., J. Verron, P. Brasseur, J. Blum, and D. Auroux, Smoothing problems in a Bayesian framework and their linear Gaussian solutions, *Mon. Weather Rev.*, *140*, 683–695, 2012.
- Counillon, F., I. Bethke, N. Keenlyside, M. Bentsen, L. Bertino, and F. Zheng, Seasonal-to-decadal predictions with the ensemble Kalman filter and the Norwegian Earth System Model: A twin experiment, *Tellus A*, *66*, 21,074, 2014.
- Counillon, F., N. Keenlyside, I. Bethke, Y. Wang, S. Billeau, M. L. Shen, and M. Bentsen, Flow-dependent assimilation of sea surface temperature in isopycnal coordinates with the Norwegian Climate Prediction Model, *Tellus A*, *68*, 1–17, 2016.
- Courtier, P., J.-N. Thépaut, and A. Hollingsworth, A strategy for operational implementation of 4D-Var, using an incremental approach, *Q J Roy. Meteor. Soc.*, *120*, 1367–1387, 1994.
- Daley, R., *Atmospheric data analysis*, Cambridge university press, 1993.
- de Rosnay, P., G. Balsamo, C. Albergel, J. Muñoz-Sabater, and L. Isaksen, Initialisation of land surface variables for numerical weather prediction, *Surveys in Geophysics*, *35*, 607–621, 2014.
- Dee, D., S. Cohn, A. Dalcher, and M. Ghil, An efficient algorithm for estimating noise covariances in distributed systems, *IEEE Trans. Automatic Control*, *30*, 1057–1065, 1985.
- Dee, D., S. Uppala, A. Simmons, P. Berrisford, P. Poli, S. Kobayashi, U. Andrae, M. Balmaseda, G. Balsamo, P. Bauer, et al., The ERA-Interim reanalysis: Configuration and performance of the data assimilation system, *Q J Roy. Meteor. Soc.*, *137*, 553–597, 2011.
- Dee, D. P., On-line estimation of error covariance parameters for atmospheric data assimilation, *Mon. Weather Rev.*, *123*, 1128–1145, 1995.
- Dee, D. P., Bias and data assimilation, *Q J Roy. Meteor. Soc.*, *131*, 3323–3343, 2005.
- Desroziers, G., J.-T. Camino, and L. Berre, 4D-EnVar: Link with 4D state formulation of variational assimilation and different possible implementations, *Q J Roy. Meteor. Soc.*, *140*, 2097–2110, 2014.
- Desroziers, G., E. Arbogast, and L. Berre, Improving spatial localization in 4D-EnVar, *Q J Roy. Meteor. Soc.*, *142*, 3171–3185, 2016, accepted for publication.
- Dijkstra, H., *Nonlinear Climate Dynamics*, Cambridge University Press, Cambridge, 2013.
- Doblas-Reyes, F. J., J. García-Serrano, F. Lienert, A. P. Biescas, and L. R. Rodrigues, Seasonal climate predictability and forecasting: Status and prospects, *Wiley Interdisciplinary Reviews: Climate Change*, *4*, 245–268, 2013.
- Douc, R., and O. Cappé, Comparison of resampling schemes for particle filtering, in *Image and Signal Processing and Analysis, 2005. ISPA 2005. Proceedings of the 4th International Symposium on*, pp. 64–69, 2005.
- Doucet, A., S. Godsill, and C. Andrieu, On sequential Monte Carlo sampling methods for Bayesian filtering, *Stat. Comput.*, *10*, 197–208, 2000.
- Doucet, A., N. de Freitas, and N. Gordon (Eds.), *Sequential Monte Carlo Methods in Practice*, Springer-Verlag New York Inc., 2001.
- Dreano, D., P. Tandeo, M. Pulido, B. Ait-El-Fquih, T. Chonavel, and I. Hoteit, Estimating model error covariances in nonlinear state-space models using Kalman smoothing and the expectation-maximisation algorithm, *Q J Roy. Meteor. Soc.*, 2017.
- Duane, G. S., J. J. Tribbia, and J. B. Weiss, Synchronicity in predictive modelling: A new view of data assimilation, *Nonlin. Proc. Geophys.*, *13*, 601–612, 2006.
- Dubinkina, S., and H. Goosse, An assessment of particle filtering methods and nudging for climate state reconstructions, *Climate of the Past*, *9*, 1141–1152, 2013.

- Elbern, H., A. Strunk, H. Schmidt, and O. Talagrand, Emission rate and chemical state estimation by 4-dimensional variational inversion, *Atmos. Chem. Phys.*, *7*, 3749–3769, 2007.
- Emili, E., S. Guroi, and D. Cariolle, Accounting for model error in air quality forecasts: an application of 4D-EnVar to the assimilation of atmospheric composition using QG-Chem 1.0, *Geosci. Model Dev.*, *9*, 3933–3959, 2016.
- Evensen, G., Using the extended Kalman filter with a multilayer quasi-geostrophic ocean model, *J. Geophys. Res.*, *97*, 17,905–17,924, 1992.
- Evensen, G., Sequential data assimilation with a nonlinear quasi-geostrophic model using Monte Carlo methods to forecast error statistics, *J. Geophys. Res.*, *99*, 10,143–10,162, 1994.
- Evensen, G., The ensemble Kalman filter: Theoretical formulation and practical implementation, *Ocean Dynamics*, *53*, 343–367, 2003.
- Evensen, G., Sampling strategies and square root analysis schemes for the EnKF, *Ocean Dynamics*, *54*, 539–560, 2004.
- Evensen, G., The ensemble Kalman filter for combined state and parameter estimation, *IEEE Control Systems Magazine*, *29*, 83–104, 2009a.
- Evensen, G., *Data Assimilation: The Ensemble Kalman Filter*, second ed., Springer-Verlag/Berlin/Heidelberg, 2009b.
- Evensen, G., Analysis of iterative ensemble smoothers for solving inverse problems, Accepted for publication in *Computat. Geosci.*, 2018.
- Fairbairn, D., S. R. Pring, A. C. Lorenc, and I. Roulstone, A comparison of 4DVar with ensemble data assimilation methods, *Q J Roy. Meteor. Soc.*, *140*, 281–294, 2014.
- Fichtner, A., H.-P. Bunge, and H. Igel, The adjoint method in seismology: II. Applications: traveltimes and sensitivity functionals, *Physics of the Earth and Planetary Interiors*, *157*, 105–123, 2006.
- Fisher, M., and E. Andersson, Developments in 4D-Var and Kalman filtering, *Technical Memorandum 347*, European Centre for Medium-Range Weather Forecasts, 2001.
- Fisher, M., and S. Gürol, Parallelization in the time dimension of four-dimensional variational data assimilation, *Q J Roy. Meteor. Soc.*, *143*, 1136–1147, 2017.
- Fisher, M., M. Leutbecher, and G. Kelly, On the equivalence between Kalman smoothing and weak-constraint four-dimensional variational data assimilation, *Q J Roy. Meteor. Soc.*, *131*, 3235–3246, 2005.
- Fisher, M., Y. Tremolet, H. Auvinen, D. Tan, and P. Poli, Weak-constraint and long-window 4D-Var, *ECMWF Techn. Rep.*, *655*, 2011.
- Fitzgerald, R., Divergence of the Kalman filter, *IEEE Transactions on Automatic Control*, *16*, 736–747, 1971.
- Frei, M., and H. R. Künsch, Bridging the ensemble Kalman and particle filters, *Biometrika*, *100*, 781–800, 2013.
- Gaspari, G., and S. E. Cohn, Construction of correlation functions in two and three dimensions, *Q J Roy. Meteor. Soc.*, *125*, 723–757, 1999.
- Gelb, A., *Applied optimal estimation*, MIT press, 1974.
- Gharamti, M., A. Samuelsen, L. Bertino, E. Simon, A. Korosov, and U. Daewel, Online tuning of ocean biogeochemical model parameters using ensemble estimation techniques: Application to a one-dimensional model in the North Atlantic, *J. Marine Systems*, *168*, 1–16, 2017a.
- Gharamti, M. E., J. Tjiputra, I. Bethke, A. Samuelsen, I. Skjelvan, M. Bentsen, and L. Bertino, Ensemble data assimilation for ocean biogeochemical state and parameter estimation at different sites, *Ocean Modell.*, *112*, 65–89, 2017b.

- Ghil, M., and P. Malanotte-Rizzoli, Data assimilation in meteorology and oceanography, *Adv. Geophys.*, *33*, 141–266, 1991.
- Ghil, M., S. Cohn, J. Tavantzis, K. Bube, and E. Isaacson, Applications of estimation theory to numerical weather prediction, in *Dynamic meteorology: data assimilation methods*, Springer-Verlag, New York, 1981.
- Golub, G. H., and C. F. van Loan, *Matrix computations*, vol. 3, JHU Press, 2013.
- Gordon, N. J., D. J. Salmond, and A. F. M. Smith, Novel approach to nonlinear/non-Gaussian Bayesian state estimation, *IEE Proc.-F*, *140*, 107–113, 1993.
- Greybush, S. J., E. Kalnay, T. Miyoshi, K. Ide, and B. R. Hunt, Balance and ensemble Kalman filter localization techniques, *Mon. Weather Rev.*, *139*, 511–522, 2011.
- Griffith, A. K., and N. K. Nichols, Adjoint methods in data assimilation for estimating model error, *Flow, turbulence and combustion*, *65*, 469–488, 2000.
- Grudzien, C., A. Carrassi, and M. Bocquet, Chaotic dynamics and the role of covariance inflation for reduced rank kalman filters with model error, *Nonlinear Proc. Geoph.*, *submitted*, 2018a.
- Grudzien, C., A. Carrassi, and M. Bocquet, Asymptotic forecast uncertainty and the unstable subspace in the presence of additive model error, *SIAM/ASA J. Uncertainty Quantification*, *submitted*, 2018b.
- Gurumoorthy, K. S., C. Grudzien, A. Apte, A. Carrassi, and C. K. Jones, Rank deficiency of Kalman error covariance matrices in linear time-varying system with deterministic evolution, *SIAM J. Control Optim.*, *55*, 741–759, 2017.
- Gustafsson, N., J. Bojarova, and O. Vignes, A hybrid variational ensemble data assimilation for the High Resolution Limited Area Model (HIRLAM), *Nonlinear Proc. Geoph.*, *21*, 303–323, 2014.
- Hamill, T. M., and C. Snyder, A hybrid ensemble Kalman filter-3D variational analysis scheme, *Mon. Weather Rev.*, *128*, 2905–2919, 2000.
- Hamill, T. M., J. S. Whitaker, and C. Snyder, Distance-dependent filtering of background error covariance estimates in an ensemble Kalman filter, *Mon. Weather Rev.*, *129*, 2776–2790, 2001.
- Hanea, R. G., G. J. M. Velders, A. J. Segers, M. Verlaan, and A. W. Heemink, A hybrid Kalman filter algorithm for large-scale atmospheric chemistry data assimilation, *Mon. Weather Rev.*, *135*, 140–151, 2007.
- Hannart, A., A. Carrassi, M. Bocquet, M. Ghil, P. Naveau, M. Pulido, J. Ruiz, and P. Tandeo, DADA: data assimilation for the detection and attribution of weather and climate-related events, *Climatic Change*, *136*, 155–174, 2016.
- Harlim, J., and A. J. Majda, Filtering turbulent sparsely observed geophysical flows, *Mon. Weather Rev.*, *138*, 1050–1083, 2010.
- Harlim, J., A. J. Majda, et al., Catastrophic filter divergence in filtering nonlinear dissipative systems, *Communications in Mathematical Sciences*, *8*, 27–43, 2010.
- Haugen, V. E., and G. Evensen, Assimilation of SLA and SST data into an OGCM for the Indian ocean, *Ocean Dynamics*, *52*, 133–151, 2002.
- Haussaire, J.-M., and M. Bocquet, A low-order coupled chemistry meteorology model for testing online and offline data assimilation schemes: L95-GRS (v1.0), *Geosci. Model Dev.*, *9*, 393–412, 2016.
- Hazeleger, W., V. Guemas, B. Wouters, S. Corti, I. Andreu-Burillo, F. Doblas-Reyes, K. Wyser, and M. Caian, Multiyear climate predictions using two initialization strategies, *Geophys. Res. Lett.*, *40*, 1794–1798, 2013.
- Hoke, J. E., and R. A. Anthes, The initialization of numerical models by a dynamic-initialization technique, *Mon. Weather Rev.*, *104*, 1551–1556, 1976.

- Horn, R. A., and C. R. Johnson, *Matrix analysis*, Cambridge university press, 2012.
- Hoteit, I., D.-T. Pham, M. Gharamti, and X. Luo, Mitigating observation perturbation sampling errors in the stochastic EnKF, *Mon. Weather Rev.*, *143*, 2918–2936, 2015.
- Houtekamer, P., and F. Zhang, Review of the ensemble Kalman filter for atmospheric data assimilation, *Mon. Weather Rev.*, *144*, 4489–4532, 2016.
- Houtekamer, P. L., and H. L. Mitchell, A sequential ensemble Kalman filter for atmospheric data assimilation, *Mon. Weather Rev.*, *129*, 123–137, 2001.
- Houtekamer, P. L., H. L. Mitchell, G. Pellerin, M. Buehner, M. Charron, L. Spacek, and B. Hansen, Atmospheric data assimilation with an ensemble Kalman filter: Results with real observations, *Mon. Weather Rev.*, *133*, 604–620, 2005.
- Hunt, B., E. J. Kostelich, and I. Szunyogh, Efficient data assimilation for spatiotemporal chaos: A local ensemble transform Kalman filter, *Physica D*, *230*, 112–126, 2007.
- Hunt, B. R., E. Kalnay, E. J. Kostelich, E. Ott, D. J. D. J. Patil, T. Sauer, I. Szunyogh, J. A. Yorke, and A. V. Zimin, Four-dimensional ensemble Kalman filtering, *Tellus A*, *56*, 273–277, 2004.
- Ide, K., L. Kuznetsov, and C. K. Jones, Lagrangian data assimilation for point vortex systems*, *J. Turbul.*, *3*, 2002.
- Janjić, T., D. McLaughlin, S. E. Cohn, and M. Verlaan, Conservation of Mass and Preservation of Positivity with Ensemble-Type Kalman Filter Algorithms, *Mon. Weather Rev.*, *142*, 755–773, 2014.
- Janjić, T., N. Bormann, M. Bocquet, J. A. Carton, S. E. Cohn, S. L. Dance, S. N. Losa, N. K. Nichols, R. Potthast, J. A. Waller, and P. Weston, On the representation error in data assimilation, *Q J Roy. Meteor. Soc.*, *0*, 0–0, 2017, accepted for publication.
- Jazwinski, A. H., *Stochastic Processes and Filtering Theory*, Academic Press, New-York, 1970.
- Kadakia, N., E. Armstrong, D. Breen, U. Morone, A. Daou, D. Margoliash, and H. D. Abarbanel, Nonlinear statistical data assimilation for hvc_ $\{\mathrm{RA}\}$ neurons in the avian song system, *Biological cybernetics*, *110*, 417–434, 2016.
- Kalman, R. E., A new approach to linear filtering and prediction problems, *J. Fluid. Eng.*, *82*, 35–45, 1960.
- Kalnay, E., *Atmospheric Modeling, Data Assimilation and Predictability*, Cambridge University Press, Cambridge, 2002.
- Kalnay, E., and A. Dalcher, Forecasting forecast skill, *Mon. Weather Rev.*, *115*, 349–356, 1987.
- Kalnay, E., and S.-C. Yang, Accelerating the spin-up of ensemble Kalman filtering, *Q J Roy. Meteor. Soc.*, *136*, 1644–1651, 2010.
- Kalnay, E., H. Li, T. Miyoshi, S.-C. Yang, and J. Ballabrera-Poy, 4-D-Var or ensemble Kalman filter?, *Tellus A*, *59*, 758–773, 2007.
- Kalnay, E., Y. Ota, T. Miyoshi, and J. Liu, A simpler formulation of forecast sensitivity to observations: application to ensemble Kalman filters, *Tellus A*, *64*, 18,462, 2012.
- Kang, J.-S., E. Kalnay, J. Liu, I. Fung, T. Miyoshi, and K. Ide, Variable localization in an ensemble Kalman filter: Application to the carbon cycle data assimilation, *J. Geophys. Res.*, *116*, D09,110, 2011.
- Keper, J. D., Covariance localisation and balance in an ensemble Kalman filter, *Q J Roy. Meteor. Soc.*, *135*, 1157–1176, 2009.
- Kleist, D. T., and K. Ide, An OSSE-based evaluation of hybrid variational–ensemble data assimilation for the NCEP GFS. Part I: System description and 3D-hybrid results, *Mon. Weather Rev.*, *143*, 433–451, 2015.

- Kondrashov, D., C. Sun, and M. Ghil, Data assimilation for a coupled ocean–atmosphere model. Part II: Parameter estimation, *Mon. Weather Rev.*, *136*, 5062–5076, 2008.
- Kong, A., J. S. Liu, and W. H. Wong, Sequential imputations and Bayesian missing data problems, *Journal of the American statistical association*, *89*, 278–288, 1994.
- Kotsuki, S., T. Miyoshi, K. Terasaki, G. Y. Lien, and E. Kalnay, Assimilating the global satellite mapping of precipitation data with the nonhydrostatic icosahedral atmospheric model (NICAM), *Journal of Geophysical Research*, *122*, 631–650, 2017.
- Kuptsov, P. V., and U. Parlitz, Theory and computation of covariant Lyapunov vectors, *J. Non-linear Sci.*, *22*, 727–762, 2012.
- Kuznetsov, L., K. Ide, and C. K. Jones, A method for assimilation of lagrangian data, *Mon. Weather Rev.*, *131*, 2247–2260, 2003.
- Lakshmivarahan, S., and J. M. Lewis, Nudging methods: A critical overview, in *Data Assimilation for Atmospheric, Oceanic and Hydrologic Applications (Vol. II)*, edited by S. K. Park and L. Xu, pp. 27–57, Springer Berlin Heidelberg, 2013.
- Laloyaux, P., M. Balmaseda, D. Dee, K. Mogensen, and P. Janssen, A coupled data assimilation system for climate reanalysis, *Q J Roy. Meteor. Soc.*, *142*, 65–78, 2016.
- Lauvernet, C., J.-M. M. Brankart, F. Castruccio, G. Broquet, P. Brasseur, and J. Verron, A truncated Gaussian filter for data assimilation with inequality constraints: Application to the hydrostatic stability condition in ocean models, *Ocean Modell.*, *27*, 1–17, 2009.
- Law, K., A. Stuart, and K. Zygalakis, *Data assimilation: A mathematical introduction*, vol. 62, Springer, 2015.
- Lawless, A., N. Nichols, C. Boess, and A. Bunse-Gerstner, Using model reduction methods within incremental four-dimensional variational data assimilation, *Mon. Weather Rev.*, *136*, 1511–1522, 2008.
- Le Dimet, F.-X., and O. Talagrand, Variational algorithms for analysis and assimilation of meteorological observations: theoretical aspects, *Tellus A*, *38*, 97–110, 1986.
- Legras, B., and R. Vautard, A guide to Liapunov vectors, in *Proceedings 1995 ECMWF Seminar on Predictability*, vol. 1, pp. 143–156, Citeseer, 1996.
- Leutbecher, M., and T. N. Palmer, Ensemble forecasting, *J. Comput Phys*, *227*, 3515–3539, 2008.
- Lewis, J. M., and J. C. Derber, The use of adjoint equations to solve a variational adjustment problem with advective constraints, *Tellus A*, *37*, 309–322, 1985.
- Li, H., E. Kalnay, and T. Miyoshi, Simultaneous estimation of covariance inflation and observation errors within an ensemble Kalman filter, *Q J Roy. Meteor. Soc.*, *135*, 523–533, 2009.
- Li, L., H. Zhou, H. J. Hendricks Franssen, and J. J. Gómez-Hernández, Groundwater flow inverse modeling in non-MultiGaussian media: Performance assessment of the normal-score Ensemble Kalman Filter, *Hydrology and Earth System Sciences*, *16*, 573–590, 2012.
- Liang, X., X. Zheng, S. Zhang, G. Wu, Y. Dai, and Y. Li, Maximum likelihood estimation of inflation factors on error covariance matrices for ensemble Kalman filter assimilation, *Q J Roy. Meteor. Soc.*, *138*, 263–273, 2012.
- Lien, G. Y., E. Kalnay, and T. Miyoshi, Effective assimilation of global precipitation: Simulation experiments, *Tellus A*, *65*, 2013.
- Lien, G.-Y., E. Kalnay, T. Miyoshi, and G. J. Huffman, Statistical Properties of Global Precipitation in the NCEP GFS Model and TMPA Observations for Data Assimilation, *Mon. Weather Rev.*, *144*, 663–679, 2016a.
- Lien, G.-Y., T. Miyoshi, and E. Kalnay, Assimilation of TRMM Multisatellite Precipitation Analysis with a Low-Resolution NCEP Global Forecast System, *Mon. Weather Rev.*, *144*, 643–661,

- 2016b.
- Lindskog, M., D. Dee, Y. Tremolet, E. Andersson, G. Radnoti, and M. Fisher, A weak-constraint four-dimensional variational analysis system in the stratosphere, *Q J Roy. Meteor. Soc.*, *135*, 695–706, 2009.
- Lions, J. L., *Optimal control of systems governed by partial differential equations*, Springer, 1971.
- Lisæter, K. A., J. Rosanova, and G. Evensen, Assimilation of ice concentration in a coupled ice-ocean model, using the ensemble Kalman filter, *Ocean Dynamics*, *53*, 368–388, 2003.
- Liu, C., Q. Xiao, and B. Wang, An ensemble-based four-dimensional variational data assimilation scheme. Part I: Technical formulation and preliminary test, *Mon. Weather Rev.*, *136*, 3363–3373, 2008.
- Liu, C., Q. Xiao, and B. Wang, An ensemble-based four-dimensional variational data assimilation scheme. Part II: Observing system simulation experiments with advanced research WRF (ARW), *Mon. Weather Rev.*, *137*, 1687–1704, 2009.
- Liu, Y., J.-M. Haussaire, M. Bocquet, Y. Roustan, O. Saunier, and A. Mathieu, Uncertainty quantification of pollutant source retrieval: comparison of bayesian methods with application to the Chernobyl and Fukushima-Daiichi accidental releases of radionuclides, *Q J Roy. Meteor. Soc.*, *143*, 2886–2901, 2017.
- Livings, D. M., S. L. Dance, and N. K. Nichols, Unbiased ensemble square root filters, *Physica D*, *237*, 1021–1028, 2008.
- Lorenc, A., Analysis methods for numerical weather prediction, *Q J Roy. Meteor. Soc.*, *112*, 1177–1194, 1986.
- Lorenc, A., Recommended nomenclature for EnVar data assimilation methods, Online: http://www.wcrp-climate.org/WGNE/BlueBook/2013/individual-articles/01_Lorenc_Andrew_EnVar_nomenclature.pdf, 2013.
- Lorenc, A. C., The potential of the ensemble Kalman filter for NWP — a comparison with 4D-Var, *Q J Roy. Meteor. Soc.*, *129*, 3183–3203, 2003.
- Lorenc, A. C., and T. Payne, 4D-Var and the butterfly effect: Statistical four-dimensional data assimilation for a wide range of scales, *Q J Roy. Meteor. Soc.*, *133*, 607–614, 2007.
- Lorenc, A. C., N. E. Bowler, A. M. Clayton, S. R. Pring, and D. Fairbairn, Comparison of hybrid-4DVar and hybrid-4DVar data assimilation methods for global NWP, *Mon. Weather Rev.*, *143*, 212–229, 2015.
- Lorenz, E., Deterministic non-periodic flow, *J. Atmos. Sci.*, *20*, 130–141, 1963.
- Lorenz, E. N., Predictability – a problem partly solved, in *Seminar on Predictability*, vol. 1, 1996.
- Lorenz, E. N., Designing chaotic models, *J. Atmos. Sci.*, *62*, 1574–1587, 2005.
- Lorenz, E. N., and K. A. Emanuel, Optimal sites for supplementary weather observations: simulation with a small model, *J. Atmos. Sci.*, *55*, 399–414, 1998.
- Lu, F., Z. Liu, S. Zhang, and Y. Liu, Strongly coupled data assimilation using leading averaged coupled covariance (LACC). Part I: Simple model study, *Mon. Weather Rev.*, *143*, 3823–3837, 2015.
- MacKay, D. J. C., *Information Theory, Inference and Learning Algorithms*, Cambridge University Press, Cambridge, 2003.
- Magnusson, L., M. Alonso-Balmaseda, S. Corti, F. Molteni, and T. Stockdale, Evaluation of forecast strategies for seasonal and decadal forecasts in presence of systematic model errors, *Clim. Dyn.*, *41*, 2393–2409, 2013.
- Mandel, J., E. Bergou, S. Gürol, S. Gratton, and I. Kusanický, Hybrid Levenberg-Marquardt and weak-constraint ensemble Kalman smoother method, *Nonlinear Proc. Geoph.*, *23*, 59, 2016.

- Miller, R., M. Ghil, and F. Gauthiez, Advanced data assimilation in strongly nonlinear dynamical systems, *J. Atmos. Sci.*, **51**, 1037–1056, 1994.
- Miyoshi, T., The Gaussian approach to adaptive covariance inflation and its implementation with the local ensemble transform Kalman filter, *Mon. Weather Rev.*, *139*, 1519–1535, 2011.
- Miyoshi, T., E. Kalnay, and H. Li, Estimating and including observation-error correlations in data assimilation, *Inverse Probl. Sci. Eng.*, *21*, 387–398, 2013.
- Morzfeld, M., X. Tu, E. Atkins, and A. J. Chorin, A random map implementation of implicit filters, *J. Comput Phys*, *231*, 2049–2066, 2012.
- Natvik, L. J., and G. Evensen, Assimilation of ocean colour data into a biochemical model of the North Atlantic. Part 1. Data assimilation experiments, *J. Marine. Sys.*, *40-41*, 127–153, 2003.
- Nerger, L., T. Janjić, J. Schröter, and W. Hiller, A unification of ensemble square root Kalman filters, *Mon. Weather Rev.*, *140*, 2335–2345, 2012.
- Ng, G.-H. C., D. McLaughlin, D. Entekhabi, and A. Ahanin, The role of model dynamics in ensemble Kalman filter performance for chaotic systems, *Tellus A*, *63*, 958–977, 2011.
- Ngodock, H., and M. Carrier, A 4DVAR system for the Navy Coastal Ocean Model. Part II: Strong and weak constraint assimilation experiments with real observations in Monterey Bay, *Mon. Weather Rev.*, *142*, 2108–2117, 2014.
- Ni, B., and Q. Zhang, Stability of the Kalman filter for continuous time output error systems, *Syst. Control. Lett.*, *94*, 172–180, 2016.
- Nicolis, C., Dynamics of model error: Some generic features, *J. Atmos. Sci.*, *60*, 2208–2218, 2003.
- Nino Ruiz, E. D., and A. Sandu, A derivative-free trust region framework for variational data assimilation, *J. Comput Appl Math*, *293*, 164–179, 2016.
- Nodet, M., Variational assimilation of lagrangian data in oceanography, *Inverse Probl.*, *22*, 245, 2006.
- Ott, E., B. R. Hunt, I. Szunyogh, A. V. Zimin, E. J. Kostelich, M. Corazza, E. Kalnay, D. J. Patil, and A. Yorke, A local ensemble Kalman filter for atmospheric data assimilation, *Tellus A*, *56*, 415–428, 2004.
- Palatella, L., and A. Trevisan, Interaction of Lyapunov vectors in the formulation of the nonlinear extension of the Kalman filter, *Phys. Rev. E.*, *91*, 042,905, 2015.
- Palatella, L., A. Carrassi, and A. Trevisan, Lyapunov vectors and assimilation in the unstable subspace: theory and applications, *J. Phys. A: Math. Theor.*, *46*, 254,020, 2013a.
- Palatella, L., A. Trevisan, and S. Rambaldi, Nonlinear stability of traffic models and the use of lyapunov vectors for estimating the traffic state, *Phys. Rev. E.*, *88*, 022,901, 2013b.
- Pazo, D., A. Carrassi, and J. Lopez, Data assimilation by delay-coordinate nudging, *Q J Roy. Meteor. Soc.*, *142*, 1290–1299, 2016.
- Penny, S. G., and T. M. Hamill, Coupled data assimilation for integrated earth system analysis and prediction, *Bull. Amer. Meteor. Soc.*, 2017.
- Penny, S. G., and T. Miyoshi, A local particle filter for high dimensional geophysical systems, *Nonlinear Proc. Geoph.*, *23*, 391–405, 2016.
- Pham, D. T., Stochastic methods for sequential data assimilation in strongly nonlinear systems, *Mon. Weather Rev.*, *129*, 1194–1207, 2001.
- Pham, D. T., J. Verron, and M. C. Roubaud, A singular evolutive extended Kalman filter for data assimilation in oceanography, *J. Marine Systems*, *16*, 323–340, 1998.
- Pires, C., R. Vautard, and O. Talagrand, On extending the limits of variational assimilation in nonlinear chaotic systems, *Tellus A*, *48*, 96–121, 1996.
- Poli, P., H. Hersbach, D. P. Dee, P. Berrisford, A. J. Simmons, F. Vitart, P. Laloyaux, D. G. Tan,

- C. Peubey, J.-N. Thépaut, et al., Era-20c: An atmospheric reanalysis of the twentieth century, *J. Climate*, *29*, 4083–4097, 2016.
- Poterjoy, J., A localized particle filter for high-dimensional nonlinear systems, *Mon. Weather Rev.*, *144*, 59–76, 2016.
- Poterjoy, J., and F. Zhang, Systematic comparison of four-dimensional data assimilation methods with and without the tangent linear model using hybrid background error covariance: E4DVar versus 4DEnVar, *Mon. Weather Rev.*, *143*, 1601–1621, 2015.
- Pulido, M., P. Tandeo, M. Bocquet, A. Carrassi, and M. Lucini, Stochastic parameterization identification using ensemble kalman filtering combined with expectation-maximization and newton-raphson maximum likelihood methods, *Submitted to Tellus*, 2018.
- Quinn, J. C., and H. D. Abarbanel, State and parameter estimation using Monte Carlo evaluation of path integrals, *Q J Roy. Meteor. Soc.*, *136*, 1855–1867, 2010.
- Raanes, P. N., On the ensemble rauch-tung-striebel smoother and its equivalence to the ensemble Kalman smoother, *Q J Roy. Meteor. Soc.*, *142*, 1259–1264, 2016.
- Raanes, P. N., A. Carrassi, and L. Bertino, Extending the square root method to account for additive forecast noise in ensemble methods, *Mon. Weather Rev.*, *143*, 3857–3873, 2015.
- Rampal, P., S. Bouillon, E. Ólason, and M. Morlighem, neXtSIM: a new Lagrangian sea ice model, *Cryosphere*, *10*, 2016.
- Raynaud, L., L. Berre, and G. Desroziers, Objective filtering of ensemble-based background-error variances, *Q J Roy. Meteor. Soc.*, *135*, 1177–1199, 2009.
- Raynaud, L., L. Berre, and G. Desroziers, An extended specification of flow-dependent background error variances in the Mto-France global 4D-Var system, *Q J Roy. Meteor. Soc.*, *137*, 607–619, 2011.
- Reich, S., A nonparametric ensemble transform method for Bayesian inference., *SIAM J. Sci. Comput.*, *35*, A2013–A2014, 2013.
- Reich, S., and C. Cotter, *Probabilistic Forecasting and Bayesian Data Assimilation*, Cambridge University Press, Cambridge, 2015.
- Robert, C., S. Durbiano, E. Blayo, J. Verron, J. Blum, and F. X. Le Dimet, A reduced-order strategy for 4D-Var data assimilation, *J. Marine Systems*, *57*, 70–82, 2005.
- Robert, S., and H. R. Künsch, Localizing the ensemble Kalman particle filter, *Tellus A*, *69*, 1282,016, 2017.
- Saha, S., S. Moorthi, H.-L. Pan, X. Wu, J. Wang, S. Nadiga, P. Tripp, R. Kistler, J. Woollen, D. Behringer, et al., The ncep climate forecast system reanalysis, *Bull. Amer. Meteor. Soc.*, *91*, 1015–1057, 2010.
- Sakov, P., and L. Bertino, Relation between two common localisation methods for the EnKF, *Computat. Geosci.*, *15*, 225–237, 2011.
- Sakov, P., and P. R. Oke, Implications of the form of the ensemble transform in the ensemble square root filters, *Mon. Weather Rev.*, *136*, 1042–1053, 2008a.
- Sakov, P., and P. R. Oke, A deterministic formulation of the ensemble Kalman filter: an alternative to ensemble square root filters, *Tellus, Ser. A*, *60*, 361–371, 2008b.
- Sakov, P., G. Evensen, and L. Bertino, Asynchronous data assimilation with the EnKF, *Tellus Ser A*, *62A*, 24–29, 2010.
- Sakov, P., F. Counillon, L. Bertino, K. Lisæter, P. Oke, and A. Korablev, TOPAZ4: an ocean-sea ice data assimilation system for the North Atlantic and Arctic, *Ocean Sci.*, *8*, 633, 2012a.
- Sakov, P., D. S. Oliver, and L. Bertino, An iterative EnKF for strongly nonlinear systems, *Mon. Weather Rev.*, *140*, 1988–2004, 2012b.

- Salman, H., L. Kuznetsov, C. Jones, and K. Ide, A method for assimilating Lagrangian data into a shallow-water-equation ocean model, *Mon. Weather Rev.*, *134*, 1081–1101, 2006.
- Santitissadeekorn, N., and C. Jones, Two-stage filtering for joint state-parameter estimation, *Mon. Weather Rev.*, *143*, 2028–2042, 2015.
- Sasaki, Y., Some basic formalism in numerical variational analysis, *Mon. Weather Rev.*, *98*, 875–883, 1970.
- Schölzel, C., and P. Friederichs, Multivariate non-normally distributed random variables in climate research-introduction to the copula approach, *Nonlinear Proc. Geoph.*, *15*, 761–772, 2008.
- Simon, E., and L. Bertino, Application of the Gaussian anamorphosis to assimilation in a 3-D coupled physical-ecosystem model of the North Atlantic with the EnKF: a twin experiment, *Ocean Sci.*, *5*, 495–510, 2009.
- Simon, E., and L. Bertino, Gaussian anamorphosis extension of the DEnKF for combined state parameter estimation: Application to a 1D ocean ecosystem model, *J. Marine Systems*, *89*, 1–18, 2012.
- Simon, E., A. Samuelsen, L. Bertino, and S. Mouysset, Experiences in multiyear combined state-parameter estimation with an ecosystem model of the North Atlantic and Arctic Oceans using the Ensemble Kalman Filter, *J. Marine Systems*, *152*, 1–17, 2015.
- Slivinski, L., and C. Snyder, Exploring practical estimates of the ensemble size necessary for particle filters, *Mon. Weather Rev.*, *144*, 861–875, 2016.
- Slivinski, L., E. Spiller, A. Apte, and B. Sandstede, A hybrid particle-ensemble Kalman filter for Lagrangian data assimilation, *Mon. Weather Rev.*, *143*, 195–211, 2015.
- Sluka, T. C., S. G. Penny, E. Kalnay, and T. Miyoshi, Assimilating atmospheric observations into the ocean using strongly coupled ensemble data assimilation, *Geophys. Res. Lett.*, *43*, 752–759, 2016.
- Smith, D. M., and J. M. Murphy, An objective ocean temperature and salinity analysis using covariances from a global climate model, *J. Geophys. Res. Oceans*, *112*, 2007.
- Smith, D. M., R. Eade, and H. Pohlmann, A comparison of full-field and anomaly initialization for seasonal to decadal climate prediction, *Clim. Dyn.*, *41*, 3325–3338, 2013.
- Smith, P. J., A. M. Fowler, and A. S. Lawless, Exploring strategies for coupled 4D-Var data assimilation using an idealised atmosphere–ocean model, *Tellus A*, *67*, 27,025, 2015.
- Snyder, C., T. Bengtsson, P. Bickel, and J. L. Anderson, Obstacles to high-dimensional particle filtering, *Mon. Weather Rev.*, *136*, 4629–4640, 2008.
- Snyder, C., T. Bengtsson, and T. Morzfeld, Performance bounds for particle filters using the optimal proposal, *Mon. Weather Rev.*, *143*, 4750–4761, 2015.
- Stewart, L. M., S. Dance, and N. Nichols, Correlated observation errors in data assimilation, *Int. J. Numer. Methods Fluids*, *56*, 1521–1527, 2008.
- Stockdale, T. N., Coupled ocean–atmosphere forecasts in the presence of climate drift, *Mon. Weather Rev.*, *125*, 809–818, 1997.
- Stordal, A. S., H. A. Karlsen, G. Nævdal, H. J. Skaug, and B. Vallès, Bridging the Ensemble Kalman Filter and particle filters: the adaptive Gaussian mixture filter, *Computat. Geosci.*, *15*, 293–305, 2011.
- Stott, P., M. Allen, N. Christidis, R. Dole, M. Hoerling, C. Huntingford, P. Pall, J. Perlwitz, and D. Stone, Attribution of weather and climate-related events, in *Climate Science for Serving Society: Research, Modelling and Prediction Priorities*. G.R. Asrar and J. W. Hurrell (Eds.), Springer, 2013.
- Sugiura, N., T. Awaji, S. Masuda, T. Mochizuki, T. Toyoda, T. Miyama, H. Igarashi, and

- Y. Ishikawa, Development of a four-dimensional variational coupled data assimilation system for enhanced analysis and prediction of seasonal to interannual climate variations, *J. Geophys. Res. Oceans*, *113*, 2008.
- Sun, C., Z. Hao, M. Ghil, and J. D. Neelin, Data assimilation for a coupled ocean–atmosphere model. Part I: Sequential state estimation, *Mon. Weather Rev.*, *130*, 1073–1099, 2002.
- Talagrand, O., Assimilation of observations, an introduction (special issue — data assimilation in meteorology and oceanography: Theory and practice), *J. Meteorol. Soc. Jpn.*, *75*, 191–209, 1997.
- Talagrand, O., Variational assimilation, in *Data assimilation: Making Sense of Observations*, pp. 41–67, Springer, 2010.
- Talagrand, O., and P. Courtier, Variational assimilation of meteorological observations with the adjoint vorticity equation. i: Theory, *Q J Roy. Meteor. Soc.*, *113*, 1311–1328, 1987.
- Tandeo, P., M. Pulido, and F. Lott, Offline parameter estimation using EnKF and maximum likelihood error covariance estimates: Application to a subgrid-scale orography parametrization, *Q J Roy. Meteor. Soc.*, *141*, 383–395, 2015.
- Tardif, R., G. J. Hakim, and C. Snyder, Coupled atmosphere–ocean data assimilation experiments with a low-order climate model, *Clim. Dyn.*, *43*, 1631–1643, 2014.
- Tardif, R., G. J. Hakim, and C. Snyder, Coupled atmosphere–ocean data assimilation experiments with a low-order model and CMIP5 model data, *Clim. Dyn.*, *45*, 1415–1427, 2015.
- Thacker, C., Data assimilation with inequality constraints, *Ocean Modell*, *16*, 264–276, 2007.
- Tippett, M. K., J. L. Anderson, C. H. Bishop, T. M. Hamill, and J. S. Whitaker, Ensemble square-root filters, *Mon. Weather Rev.*, *131*, 1485–1490, 2003.
- Trémolet, Y., Accounting for an imperfect model in 4D-Var, *Q J Roy. Meteor. Soc.*, *132*, 2483–2504, 2006.
- Trémolet, Y., Model-error estimation in 4D-Var, *Q J Roy. Meteor. Soc.*, *133*, 1267–1280, 2007.
- Trevisan, A., and L. Palatella, On the Kalman filter error covariance collapse into the unstable subspace, *Nonlinear Proc. Geoph.*, *18*, 243–250, 2011a.
- Trevisan, A., and L. Palatella, Chaos and weather forecasting: the role of the unstable subspace in predictability and state estimation problems, *Int. J. Bifurcat. Chaos*, *21*, 3389–3415, 2011b.
- Trevisan, A., and F. Uboldi, Assimilation of standard and targeted observations within the unstable subspace of the observation-analysis-forecast cycle, *J. Atmos. Sci.*, *61*, 103–113, 2004.
- Trevisan, A., M. D’Isidoro, and O. Talagrand, Four-dimensional variational assimilation in the unstable subspace and the optimal subspace dimension, *Q J Roy. Meteor. Soc.*, *136*, 487–496, 2010.
- Uboldi, F., and M. Kamachi, Time-space weak-constraint data assimilation for nonlinear models, *Tellus A*, *52*, 412–421, 2000.
- Uboldi, F., and A. Trevisan, Detecting unstable structures and controlling error growth by assimilation of standard and adaptive observations in a primitive equation ocean model, *Nonlinear Proc. Geoph.*, *16*, 67–81, 2006.
- Ueno, G., and N. Nakamura, Iterative algorithm for maximum-likelihood estimation of the observation-error covariance matrix for ensemble-based filters, *Q J Roy. Meteor. Soc.*, *140*, 295–315, 2014.
- Ueno, G., and N. Nakamura, Bayesian estimation of the observation-error covariance matrix in ensemble-based filters, *Q J Roy. Meteor. Soc.*, *142*, 2055–2080, 2016.
- van Leeuwen, P. J., Particle filtering in geophysical systems, *Mon. Weather Rev.*, *137*, 4089–4114, 2009.
- van Leeuwen, P. J., Y. Cheng, and S. Reich, *Nonlinear data assimilation*, vol. 2, Springer, 2015.

- Vannitsem, S., Predictability of large-scale atmospheric motions: Lyapunov exponents and error dynamics, *Chaos*, *27*, 032,101, 2017.
- Vidard, P., A. Piacentini, and F.-X. Le Dimet, Variational data analysis with control of the forecast bias, *Tellus A*, *56*, 177–188, 2004.
- Wackernagel, H., *Multivariate Geostatistics*, 3rd ed., Springer Verlag, Berlin, 2003.
- Wang, S., M. Xue, A. D. Schenkman, and J. Min, An iterative ensemble square root filter and tests with simulated radar data for storm-scale data assimilation, *Q J Roy. Meteor. Soc.*, *139*, 1888–1903, 2013.
- Wang, X., and C. H. Bishop, A comparison of breeding and ensemble transform Kalman filter ensemble forecast schemes, *J. Atmos. Sci.*, *60*, 1140–1158, 2003.
- Wang, X., C. H. Bishop, and S. J. Julier, Which is better, an ensemble of positive–negative pairs or a centered spherical simplex ensemble?, *Mon. Weather Rev.*, *132*, 1590–1605, 2004.
- Wang, X., C. Snyder, and T. M. Hamill, On the theoretical equivalence of differently proposed ensemble-3DVAR hybrid analysis schemes, *Mon. Weather Rev.*, *135*, 222–227, 2007.
- Wang, Y., F. Counillon, and L. Bertino, Alleviating the bias induced by the linear analysis update with an isopycnal ocean model, *Q J Roy. Meteor. Soc.*, *142*, 2016.
- Weber, R. J., A. Carrassi, and F. J. Doblas-Reyes, Linking the anomaly initialization approach to the mapping paradigm: a proof-of-concept study, *Mon. Weather Rev.*, *143*, 4695–4713, 2015.
- Whitaker, J. S., and T. M. Hamill, Ensemble data assimilation without perturbed observations, *Mon. Weather Rev.*, *130*, 1913–1924, 2002.
- Whitaker, J. S., and T. M. Hamill, Evaluating methods to account for system errors in ensemble data assimilation, *Mon. Weather Rev.*, *140*, 3078–3089, 2012.
- Wiener, N., *Extrapolation, Interpolation and Smoothing of Stationary Time Series, with Engineering Applications*, M.I.T. Press, Cambridge, MA, 1949.
- Wikle, C. K., and L. M. Berliner, A Bayesian tutorial for data assimilation, *Physica D*, *230*, 1–16, 2007.
- Winiarek, V., J. Vira, M. Bocquet, M. Sofiev, and O. Saunier, Towards the operational estimation of a radiological plume using data assimilation after a radiological accidental atmospheric release, *Atmos. Environ.*, *45*, 2944–2955, 2011.
- Wu, L., V. Mallet, M. Bocquet, and B. Sportisse, A comparison study of data assimilation algorithms for ozone forecasts, *J. Geophys. Res.*, *113*, D20,310, 2008.
- Xie, J., L. Bertino, F. Counillon, K. A. Lisæter, and P. Sakov, Quality assessment of the topaz4 reanalysis in the arctic over the period 1991–2013, *Ocean Sci.*, *13*, 123, 2017.
- Yang, S.-C., M. Corazza, A. Carrassi, E. Kalnay, and T. Miyoshi, Comparison of local ensemble transform Kalman filter, 3DVAR, and 4DVAR in a quasigeostrophic model, *Mon. Weather Rev.*, *137*, 693–709, 2009.
- Yano, J.-I., M. Z. Ziemiański, M. Cullen, P. Termonia, J. Onvlee, L. Bengtsson, A. Carrassi, R. Davy, A. Deluca, S. L. Gray, et al., Scientific challenges of convective-scale numerical weather prediction, *Bull. Amer. Meteor. Soc.*, 2017.
- Ye, J., N. Kadakia, P. Rozdeba, H. Abarbanel, and J. Quinn, Improved variational methods in statistical data assimilation, *Nonlinear Proc. Geoph.*, *22*, 205–213, 2015.
- Ying, M., and F. Zhang, An adaptive covariance relaxation method for ensemble data assimilation, *Q J Roy. Meteor. Soc.*, *141*, 2898–2906, 2015.
- Zhang, M., and F. Zhang, E4DVar: Coupling an ensemble Kalman filter with four-dimensional variational data assimilation in a limited-area weather prediction model, *Mon. Weather Rev.*, *140*, 587–600, 2012.

- Zhang, S., M. Harrison, A. Rosati, and A. Wittenberg, System design and evaluation of coupled ensemble data assimilation for global oceanic climate studies, *Mon. Weather Rev.*, *135*, 3541–3564, 2007.
- Zhang, Y., M. Bocquet, V. Mallet, C. Seigneur, and A. Baklanov, Real-time air quality forecasting, part II: State of the science, current research needs, and future prospects, *Atmos. Environ.*, *60*, 656–676, 2012.
- Zheng, X. G., An adaptive estimation of forecast error covariance parameters for Kalman filtering data assimilation, *Adv. Atmos. Sci.*, *26*, 154–160, 2009.
- Zhou, H., L. Li, H.-J. Hendricks Franssen, and J. J. Gómez-Hernández, Pattern Recognition in a Bimodal Aquifer Using the Normal-Score Ensemble Kalman Filter, *Math. Geosci.*, *44*, 169–185, 2012.
- Zhu, M., P.-J. van Leeuwen, and J. Amezcuca, Implicit equal-weights particle filter, *Q J Roy. Meteor. Soc.*, *142*, 1904–1919, 2016.
- Zupanski, D., A general weak constraint applicable to operational 4DVAR data assimilation systems, *Mon. Weather Rev.*, *125*, 2274–2292, 1997.
- Zupanski, M., A preconditioning algorithm for four-dimensional variational data assimilation, *Mon. Weather Rev.*, *124*, 2562–2573, 1996.
- Zupanski, M., Maximum likelihood ensemble filter: Theoretical aspects, *Mon. Weather Rev.*, *133*, 1710–1726, 2005.